UNIVERSIDADE D
COIMBRA

Beatriz Anjos Caramelo Ferreira

Development of New Imaging and Biochemical Markers of Diabetic Complications

Early Neurometabolic alterations in obesity and type 2 diabetes *mellitus*

Dissertação no âmbito do Mestrado em Biologia Celular e Molecular orientada pelo Professor Doutor Paulo Nuno Centeio Matafome e pela Professora Doutora Emília da Conceição Pedrosa Duarte e apresentada à Faculdade de Ciências e Tecnologia da Universidade de Coimbra, Departamento de Ciências da Vida

Julho de 2022

Beatriz Anjos Caramelo Ferreira

DEVELOPMENT OF NEW IMAGING AND BIOCHEMICAL MARKERS OF DIABETIC COMPLICATIONS

EARLY NEUROMETABOLIC ALTERATIONS IN OBESITY AND TYPE 2 DIABETES *MELLITUS*

Dissertation regarding the Master of Cellular and Molecular Biology oriented by Professor Doctor Paulo Nuno Centeio Matafome and by Professor Doctor Emília da Conceição Pedrosa Duarte and presented to the Faculty of Sciences and Technology of University of Coimbra, Department of Life Sciences

July 2022

Acknowledgments:

Hoje termina aquela que foi até agora, possivelmente, a etapa mais desafiante da minha vida académica e profissional, mas também a mais enriquecedora. No entanto, este percurso não foi feito sozinha, foi repleto de pessoas incríveis ao meu lado a cada momento deste último ano. Por isso, não poderia terminar esta fase sem vos deixar o maior dos agradecimentos.

Primeiramente, gostaria de deixar o meu "obrigada" ao Professor Doutor Paulo Matafome que desde sempre demonstrou confiança em mim e nas minhas capacidades, tendo-me aberto as portas do seu laboratório e me confiado este projeto que deu origem à minha dissertação de mestrado. Obrigada por todas as oportunidades que me foram concedidas, das quais eu adquiri tantos conhecimentos que vou levar para o resto da minha vida profissional. Tal inclui não só aprendizagens de prática-laboratorial e teórica, mas também a extraordinária ética de trabalho que incute nos seus alunos.

Seguidamente, gostaria de agradecer à minha co-orientadora e supervisora, Professora Doutora Emília Duarte, pelo acompanhamento e disponibilidade que me ofereceu durante a totalidade deste percurso.

Gostaria ainda de agradecer ao Professor Doutor Miguel Castelo-Branco por me ter aceitado na equipa formada para a concretização deste projeto e me ter confiado várias etapas deste (de imagem) nas quais eu não tinha qualquer experiência, mas das quais tanto aprendi, demonstrando sempre paciência e compreensão. Adicionalmente, gostaria de agradecer a disponibilidade que sempre me apresentou. Estendo o meu agradecimento aos membros da sua equipa, nomeadamente ao Doutor João Castelhano, ao Doutor João Martins e ao Doutor José Sereno, por todos os valiosos ensinamentos e paciência durante este último ano.

Adicionalmente, deixo um especial obrigada àquela que me apresentou o trabalho num laboratório no âmbito de investigação científica e, por isso, apelido carinhosamente "mamãe científica", a Doutora Tamaeh Alfredo-Monteiro. Obrigada por tudo o que me proporcionaste enquanto minha co-orientadora e professora, que fez de mim a investigadora que sou hoje, desde os ensinamentos, à paciência, à serenidade e ao companheirismo. É e sempre será um enorme orgulho poder dividir contigo, uma

grande investigadora, o meu primeiro artigo. E agora, inda que longe, os ensinamentos continuam, mas principalmente a amizade continua. É por esta que, acima de tudo, te agradeço. Faltou apenas me ensinares a não esquecer de responder a mensagens, mas hei-de aprender.

Agora, gostava de deixar o maior dos agradecimentos àquelas que tornaram toleráveis os momentos de stress e desespero experienciados este ano, incluindo dormidas em aeroportos e western blots falhados: Andreia Amaro, Daniela Rosendo da Silva, Diana Sousa e Mariana Rocha. Obrigada por todo o apoio dentro do laboratório, desde o desvendar dos problemas nos blots, dando um estilo "Sherlock Holmes" aos meus dias, à paciência com a complexidade que é o cérebro desta porteira durante as tardes de "Código Secreto". Mas obrigada também a todo o companheirismo e momentos fora do laboratório, àquelas que se tornaram de colegas a amigas fontes de inúmeras "catchphrases".

Seguidamente, agradeço aos meus amigos Diana Monteiro, Guilherme Faria, Isa Mota, Luiz Piochi, Mariana Pires e Vasco Santos. Aos melhores companheiros que poderia ter tido durante a faculdade, que tornaram tudo mais fácil e divertido, mesmo nos momentos mais desesperantes e que tornaram a faculdade algo que ansiava diariamente. Ainda que agora com menos interações visto a vida nos ter levado em caminhos agora separados, quando nos reencontramos, tudo permanece igual, como se esses encontros diários se mantivessem. Vocês são quem eu sempre ansiarei primeiro contar as minhas vitórias e as minhas derrotas, e obrigada por estarem sempre lá quer para me celebrar comigo, quer para me consolar.

Agora, queria agradecer aos mais antigos: Renata Craveiro, Mauro Dinis, Sara Ribeiro, Rogério Velindro e Carlos Marques. Obrigada por ouvirem sobre as minhas experiências, resultados e ratinhos e se fingirem interessados durante tantas ocasiões, e de facto prestarem atenção para eu não dar conta do desinteresse. Obrigada por todos os momentos, conselhos e companheirismo. Mas, principalmente, obrigada a ti Renata! Por acreditares mais em mim do que eu em mim própria, de acreditares piamente em todas as minhas capacidades e me relembrares delas sempre que me esqueço. Obrigada por estares sempre comigo para celebrar as minhas conquistas comigo e quereres estar presente em todos os passos do meu percurso (nem que por videochamada), por me

socorreres nos momentos maus, pela constante preocupação. O maior dos obrigadas a ti, melhor amiga.

Por fim, obrigada aos meus pais, Joaquina e Paulo Ferreira, à minha irmã, Emília Ferreira, por toda a compreensão, força, encorajamento e o inalcançável para que os meus objetivos se possam concretizar. Mas também agradeço a todos os meus primos, tios e amigos de família que desde cedo vivenciaram a minha paixão pela ciência e que sempre me encorajaram a segui-la.

Index:

Pages

Abstract:

Introduction and objectives: Type 2 diabetes *mellitus* (T2DM) is associated with a great risk of developing neurological comorbidities, which are, at least partly, responsible for the elevated mortality and low life quality of these patients. Therefore, these conditions require monitoring and, ideally, an early diagnosis through biochemical and imaging markers. However, in regard to cerebral complications, the monitoring procedures are limited, mostly focusing on structural alterations which are usually present only at later stages and are irreversible. For several years, it has been showcased that both hyperglycaemia and insulin resistance induce an excitatory synaptic remodelling. However, only recently an equivalent effect was observed in the GABAergic synapse. Furthermore, these alterations have also been related with the onset of oxidative stress. A recent ^{1}H-magnetic resonance spectroscopy (MRS) sequence has been developed entitled Hadamard Encoding and Reconstruction of MEGA-Edited Spectroscopy (HERMES) which enables the simultaneous cerebral assessment of gamma-aminobutyric acid (GABA) and glutathione (GSH), thus inhibitory synapse and oxidative stress, respectively. This project aims to optimize the use of the HERMES sequence on animal models of obesity and type 2 diabetes, while identifying early neurometabolic alterations in the hippocampus and visual cortex that could be clinically applied.

Materials and methods: Three experimental groups were designed: (1) Control group of male Wistar rats only fed standard diet (SD, 10 weeks) (SD group); (2) high-fat diet (HFD) induced obese rats for 10 weeks (HFD group); and (3) Obese rats induced to T2DM by an intraperitoneally injected low dose (35 mg/kg) of streptozotocin on week 4 (HFD+STZ group). Upon a 10-week period, all rats were subjected to MRS recurring to the HERMES sequence. This was followed by their sacrifice, moment in which the hippocampus and visual cortex were collected and frozen for later use in biochemical experiments.

Results: Resorting to the HERMES sequence, GABA levels were obtained with a coefficient of variance (CV) of 20.91% and 39.89% in the hippocampus and visual cortex,

respectively. Likewise, GSH levels presented in the hippocampus a CV of 23.82%; while, in the visual cortex, it equalled 23.61%. Glutamine (Gln), but not glutamate (Glu), levels were elevated in the visual cortex of the HFD+STZ group ($p = 0.0252$), as well as in the hippocampus of the HFD+STZ group ($p = 0.0088$). Moreover, unlike what is observed in the visual cortex, HFD potentiated the N-acetylaspartylglutamate (NAAG) formation in the hippocampus ($p = 0.0365$), which are not observed in HFD+STZ rats. Similarly, in the hippocampus only, an increment of GSH levels was observed in the HFD group ($p = 0.0494$). Altogether, both these molecules shared a similar variation pattern, suggesting a compensatory mechanism mediated between the two ($r = 0.4652$, $p = 0.0336$). The latter was, however, absent in the visual cortex ($r = - 0.2111$, $p = 0.3857$). Moreover, GABA levels and GABA type A receptor ($GABA_AR$) were not altered. No changes were observed for other antioxidant defences, including catalase, nor for the marker for cellular viability, N-acetylaspartate (NAA).

Conclusion: Through the apparent accurate measurements obtained by the HERMES sequence, we concluded that, in the hippocampus of the HFD model, Glu synthesis was not affected. Through the inhibitory effect of NAAG, Glu release into the synaptic cleft is apparently prevented in order to promote the formation of GSH as a compensatory mechanism. However, this effect is lost in the HFD+STZ model, showing the noxious effects of T2DM in the brain occur even before a compromised cellular viability. The metabolite NAAG and GSH may be valuable early markers of neurometabolic alterations.

Keywords: HERMES sequence, N-acetylaspartylglutamate, glutathione, obesity, hippocampus

Resumo:

Introdução e objetivos: Diabetes *mellitus* tipo 2 (T2DM) é associada a um risco aumentado para o desenvolvimento de complicações neurológicas, as quais são, pelo menos em parte, responsáveis pela elevada mortalidade e baixa qualidade de vida destes pacientes. Desse modo, estas necessitam monitorização e, idealmente, um diagnóstico numa fase inicial através de marcadores bioquímicos e de imagem. Contudo, no que diz respeito a estas complicações, os procedimentos de monitorização são limitados, focando-se maioritariamente em alterações estruturais, as quais estão comumente presentes em fases tardias exclusivamente e são irreversíveis. Há diversos anos que é sabido que a hiperglicemia e a resistência à insulina induzem remodelação sináptica excitatória. No entanto, só recentemente foram também observadas modificações ao nível da sinapse GABAérgica. Consequentemente, estas alterações culminam no desenvolvimento de stress oxidativo. Uma sequência de espetroscopia de ressonância magnética (^{1}H-MRS) foi recentemente desenvolvida denominada "Hadamard Encoding and Reconstruction of MEGA-Edited Spectroscopy" (HERMES), a qual possibilita a deteção cerebral simultânea do ácido gama-aminobutírico (GABA) e glutationa (GSH), medindo, por conseguinte, a sinapse inibitória e stress oxidativo, respetivamente. Este projeto tem como objetivo otimizar o uso da sequência HERMES em modelos animais de obesidade e T2DM, enquanto são identificadas alterações neurometabólicas em fases iniciais destas doenças metabólicas no hipocampo e córtex visual que possam ser futuramente aplicadas na clínica.

Materiais e métodos: Três grupos experimentais foram desenhados: (1) grupo controlo composto por ratos Wistar machos exclusivamente alimentados com dieta *standard* (SD, 10 semanas) (grupo SD); (2) obesidade foi induzida em ratos através da limitação da sua alimentação a dieta gorda (HFD) por 10 semanas (grupo HFD); e (3) ratos obesos foram injetados com uma dose baixa (35 mg/kg, intraperitoneal) de estreptozotocina (STZ) na quarta semana (grupo HFD+STZ). Após as 10 semanas, todos os ratos foram sujeitos a MRS com recurso à sequência HERMES. Este procedimento foi seguido pelo sacrifício destes, momento no qual o hipocampo e córtex visual foram recolhidos e congelados para uso futuro em experiências bioquímicas.

Resultados: Recorrendo à sequência HERMES, os níveis de GABA foram obtidos com um coeficiente de variação (CV) de 20.91% e 39.89% no hipocampo e córtex visual, respetivamente. Do mesmo modo, os níveis de GSH apresentaram no hipocampo um CV de 23.82%, enquanto que, no córtex visual, este parâmetro igualou 23.61%. Os níveis de glutamina (Gln), ao contrário do glutamato (Glu), estavam aumentados no córtex visual do grupo HFD+STZ ($p = 0.0252$), assim como no hipocampo do mesmo grupo ($p = 0.0088$). Além disso, em contraste ao que é observado no córtex visual, a dieta gorda potenciou a formação de N-acetilaspartilglutamato (NAAG) no hipocampo ($p = 0.0365$), o que não é observado na mesma região em ratos do grupo HFD+STZ. Similarmente, apenas no hipocampo, um aumento dos níveis de GSH foi observado no grupo HFD ($p = 0.0494$). Ambas as moléculas partilharam um padrão de variação similar, sugerindo a presença de um mecanismo de compensação mediado pelas duas ($r = 0.4652$, $p = 0.0336$). Em contrapartida, este está ausente no córtex visual ($r = - 0.2111$, $p = 0.3857$). Já no que diz respeito aos níveis de GABA e do recetor de GABA do tipo A ($GABA_AR$), alterações não foram verificadas. Adicionalmente, nenhuma modificação foi observada noutras defesas antioxidantes, nomeadamente na catálase, nem no marcador de viabilidade celular, N-acetilaspartato (NAA).

Conclusão: Através das medidas aparentemente exatas obtidas pela sequência HERMES, é possível concluir que, no hipocampo do modelo HFD, a síntese de Glu não foi afetada. Por intermédio do efeito inibitório de NAAG, a libertação de Glu para a fenda sináptica é presumivelmente impedida para a indução da formação de GSH num mecanismo compensatório. Porém, este efeito é perdido no grupo HFD+STZ, evidenciando que os efeitos danosos da T2DM no cérebro se dão previamente ao comprometimento da viabilidade celular. Os metabolitos NAAG e GSH poderão constituir úteis marcadores de alterações neurometabólicas em fases iniciais destas comorbidades.

Palavras-chave: sequência HERMES, N-acetilaspartilglutamato, glutationa, obesidade, hipocampo

Master's degree (MSc): publications and scientific communications

Scientific communications:

1. **Congress:** 18th Portuguese Congress of Diabetes
   Held in: Vilamoura, Portugal
   Date: 10th-12th March 2022
   Communication format: Oral Presentation
   Title: Type 2 diabetes *mellitus* promotes early neurometabolic alterations: *in vivo* evaluation by magnetic resonance in animal models
   Status: Presented

2. **Congress:** 56th European Society for Clinical Investigation (ESCI) Annual Scientific Meeting
   Held in: Bari, Italy
   Date: 8th-10th June 2022
   Communication format: Oral Presentation
   Title: Type 2 diabetes *mellitus* promotes early neurometabolic alterations: *in vivo* evaluation by magnetic resonance in animal models
   Status: Presented

3. **Congress:** 58th European Association for the Study of Diabetes (EASD) Annual Meeting
   Held in: Stockholm, Sweden
   Date: 19th-23rd September 2022
   Communication format: Short Oral Presentation
   Title: Neurometabolic changes in the hippocampus of type 2 diabetic rats: an imaging perspective towards clinical applications
   Status: Accepted, but not yet presented

Scientific publications:

1. **Title:** A HERMES sequence revealed a compensatory mechanism mediated by NAAG and GSH in response to obesogenic conditions
   Type: Research article
   Status: In preparation
2. **Title:** Let's Take a Look: Early diagnosis of metabolic and vascular diabetic complications in brain and heart through state-of-the-art imaging
   Type: Narrative review
   Status: In preparation

Financing:

1. European Foundation for the Study of Diabetes (EFSD)

List of abbreviations (in order of appearance in the manuscript):

T2DM: Type 2 diabetes *mellitus*

WHO: World Health Organization

AT: Adipose tissue

IR: Insulin resistance

AGE: Advanced Glycation End Products

BBB: Blood-brain barrier

Glu: Glutamate

CNS: Central Nervous System

Gln: Glutamine

Cys: Cysteine

SNAT: Sodium-coupled neutral amino acid transporters

EAAT: Excitatory amino acid transporters

Glut. C: Glutaminase C

α-KG: Alpha-ketoglutarate

GDH: Glutamate dehydrogenase

Asp: Aspartate

AST: Aspartate aminotransferase

Ala: Alanine

ALT: Alanine aminotransferase

vGLUT: Vesicular glutamate transporters

ATP: Adenosine triphosphate

NMDAR: N-methyl-D-aspartate receptor

AMPAR: Alpha-amino-3-hydroxy-5-methyl-4-isoxazolepropionic acid receptor

PSD-95: Postsynaptic density protein 95

GS: Glutamine synthetase

GABA: Gamma-aminobutyric acid

GABA-T: Gamma-aminobutyric acid transaminase

SSADH: Succinic semialdehyde dehydrogenase

GAD: Glutamic acid decarboxylase

vGAT: Vesicular gamma-aminobutyric acid transporter

$GABA_AR$: Gamma-aminobutyric acid type A receptor

GAT: Gamma-aminobutyric acid transporter

NIH: National Institutes of Health

CT: Computed tomography

MRI: Magnetic Resonance Imaging

PET: Positron Emission Tomography

SPECT: Single photon emission computed tomography

VAT: Visceral adipose tissue

SAT: Subcutaneous adipose tissue

SOCS3: Suppressor of cytokine signalling 3

GM: Grey matter

WM: White matter

DTI: Diffusion tensor imaging

CB_1R: Cannabinoid type 1 receptor

D2R: Dopamine type 2 receptor

SERT: Serotonin transporter

5-HT_4: Serotonin

BOLD: Blood oxygen level-dependent

CBF: Cerebral blood flow

IRS: Insulin receptor substrate

GSK3β: Glycogen synthase kinase beta 3

ROS: Reactive oxygen species

RNS: Reactive nitrogen species

MCI: Mild cognitive impairment

DKI: Diffusion kurtosis imaging

MRS: Magnetic resonance spectroscopy

NAA: N-acetylaspartate

^{18}F-FDG: ^{18}F-fluorodeoxyglucose

GK: Goto-Kakizaki

^{1}H-MRS: Proton magnetic resonance spectroscopy

Cho: Choline

fMRI: Functional magnetic resonance imaging

NO: Nitric oxide

DMN: Default mode network

HFD: High-fat diet

HERMES: Hadamard Encoding and Reconstruction of MEGA-Edited Spectroscopy

GSH: Glutathione

ELISA: Enzyme-linked immunosorbent assay

Glo-1: Glyoxalase-1

HO-1: Heme oxygenase 1

Nitrotyr: Nitrotyrosine

p-IR: Phosphorylated insulin receptor

GLUT3: Glucose transporter 3

ArgPyr: Argpyrimidine

MG-H1: Nδ-(5-hydro-5-methyl-4-imidazolon-2-yl)ornithine

APP: Amyloid precursor protein

IR-T: Total insulin receptor

p-GSK3β: Phosphorylated glycogen synthase kinase beta 3

SD: Standard diet

STZ: Streptozotocin

ITT: Insulin tolerance test

AUC: Area under curve

Tris-HCl: Tris-hydrochloride

NaCl: Sodium chloride

EDTA: Ethylenediaminetetraacetic acid

EGTA: Ethylene glycol-bis(2-aminoethylether)-N, N, N', N'-tetraacetic acid

NaF: Sodium fluoride

$NaVO_3$: Sodium metavanadate

PMSF: Phenylmethylsulfonyl fluoride

rpm: Rotations per minute

BSA: Bovine serum albumin

SDS: Sodium dodecyl sulphate

APS: Ammonium persulfate

TEMED: N-tetramethylethylenediamine

PVDF: Polyvinylidene difluoride

CAPS: 3-(Cyclohexylamino)-1-propanesulfonic acid

NaOH: Sodium hydroxide

TBS: Tris-buffered saline

ECL: Enhanced chemiluminescence

IHC: Immunohistochemistry

PBS: Phosphate-buffer saline

DHE: Dihydroethidium

DAPI: 4',6-diamidino-2-phenylindole

SEM: Standard error of the mean

ANOVA: Analysis of variance

MG: Methylglyoxal

NAAG: N-acetylaspartylglutamic acid

NAA: N-acetylaspartate

%SD: Estimated standard deviations

CV: Coefficient of variance

MEGA-PRESS: Mescher–Garwood Point Resolved Spectroscopy

mGluR3: Metabotropic glutamate receptor 3

TGF-β: Transforming growth factor β

List of figures:

List of tables:

Introduction

1. Obesity and type 2 diabetes: the new pandemic of the 21st century?

Although genetic factors contribute to the development of both obesity and type 2 diabetes *mellitus* (T2DM), the pronounced sedentary lifestyle of worldwide population in the 21st century is a greater factor for the development of these metabolic diseases. Among the convenience of fat and sugar-enriched fast food and diminished physical activity, the poorer lifestyle of today's population has compromised their quality of life, while also being reported as a death risk factor[1]. The latter incidence is supported by the exponentially increasing incidence over the years, which has tripled since 1975, according to the World Health Organization (WHO). In fact, in 2016, 1.9 billion (39%) adults were considered overweight, among which 650 million were obese. Such corresponds to 13% of the entire world population, which is an alarming number. The obesity phenotype enhances the risk for the onset of T2DM, given that a dysfunctional adipose tissue (AT), meaning a exacerbated lipid accumulation is present, promotes insulin resistance (IR) through inflammatory responses and lipotoxicity[2]. Thus, the latter has similarly and dramatically worsened. In fact, in 2021, 537 million patients lived with this diagnosis.

While obesity is associated with cellular leptin resistance[3], T2DM is characterized by IR[4]. Hence, although there are some overlapping hallmarks, these metabolic phenotypes result in and from different physiological and cellular outcomes. Leptin, an AT-produced protein, is related to inflammation, lipolysis, angiogenesis and brain-related appetite control. Therefore, once leptin resistance occurs, food intake and energy expenditure are unregulated[5], leading to a greater lipid accumulation namely in organs with a higher expression of leptin receptor, which includes the AT, liver and heart[3]. Hence, most of obesity-related diseases reflect this increased steatosis, including non-alcoholic fatty liver disease and muscular/ cardiac steatosis, being all a risk factor for insulin resistance and T2DM. The IR-characterized pathology compromises the glucose metabolism and homeostasis. Given that insulin is involved in cellular anabolism and storage mechanisms, glucose's entrance into the cells is compromised, thus culminating in hyperglycemia[6]. The latter induces, among others, mitochondrial dysfunction and

energy deficit, oxidative stress, advanced glycation end products (AGE) production and inflammation[4]. All of which promote the onset of various diabetic complications, including nephropathy, cardiovascular diseases and atherosclerosis and neurological comorbidities, both at vascular and metabolic levels.

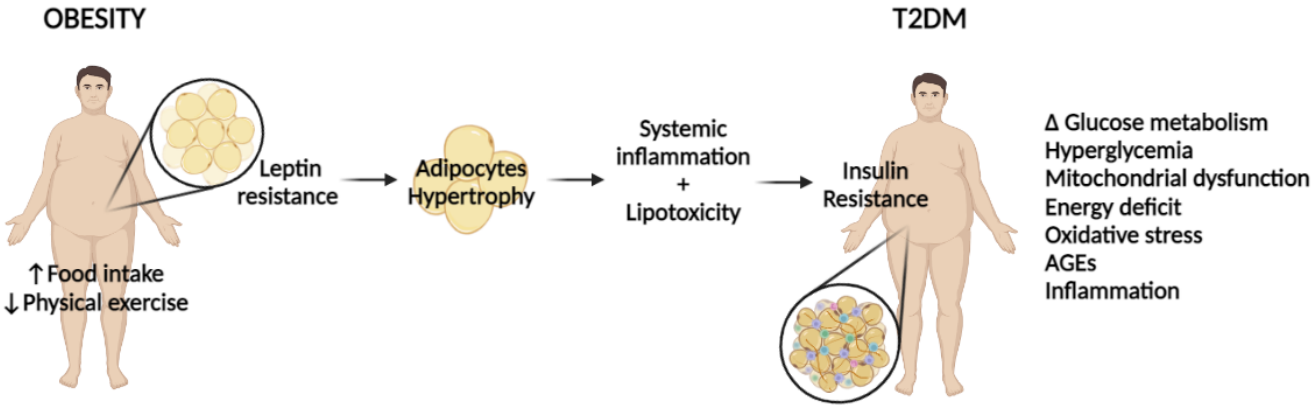

Figure 1. The progression from obesity to T2DM.

The excessive food intake and minimal physical exercise typically observed in the population of the 21st century potentiates leptin resistance. In turn, given its role appetite control and lipidic homeostasis, the latter promotes an intensified lipid accumulation (hypertrophy) in organs with a greater expression of the leptin receptor which includes the adipose tissue. Ultimately, it culminates in lipotoxicity and inflammation, which are known to induce insulin resistance. This main T2DM hallmark promotes others, including hyperglycemia, altered glucose metabolism, oxidative stress and inflammation. Image created with Biorender.com.

2. The glutamatergic synapse: synthesis and activity

The blood-brain barrier (BBB) is a vast capillary network surrounding the entire brain, which allows for a selective entrance of molecules into this organ and is, in turn, surrounded by a layer of astrocytes. This primary resistance is achieved by the endothelial cells of the capillaries which are composed of the luminal (blood facing) and abluminal (brain facing) membranes. However, they provide different permeability to distinct molecules. Glutamate (Glu) is the main excitatory neurotransmitter in the mammalian central nervous system (CNS). Regarding Glu and glutamine (Gln), the luminal membrane allows an overall bidirectional facilitative transport (sodium-independent mechanism) from the bloodstream into the endothelial cell. While Glu is

transported by the system X_C^- at the expense of cysteine (Cys), the uptake of Gln is promoted by the system n and system L. Given the non-energy-potentiated transport mechanisms, a large concentration of these amino acids passes from the bloodstream to the endothelial cells. However, to a lower extent, Gln can also be transported through the luminal membrane by the sodium-coupled neutral amino acid transporter 3 (SNAT3), unidirectionally. Likewise, through the abluminal membrane, 80% of Gln transport is accomplished by the system L, while 20% is promoted by SNAT3. The preferentially facilitative transport is enabled since Gln has been shown to be present in the extracellular space in concentrations equivalent to the ones in the bloodstream. This effect is highly valuable given it not only (1) allows a constant substrate pool for the synthesis of Glu, but it also (2) supresses the neurotoxic ammonium accumulation which could arise from the constant conversion of Gln into Glu which involves a deamination process. However, Glu passage through the abluminal membrane is, exclusively, an energy-consuming process accomplished by sodium-dependent glutamate transporters: 1, 2 and 3 (excitatory amino acid transporters, EAAT). This mechanism enables the tight control of the Glu levels in the extracellular space in comparison to the bloodstream, thus avoiding excitotoxicity, a highly deleterious event. Considering the compensatory mechanisms mentioned above, it is perceptible the differential concentrations of Glu and Gln in the extracellular space. It is also worth considering the speed of action potential propagation. Therefore, the greater Gln levels allow these to be readily taken up and used by neurons upon an excitatory stimulus, while supressing potentially toxic events (Reviewed by Zaragozá *et al. 2020* and Hawkins *et al. 2009*)[7,8]. Such is further supported by the inability to uptake Glu present in neurons.

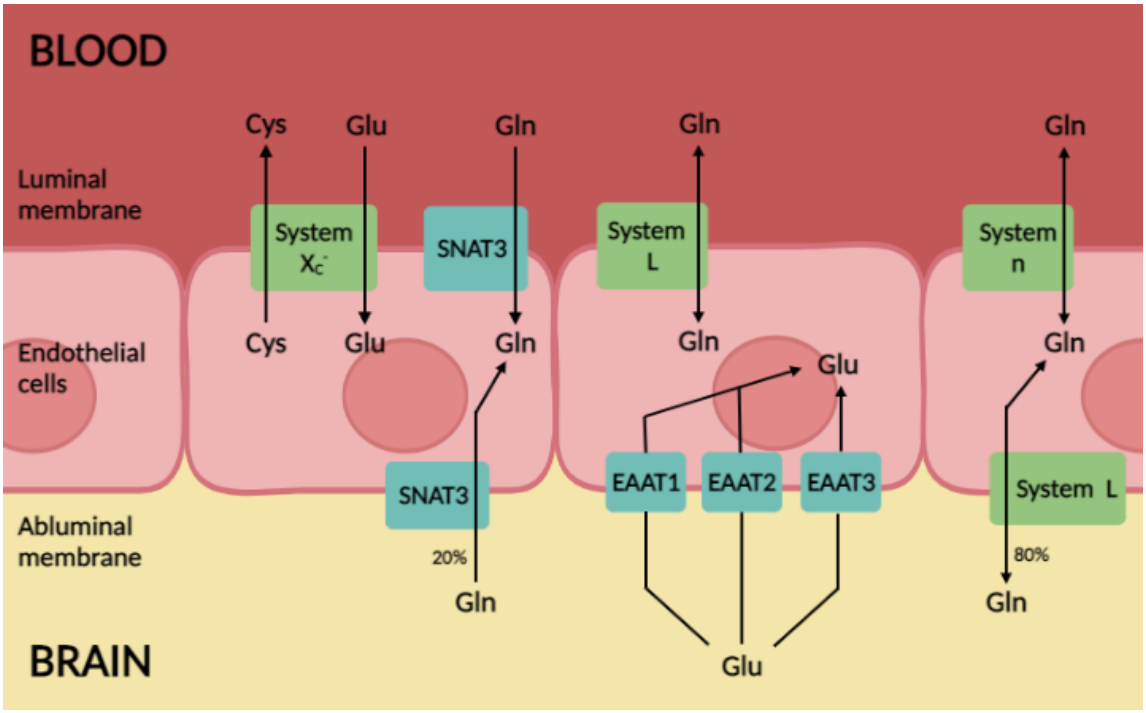

Figure 2. Glutamate and glutamine transport through the BBB.

Differential transport is observed for Gln and Glu. Gln, being the only amino acid present in a similar concentration in the brain and blood, presents an overall (80%) facilitative transport (represented in green) in both the luminal and abluminal membrane, including the system L and system n. Nevertheless, 20% of Gln transport is potentiated by an active form of transport (represented in blue), ie sodium-dependent, enabled by the SNAT3 in both membranes. Regarding Glu, the transport is more tightly regulated. In the luminal membrane, the excitatory neurotransmitter is transported by the system X_C^- at the expense of Cys uptake into the blood. In contrast, in the abluminal membrane, only active transport is observed through 3 different isoforms of EAAT: 1, 2 and 3. Image created with Biorender.com.

Glu is predominantly formed through the deamination of Gln, in a process catalysed by the enzyme glutaminase C (Glut. C)[9]. Nevertheless, Glu can also be formed through several other metabolic pathways. Firstly, the glucose-derived α-ketoglutarate (α-KG) is transformed into Glu, resorting to Glu dehydrogenase (GDH), while simultaneously converting glucose-generated oxaloacetate into aspartate (Asp) through a process mediated by aspartate aminotransferase (AST). Conversely, instead of its conversion into Asp, the enzyme GDH may function with the transformation of alanine (Ala) into pyruvate, which is mediated by alanine aminotransferase (ALT). Biochemically, both

metabolic reactions occur concomitantly, given their low thermodynamic equilibrium constant[10]. It is, therefore, easy to comprehend how the glutamatergic synapse is estimated to consume 80% of the entire brain energy expenditure.

Once the excitatory neurotransmitter is formed, it is stored in vesicles which is facilitated by vesicular glutamate transporters (vGLUT) through an adenosine triphosphate (ATP)-mediated process, which assures its neurotransmitter activity over the metabolic function[11]. Then, these get accumulated in the presynaptic terminal ready for their release. Once a given excitatory stimulus occurs, Glu is induced to be released from the presynaptic terminal. Simultaneously, the excitatory N-methyl-D-aspartate (NMDAR) and α-amino-3-hydroxy-5-methyl-4-isoxazolepropionic acid receptors (AMPAR) are translocated to the postsynaptic membrane, where these are anchored by several scaffolding proteins, including postsynaptic density protein 95 (PSD-95)[12]. Consequently, an excitatory response and action potential is propagated. Given the lack of Glu transporters in neurons, upon the end of the stimulus, Glu is taken up by astrocytes, namely through EEAT1/2. Once in the astrocytes, Glu is transformed into Gln as mentioned previously. The latter amino acid can now be released through SNAT3/5. In turn, Gln is actively transported into the astrocytes transported into neurons through SNAT1/2, where it is converted into Glu by the enzyme Gln synthetase (GS)[13], which can be taken up by neuron afterwards and the cycle restarts (Reviewed by Andersen *et al. 2021*)[14].

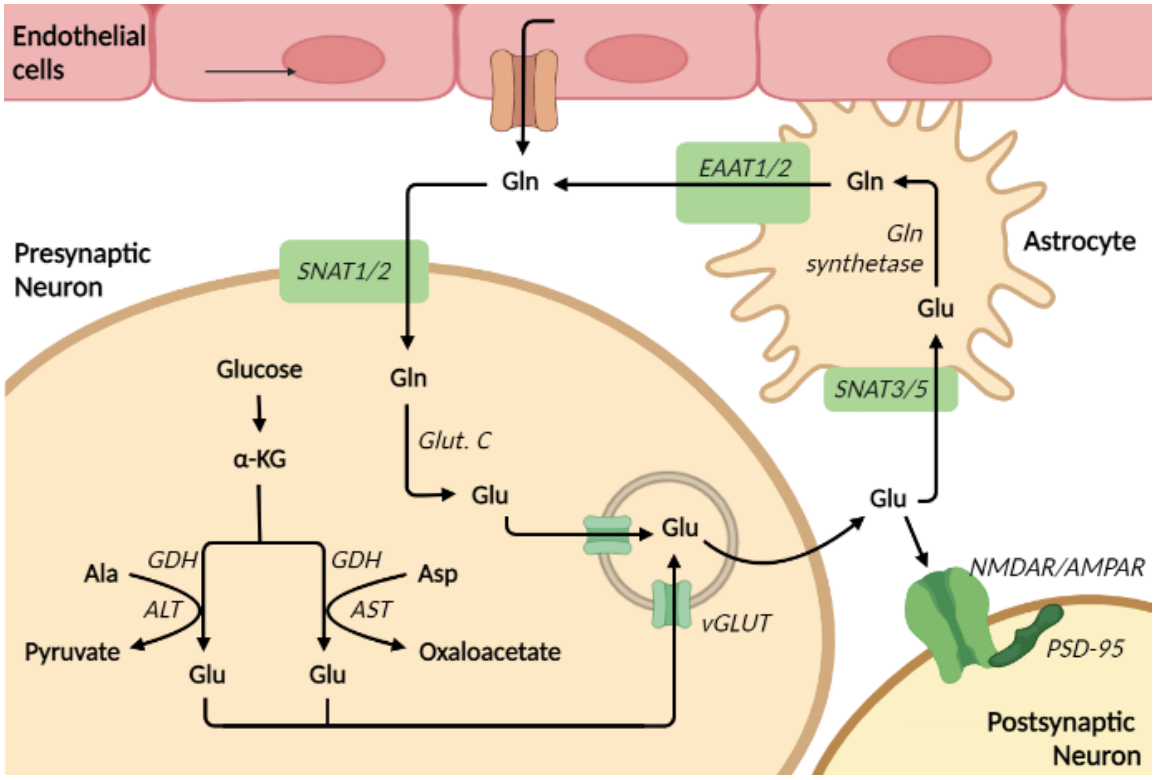

Figure 3. Glutamate synthesis and synaptic activity

Glu is mainly formed by the conversion of Gln through a reaction catalysed by Glut. C. Moreover, glucose, through the Krebs cycle, promotes the formation of α-KG. In turn, through a reaction mediated by GDH, the latter is converted into glutamate. However, this reaction can only occur in case one of these reactions occurs simultaneously: (1) Ala transformed into pyruvate by ALT; or (2) Asp converted into oxaloacetate which is mediated by AST. Following, Glu is incorporated in vesicles through vGLUTs. Once a stimulus occurs, the vesicle-located Glu is released into the synaptic cleft, where it activates glutamatergic receptors (NMDAR and AMPAR) anchored by PSD-95. Upon the stimulus ceasing, Glu is taken up by astrocytes through SNAT3/5. In this cells, Glu is transformed into Gln by the enzyme Gln synthetase, which is followed by the release of the latter metabolite through EAAT1/2. Finally, Gln is taken up by SNAT 1/2 into neurons, where the cycle is repeated. Image created with Biorender.com.

3. The GABAergic synapse: synthesis and activity

Gamma-aminobutyric acid (GABA) is the main inhibitory neurotransmitter of the mammalian CNS. This molecule is mainly formed by a metabolic pathway named the "GABA shunt". Firstly, in the mitochondria, α-KG undergoes a transamination process

catalysed by the enzyme GABA transaminase (GABA-T), which produces Glu. However, the previous reaction occurs at the expense of a GABA molecule, which transfers an amino group to α-KG. As a result of the deamination, the GABA molecule gives rise to succinic semialdehyde, which is, in turn, metabolized by succinic semialdehyde dehydrogenase (SSADH), forms succinic acid, an intermediary of the Krebs cycle. Then, Glu is released into the cytosol, where it forms GABA through the enzyme glutamic acid decarboxylase (GAD) (Reviewed by Roth and Draguhn)[15]. These enzymes, especially the isoform GAD65 in comparison to GAD67, are usually bound to small vesicles, to guarantee their rapid uptake through ATP-dependent vesicular GABA transporters (vGAT)[16]. These vesicles, similar to the glutamatergic ones, are concentrated in the active zone present near the plasma membrane, thereby enabling their prompt fusion and content release upon a stimulus. Meanwhile, in the postsynaptic neuron, the GABA receptors are translocated into the membrane, namely the most expressed isoform GABA type A receptor ($GABA_AR$). At the synapse, these tend to cluster and interact with intracellular proteins, namely gephyrin, which anchors these receptors, while stabilizing these by binding to the cytoskeleton[17].

In contrast to the excitatory neurotransmitter, once the stimulus ceases, GABA can undergo two different pathways: (1) it can be taken up by the presynaptic terminal through the GABA transporter (GAT) 1, where it is accumulated in vesicles and hence recycled for novel usage[18]; or (2) it can be taken up by astrocytes-located GAT-3 [19]. The latter cells lack GAD, which hampers GABA formation in these. It has, however, GABA transaminase. Thereby, the captured inhibitory neurotransmitters are metabolized into succinic semialdehyde through the transfer of an amino group to α-KG. Simultaneously, this Krebs cycle's intermediary is converted into Glu by the same enzyme, which, in turn, is converted into Gln by the action of glutamine synthetase. This amino acid can now be taken up by the nerve terminal, in which Glu is produced and converted into GABA again (Reviewed by Schousboe *et al. 2013*)[10].

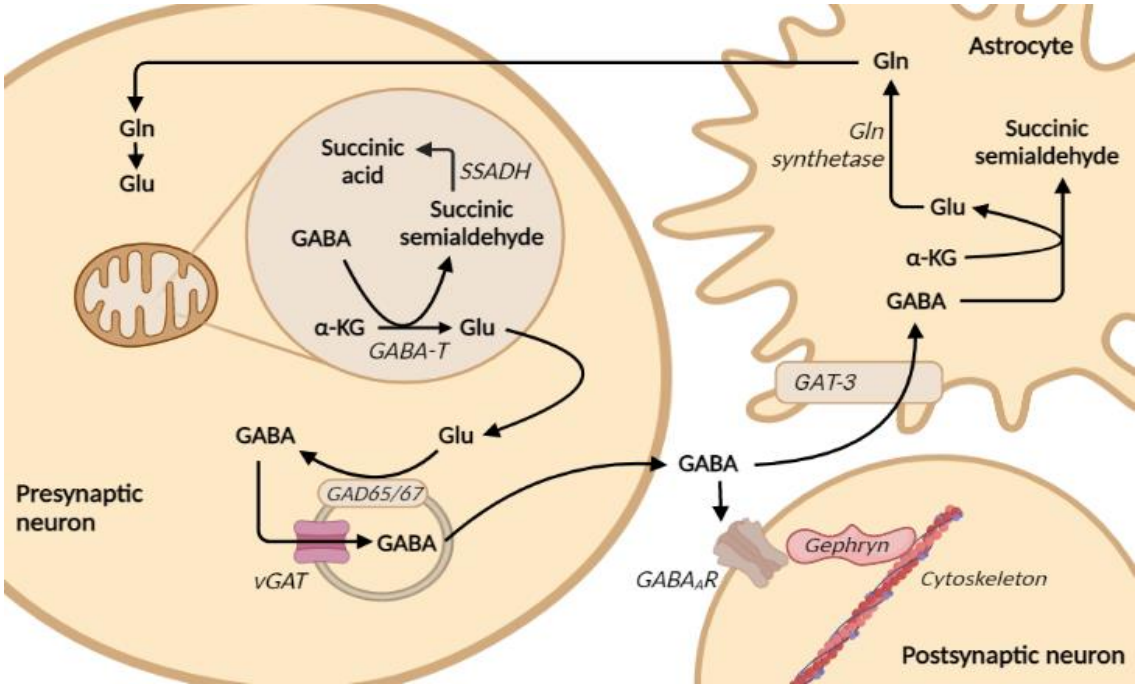

Figure 4. GABA synthesis and synaptic activity.

In the mitochondria, α-KG is converted into Glu through the action of GABA-T, at the expense of a GABA molecule which is, in turn, transformed into succinic semialdehyde. The latter is then converted into succinic acid in a reaction catalysed by SSADH. Following, the formed Glu is translocated into the cytosol where it is transformed in GABA through the small vesicle-located GAD65/67. Such facilitates its transport into these vesicles through vGAT. Upon a stimulus, GABA is released into the synaptic cleft where it will activate GABA receptor, namely type A which is anchored to the cytoskeleton by gephyrin. Once the stimulus ceases, GABA enters the astrocytes through GAT-3, where, through the same mechanisms observed in the neuronal mitochondria, GABA is transformed into α-KG, succinic semialdehyde and Glu. Later, Glu is converted into Gln by the Gln synthetase. The latter amino acid is then released into the synaptic cleft and taken up by neurons, where it is transformed into Glu and the cycle restarts. Image created with Biorender.com.

4. Let's take a look: Early Diagnosis of Neurological Complications Through State-of-the-art Imaging

Little are the biochemical biomarkers assessed in blood samples that predict or diagnose neurological alterations. Therefore, in the clinic, imaging markers are resorted routinely to identify these comorbidities. According to the National Institutes of Health

(NIH), the most common imaging techniques used to detect neurological complications are: computed tomography (CT), magnetic resonance imaging (MRI), positron emission tomography (PET) and single photon emission computed tomography (SPECT). While CT and MRI enable the indirect observation of blood vessels and brain tissue, SPECT and PET allow the *in vivo* assessment of the brain function in real time. However, the latter are extremely expensive and are not present in every hospital, hence not being in the first line of diagnosis. On the other hand, MRI and CT only allow structural alterations, which are often already in an irreversible status. There is, therefore, an urgency to identify novel early imaging and functional biomarkers for neurological comorbidities.

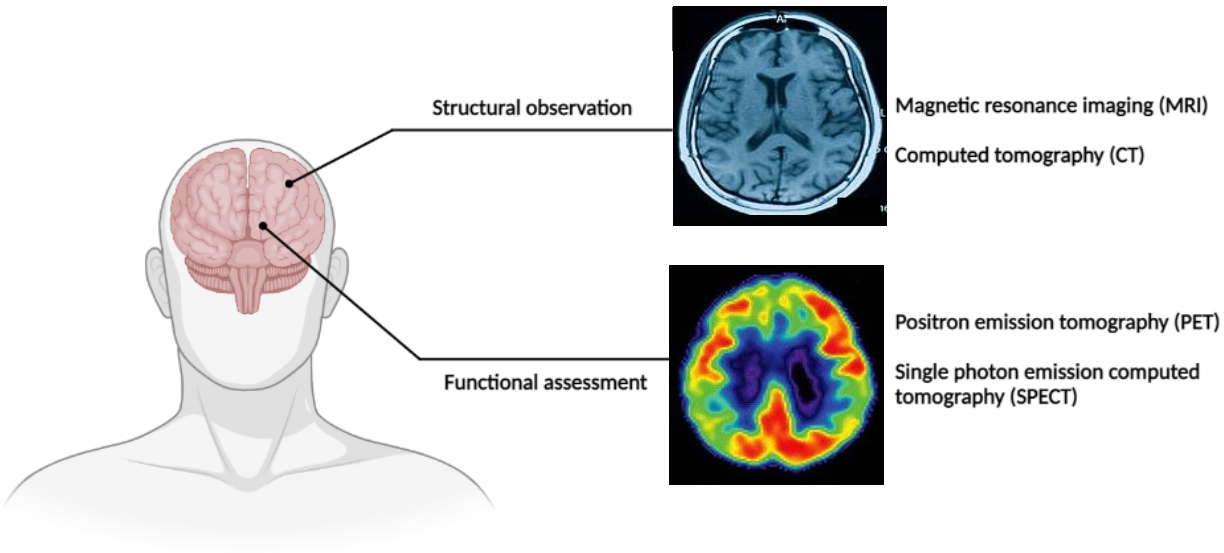

Figure 5. Neurological complications and the clinically-used imaging techniques.

The monitoring and diagnosis of neurological complications is accomplished through 2 main factors: (1) structural observation enabled though MRI and CT; and (2) assessment of cerebral function evaluated by PET and SPECT. Image created with Biorender.com.

a. Imaging of obesity's impact in the brain

i. Relation of obesity with brain's morphological and structural modifications

Leptin is mainly produced by visceral adipose tissue (VAT) in rodents and by subcutaneous adipose tissue (SAT) in humans[20]. Hyperleptinemia promotes the activation of the suppressor of cytokine signalling 3 (SOCS3), which, in turn, induces leptin resistance, which also causes, among others, insulin resistance (Review by Li *et al. 2020*)[21] and hinder Akt function, a protein involved in cellular apoptosis[22]. Accordingly, in obese subjects, Karlsson *et al.* demonstrated that an augmented SAT, possibly due to leptin resistance, is associated with grey matter (GM) atrophy, but not white matter (WM)[23]. In contrast, in the same population, hypertrophy was observed in the thalamus and amygdala[24], which are both believed to be involved in anxiety[25], as well as in the left putamen, an area involved in reward and addiction[26]. Also, the right orbitofrontal and prefrontal cortex areas, both of which are decision-making regions, were diminished, which, when damaged, promotes impulsivity[26,27]. Taken together, these alterations might culminate in an excessive food intake, which, given the anxiety-like feelings, might become an event commonly named "emotional binge eating" , in which an individual uses food as a copying mechanism instead of satiety fulfilling. As a consequence of overeating, a greater lipidic accumulation in the AT, namely in VAT, is induced and, consequently, systemic inflammation is promoted, creating a vicious circle between obesity, impulsivity, binge eating and systemic and brain inflammation[23].

WM is mainly composed of axons which enable signal transmission between distinct brain regions, spinal cord and peripheral nervous system. In order to facilitate the propagation of the action potential, axons are enriched in capillaries-veined lipidic myelin. AT-induced neuroinflammation[27] and hyperglycemia[28,29] induce endothelial dysfunction. In fact, dysfunctional cerebral blood flow has been associated with a hindered myelin content[30,31]. Concurrently, through diffusion tensor imaging (DTI) experiments have shown a reduced myelin content and consequent diminished WM integrity in the fornix, internal capsule, corona radiata and corpus callosum in overweight subjects[31,32]. Since these connect limbic regions, the reward system and

appetite are hindered, which promote a greater food intake and further worsening the obesity phenotype[23,33].

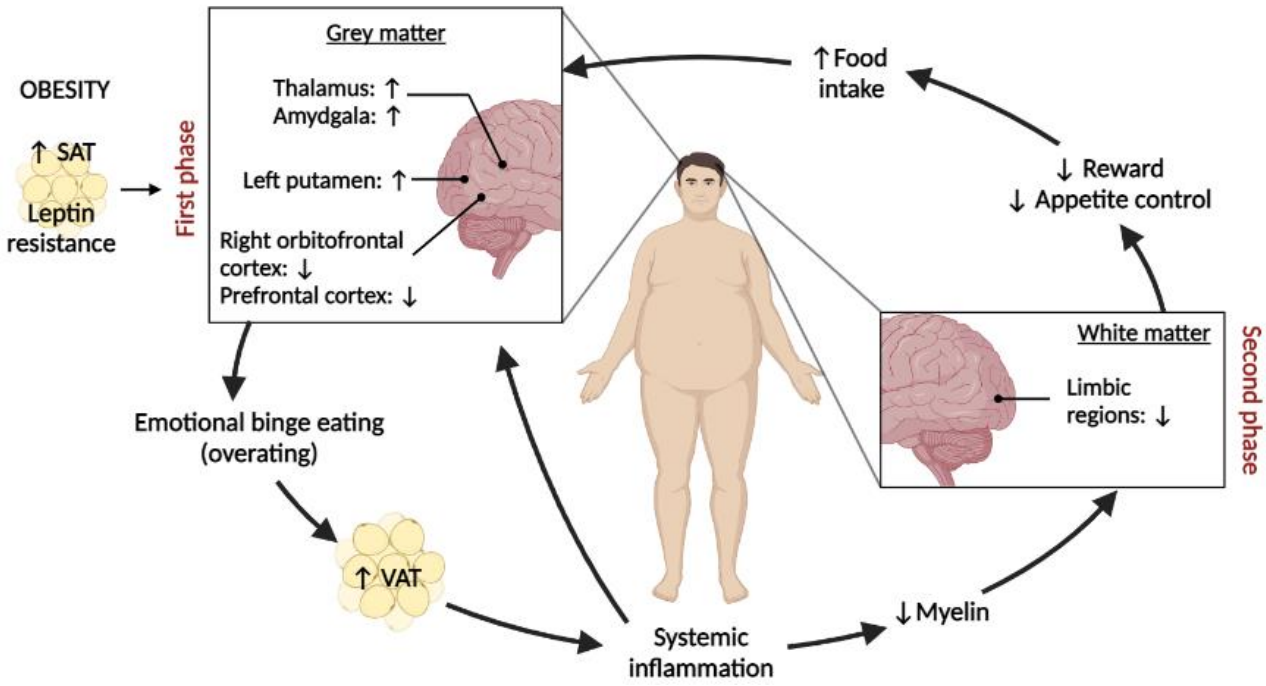

Figure 6. Obesity and its cerebral structural alterations.

In the early stage of obesity, an hypertrophic SAT and leptin resistance is developed which have been shown to be related with GM modifications, but not with the WM. The alterations in these brain regions are predominantly located in the thalamus, amygdala and left putamen, all of which are hypertrophic (signalled by ↑) in these conditions, while the right orbitofrontal and prefrontal cortices suffered atrophy (identified with ↓). Altogether, these variations in volumes culminate in "emotional binge eating", which ultimately leads to overeating. In turn, a greater lipidic accumulation in the VAT is noted and inflammation is potentiated, which affects both GM and WM. The inflammatory reaction reduces myelin content, compromising the cellular viability of limbic regions, leading to an hampered reward and appetite control system. Consequently, food intake is potentiated, further aggravating the previous comorbidities in a cycle. Image created with Biorender.com.

ii. Obesity and neurometabolic alterations

Obesity and the associated visceral adiposity are postulated to promote cerebral inflammation[34,35], which might compromise brain areas involved in reward and appetite. Among the affected areas, the hypothalamus compromises satiety; the orbitofrontal cortex, a decision-making region, may impact food selection; and the amygdala[36]. In the hypothalamus of obese subjects, the inflammation and associated activated glial cells promote neuronal damage as assessed though DTI[37,38].

Leptin has been shown to negatively regulate food intake through hypothalamic endocannabinoids' modulation in cannabinoid receptor type 1 (CB_1R)-knockout mice[39]. Given that obesity presents an impaired sensitivity to this hormone, a decreased expression of μ-opioid receptors and CB_1R expression occurs, as identified with [^{11}C]-carfentanil and [^{18}F]-FMPEP-d_2 in PET[40]. Consequently, these patients tended to overeat and further worsen their obese status, suggesting a loss of sensitivity of nutrient-sensing mechanisms[41]. Accordingly, a diminished activation of this food reward system in chronically obese men occurs in response to the consumption of a given meal, which is partially recovered in patients undergoing a weight-loss program. These differences were mostly observed in the temporal and frontal cortices, brain areas that are involved in emotional and decision-making responses, respectively[42]. Such suggests this mechanism may also contribute to "emotional eating", further contributing to an obese phenotype. The greater difficulty to satisfy their satiety is further worsened by the leptin-induced diminished dopamine type 2 receptor (D2R) in the ventral tegmental area of obese women, as assessed through PET scans with the radioligand [^{18}F]-fallypride[43]. In fact, the dopaminergic and opioid systems have been postulated to interact[44]. In non-obese patients, GABAergic neurons inhibit dopamine release and synaptic activity, inducing hunger. Normally, upon a meal, μ-opioid receptors, which are localized in GABAergic neurons, hamper this inhibitory activity. In turn, dopaminergic synaptic activity is ameliorated, promoting satiety. However, the opioid receptors inhibit this signal, which culminates in dopamine release in the nucleus accumbens, a brain region involved in the reward system[45]. Taken this together, we can hypothesize that, in an obese phenotype, the lower endocannabinoids' expression hinders dopamine

release and consequently impairs the reward system. Such might further compromise satiety.

Likewise, through the resorting of PET and the radioligand [^{11}C]DASB, impaired cerebral serotonin transporter (SERT) binding observed in an obese cohort and consequent feelings of anxiety and depression may aggravate this phenomenon of "emotional eating" [46]. However, studies concerning obesity and serotoninergic system provide contradictory data. Through PET scans using the tracer [^{11}C]SB207145, obese patients presented high levels of serotonin (5-HT$_4$) receptor in reward-involving brain areas, including the nucleus accumbens and left hippocampus. On the left hippocampus, the higher serotoninergic activity might not only be involved in the pleasurable sensation of food[47], but also, given this is a brain region involved in memory and learning functions, the enhanced activity might evoke appetite responses when exposed to given environmental stimuli. In contrast, the enhanced activity in the nucleus accumbens would suggest an impairment of food intake, which goes against clinical observations[48].

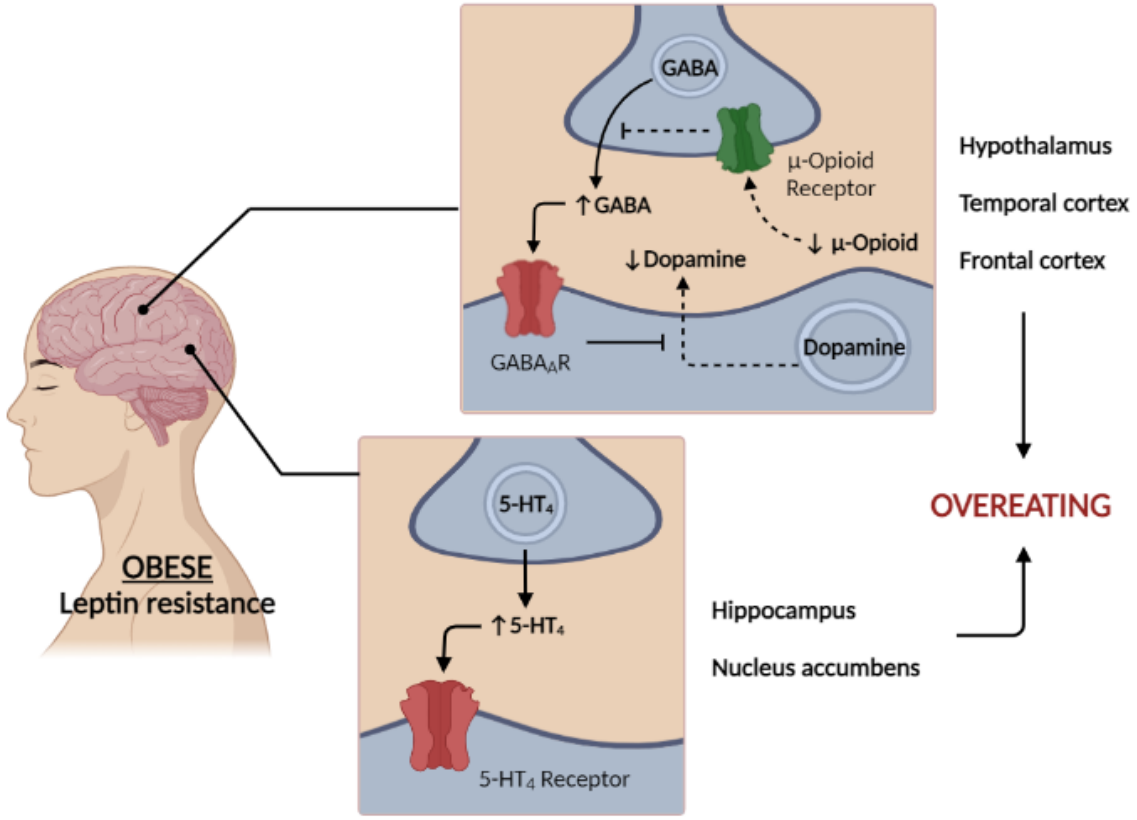

Figure 7. Obesity and its cerebral neurometabolic alterations.

The lost sensitivity to leptin observed in obesity potentiates a decreased μ-opioid receptor-mediated synaptic activity (identified with ↓). The hampered effect intensifies the inhibitory activity of the GABAergic synapse (represented with ↑), which, in turn, weakens dopamine release in the hypothalamus (reward system), temporal (emotion regulation) and frontal (decision-making) cortices. Taken together, these alterations culminate in overeating. The latter is further potentiated by increased levels of 5-HT$_4$ in the hippocampus (memory) and nucleus accumbens (reward system). Weakened activities are represented by dashed arrows, while the ameliorated activities are symbolized by continuous arrows. Image created with Biorender.com.

iii. Obesity, vascular modifications and dementia

Metabolically, in obesogenic phenotypes, the brain encodes eating as an addiction, in comparison to an energy gain event. In concordance, in patients with obesity, insulin-induced hemodynamic response in the hypothalamus is reduced, as measured by fMRI-obtained blood oxygen level-dependent (BOLD) measurements. It is

inversely correlated with visceral adiposity, suggesting that cerebral insulin resistance and metabolically unfavourable adiposity are linked[49].

Physiological shift from normoglycaemia to hyperglycaemia seems to modulate the brain response to food stimulus. Prior to a highly desirable meal during a fasting state, high blood glucose promoted an hyperresponsivity between the ventral anterior insula and putamen in obese subjects[50,51] and experienced an adiposity-induced greater neural response to the sensory stimulation in the insular cortex[52]. Given that the insula is primarily involved in sensorial processing and the putamen constitutes part of the reward system, these might contribute to the predisposition and desire for foods with a given odour and flavour, namely high-caloric food[50]. Likewise, the medial hypothalamus network activity (ventral striatum, orbitofrontal cortex and occipital gyrus) is increased in obese individuals[53–55]. While the orbitofrontal cortex is involved in decision making in reward-related behaviours, the occipital cortex is involved in visual processing. Thus, other than smell and flavour, food-potentiated vision stimulation can activate the reward system, which has been associated with a lower D2R availability and consequent hyperstimulated eating. Altogether, this effect is alluded to be an independent response to hunger and peripheral signals regarding the energy storage of the body[56–58].

Similarly, an augmented cerebral blood flow (CBF) between the ventral striatum (ie nucleus accumbens), prefrontal and parietal cortices as a result of a decreased peripheral insulin sensitivity. Given that this network connects the reward system (ventral striatum), impulsivity control-related region (prefrontal cortex) and sensorial system (parietal cortex), it is suggested that food satiety relies more in sensorial stimulus and hedonic feeding in obese patients, in comparison to normal weight patients[49,59]. In fact, Avery *et al.*, 2019 have demonstrated that patients with obesity experienced an enhanced connectivity between the insula and the dorsal striatum, a hedonism-related brain area, between fasted and fed scans, in contrast to healthy weight individuals in proportion to the meal pleasantness[54]. The D2R shift from the ventral to the dorsal striatum occurs with the hedonic response to food in obesity, similarly to what occurs with the development of substance addiction. It is, hence, suggestive that overeating may result from an addiction to high-caloric food[60]. An increased desire for high-caloric food has also been correlated with a reduced connectivity of anterior cingular cortex

and an enhanced insula connectivity in obese patients. Such alludes that these subjects require more caloric food to satisfy their food desires and feel satiated[61]. Taken together, it seems that, in healthy subjects, the feeding process is an energy gain-potentiated event; in obese patients, hunger might be perceived as a reward-absent feeling. In contrast, in a postprandial state, under food stimuli, an enhanced connectivity between the caudate (reward) and amygdala (emotional salience) is observed in obese subjects. This alludes to a heightened reward response only after a meal consumption and not during, which may induce overeating[62].

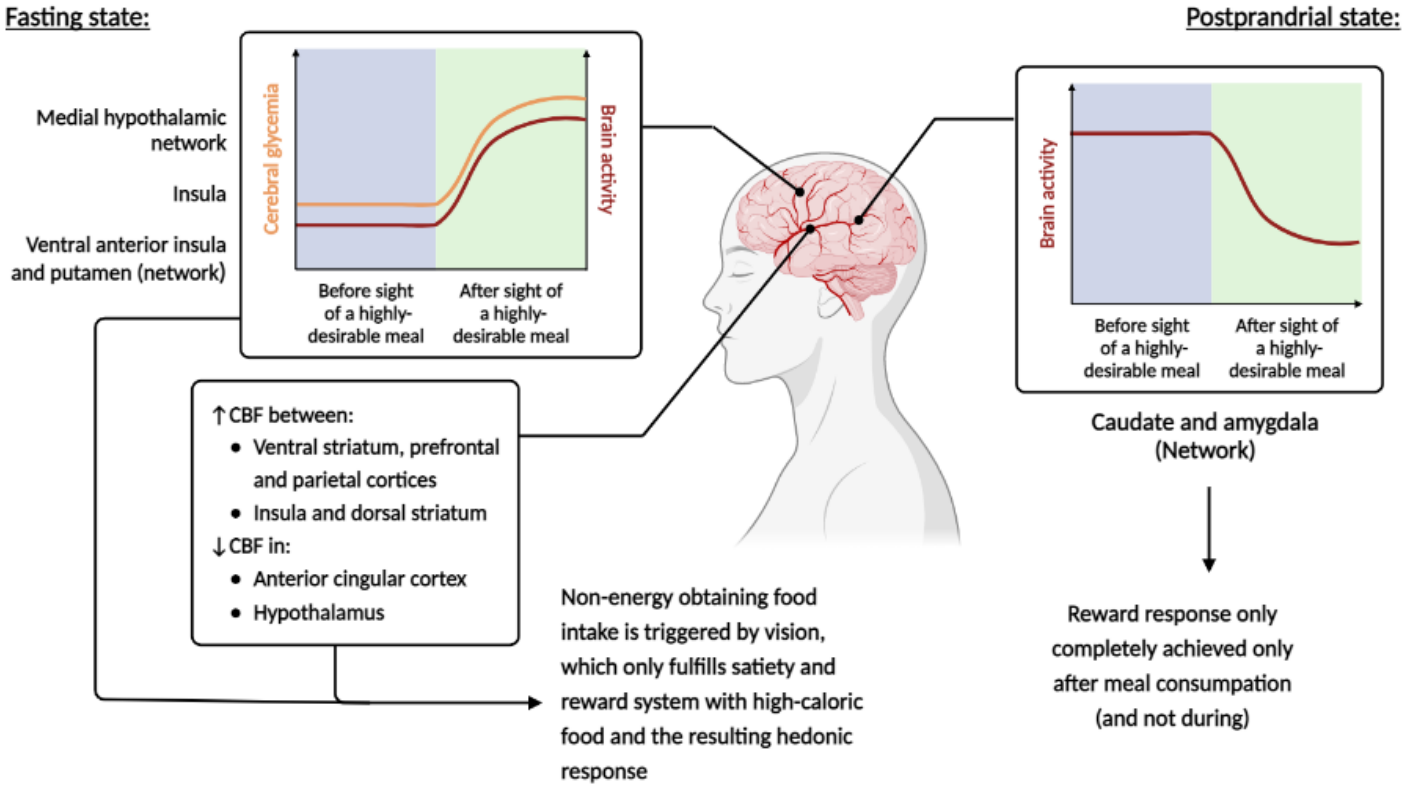

Figure 8. Obesity and its cerebral vascular alterations.

Upon a high-caloric meal-mediated stimulus, during a fasting state, visual stimulation (occipital gyrus, parietal cortex and insula) induced hyperactivity of the interconnected reward-involving (putamen, ventral and dorsal striatum) and decision-making brain regions (orbitofrontal, anterior cingular and prefrontal cortex), suggesting a stronger reward response (identified with ↑) with high-caloric food. Meanwhile, after meal consumption, an enhanced cerebral activity between caudate (reward) and amygdala (emotional salience) was observed in obesity, proposing that a reward response only occurs in a fed state. Image created with Biorender.com.

b. Imaging of T2DM impact in the brain

i. Relation of T2DM with brain's morphological and structural modifications

The process of adipose tissue dysfunction in obesity is associated with the development of central and peripheral insulin resistance and prediabetes. Thus, it indirectly contributes to the changes in brain morphology and function driven by hyperglycaemia and insulin resistance. However, the deleterious effect of adipose tissue on the brain seems to be mainly exerted through AT-potentiated inflammation and impaired secretion of adipokine, ie AT-produced cytokines[63,64]. While the latter event compromises predominantly more superficial brain regions in obesity, the deleterious effect reaches more centrally located regions in T2DM. However, similar to what is observed in obesogenic conditions, the grey and white matters of the brain are differently conditioned by T2DM, not to mention at different rates.

Although some adipokines can cross the BBB, its majority promote the pro-inflammatory function through the modulation of BBB-present endothelial cells, compromising their function and integrity[65]. It is, therefore, likely BBB is the primary cerebral defence to be compromised in prediabetes, priorly to GM or WM integrity loss. Since insulin is transported through the BBB by a saturable transport system, endothelial impairment may promote its inadequate transport, diminishing insulin bioavailability in the brain[66]. Therefore, simultaneous to the already diminished peripheral insulin sensitivity present in prediabetes, central insulin insensitivity and impaired activity may be observed in these same conditions. Consequently, given the role of insulin on neuronal viability[69], it comes as no surprise that GM abnormalities are present in in prediabetes, while the WM impairment is absent as assessed through MRI-involving studies[67–70]. Inhibition of the insulin receptor substrate (IRS)-Akt pathway upregulates cell cycle inhibitors (p21Cip1/WAF1 and p27Kip1) and pro-apoptotic proteins and mediators involved in the intrinsic pathway of apoptosis (BAX, BAD and caspase 9) (reviewed by Boucher *et al.*)[71]. Moreover, impairment of insulin receptor pathway yet promotes the activation of glycogen synthase kinase beta 3 (GSK3β), which induces the formation of neurofibrillary tangles[72]. Moreover, inflammation promotes an

overactivation of microglia and astrocytes, which produce and release pro-inflammatory cytokines and reactive oxygen (ROS) and nitrogen (RNS) species. As a consequence, protein degradation, mitochondrial dysfunction, defects on axonal transport and apoptosis are potentiated[47]. These mechanistic events are further worsened once IR is fully developed, which occurs in T2DM. Hence, it is understandable why the mainly affected brain regions observed, in T2DM individuals, present the higher concentrations of the insulin receptor in the brain[44], which include the hippocampus, amygdala[73] and cerebral cortex[74].

Although insulin is not required for glucose metabolism in the brain, the overall systemic glucose metabolism depends on this hormone[75]. Therefore, cerebral hyperglycemia is only expected in T2DM in which chronic hyperglycemia is present. The latter promotes oxidative stress and increases AGE levels, both of which contribute to inflammation and endothelial dysfunction. Moreover, the high blood glucose also promotes the loss of neuronal integrity, potentiating apoptosis, as observed through MRI[76–78]. Such aggravates GM lesions[69,79] and BBB integrity through vascular impairment[80] in T2DM subjects. Hyperglycemia[81], VAT-promoted inflammation and IR promote an enhancement of the total hippocampal area[82], which is then replaced by its atrophy, primarily in the left tail region[81], the dentate gyrus and CA2/3 subregions[78,83]. The hippocampus is highly sensitive to interleukin-6-based neuroinflammation, which promotes cellular death. Consequently, executive dysfunction, namely working memory, may be hampered[84,85]. Similarly, cortical regions are prone to diabetic-induced damage. In retinopathy-free diabetic subjects, reduced GM was observed in the left occipital cortex, an early visual-processing brain area. In turn, the visual performance was compromised in the absence of retinal abnormalities[86]. Similarly, in obese T2DM patients, hyperglycaemia-induced atrophy in GM can already be observed in the insular, temporal, occipital and superior parietal cortexes, all of which are involved in sensorial responses[25]. Altogether, GM constitutes the primary cerebral area affected by diabetic environment, although primarily unilaterally. Nevertheless, given the long duration of the disease and the poorer control of the pathology, the atrophic effect gets further worse and reaches both hemispheres[80], suggesting a cumulative effect of T2DM[87].

Mild cognitive impairment (MCI), an advanced stage of neurological complications, is only observed in T2DM subjects with WM atrophy, namely in the left posterior cingulate, precuneus, insula and right rostral middle frontal gyrus[88], all of which are involved in executive functions (memory and decision-making) and emotion regulation. Furthermore, in T2DM patients, a reduced and compromised WM integrity is observed in: (1) the splenium of the corpus callosum which connect temporal, posterior parietal and occipital cortices, all of which are involved in the processing of sensorial input; (2) the external capsule that connects the outer segment of the lentiform nucleus (putamen) and the claustrum, which are involved in salience and reward system; and (3) the pons that enables the connection between the forebrain to the cerebellum, a network involved in the regulation of involuntary processes (including breathing)[54,59,89,90]. Through diffusion kurtosis imaging (DKI) experiments, the loss of WM integrity in T2DM subjects was attributed to the axon fibers' degeneration which seemed to be related with the formation of neurofibrillary tangles[91]; demyelination and subsequent increased interstitial space between myelin-covered axons[87,91,92]. Due to the previously mentioned dependence of myelin maintenance and the axon-surrounding capillaries, the alterations on myelin sheath were attributed to an hypoperfusion[92] associated with VAT-potentiated inflammation[88,90,91], endothelial dysfunction, and IR[94,95].

The relation between morphological alterations and cognitive impairments supports the urgency of novel imaging biomarkers to detect early cerebral abnormalities before massive neuronal loss, since the earlier symptoms are mostly "silent". Unfortunately, most diabetic subjects only resort to medical aid when the metabolic dysregulation is already established.

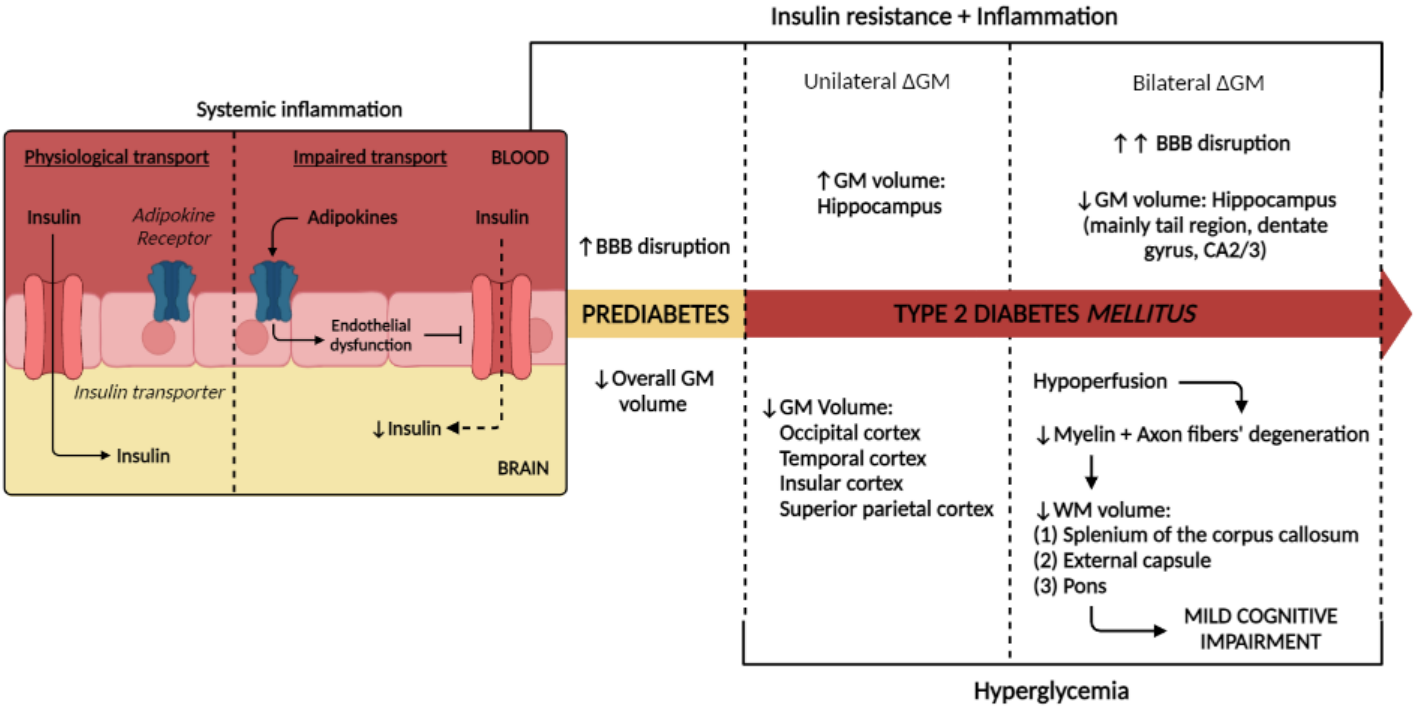

Figure 9. Prediabetes, T2DM and its cerebral structural alterations.

As a consequence of systemic inflammation promoted by AT, endothelial dysfunction hinders insulin transport (identified with ↓) through the BBB. The latter is further worsened in prediabetes, moment in which GM abnormalities are already observed due to the weakened sensitivity to the previous hormone. However, IR is only fully established in T2DM, in which hyperglycemia is verified as well. In this metabolic disease, in an earlier stage, the volumes of the occipital, temporal, insular and superior parietal cortices are diminished unilaterally, while an enhanced hippocampal volume (represented with ↑) is observed. Nonetheless, the latter is lost with the progression of the disease, compromising primarily the tail region, dentate gyrus and CA2/3 areas, bilaterally. Furthermore, IR and hyperglycemia further compromises BBB integrity and promotes a diminished hypoperfusion. Such reduces the myelin pool and promotes the degeneration of axon fibers, promoting axonal death. Therefore, a reduction of WM volume can be observed in the splenium of the corpus callosum, external capsule and pons, all which contribute to MCI. Weakened activities are represented by dashed arrows, while the ameliorated activities are symbolized by continuous arrows. Image created with Biorender.com.

ii. T2DM and neurometabolic alterations

In animal models and subjects with T2DM, studies resorting to magnetic resonance spectroscopy (MRS) showed lower levels of N-acetylaspartate (NAA), a neuronal viability marker, in the caudate-putamen, prefrontal cortex, left lenticular nucleus[81–83] and parietal white matter[96]. Therefore, it has been postulated that neurometabolic alterations may precede structural changes and even the establishment of chronic hyperglycaemia. Although they are still difficult to evaluate in clinical studies, their assessment would enable an early detection of cerebral alterations, prior to structural modifications, and have a preventive action over these diabetic outcomes.

During a prediabetic stage, although the impaired glucose metabolism is observed in both female and male subjects, its effect in cognitive impairment seems to be specific for women in the frontal cortex-involved tasks, ie, executive function and language performance. Such was postulated to be associated with a more severe effect of IR on female individuals, when compared to men[97]. Likewise, it has been suggested a possible effect of the SAT-potentiated inflammation, which is usually augmented prominently in women.

In a diabetic environment, it is widely accepted that IR is associated with an altered cerebral glucose metabolism, namely in frontal, temporal-parietal and cingulate regions, as observed by ^{18}F-*fluorodeoxyglucose* (^{18}F-FDG)-involving PET and [^{13}C]-MRS[98,99]. Specifically, IR seems to reduce the Krebs cycle's activity[100] and hamper glycogen metabolism[101] in neurons. Simultaneously, the latter is enhanced in astrocytes and glial cells, a nervous system-specific immune cells, as observed in Goto-Kakizaki (GK) rats[56]. This glucose metabolism deviation supports a synaptic imbalance, given that glucose is the main energy substrate of the brain and is involved in the synthesis of neurotransmitters. Furthermore, since astrocytes transform glucose into lactate and neurons are unable to process glucose[102], a lactate-focused metabolism is potentiated as a secondary form of energy source[56,103]. The latter is further supported by increased myo-inositol levels, a putative marker of glial cells, ie inflammation, in the frontal cortex[84].

In an earlier state of the metabolic disease, the enhanced glutamatergic pool, ie the main excitatory neurotransmitter, in the hippocampus, was observed by proton (^{1}H)-MRS in both animal models and patients with diabetes[100,104]. Consequently, it induces an augmented synaptic activity, possibly as a compensatory mechanism, that is later lost. With the progression of the disease and poor glycaemic control, Glu levels are decreased, while Gln are increased in the occipital cortex[104], due to a reduced rate of Glu-Gln cycle in GK rats[56]. Individuals with diabetes and severe depression present low levels of both Glu and Gln in WM regions, possibly due to an aberrant activation of glial cells[105]. The latter is corroborated by the enhanced levels of the proton MRS-assessed myo-inositol, a putative marker of neuroinflammation, which was suggested to be potentiated by VAT hypertrophy and consequent systemic inflammation[57]. Glial cells might yet promote demyelination and membrane turnover[58], as given by increased choline (Cho) levels in T2DM patients, known to be involved in the metabolism of myelin and other phospholipids of the cell membrane[106]. Given the role of myelin on propagation of action potential, its decrease further contributes to an impaired synaptic activity and a weakened intercommunication between different brain areas. Additionally, Cho is a precursor for acetylcholine, which constitutes an excitatory neurotransmitter. Therefore, it is postulated that T2DM impairs the conversion of Cho into acetylcholine[58]. Hence, the excitatory activity is further hampered, along with the decreased Glu levels. While the lenticular nucleus[98] and frontal cortical region[96] undergo enhanced levels of Cho in T2DM subjects; the thalamus[98], right frontal, right parieto-temporal and right parieto-occipital regions are unaltered[106]. Nevertheless, simultaneous to a modified glutamatergic pool, depression-free diabetic subjects undergo enhanced cerebral GABA levels in the hippocampus[100,103] and medial prefrontal cortex, potentiating neuronal inhibitory activity, hence compromising episodic memory[108]. In patients with prediabetes and T2DM, IR potentiates the formation of neurofibrillary amyloid-beta plaques, as assessed through ^{18}F-Florbetaben or [^{11}C]- Pittsburgh compound-involving PET imaging[109,110].

Interestingly, similarly to neuronal structural changes, metabolic alterations in the brain occur predominantly in the left hemisphere in right-handed individuals, probably due to higher energy requirements of the dominant hemisphere[98].

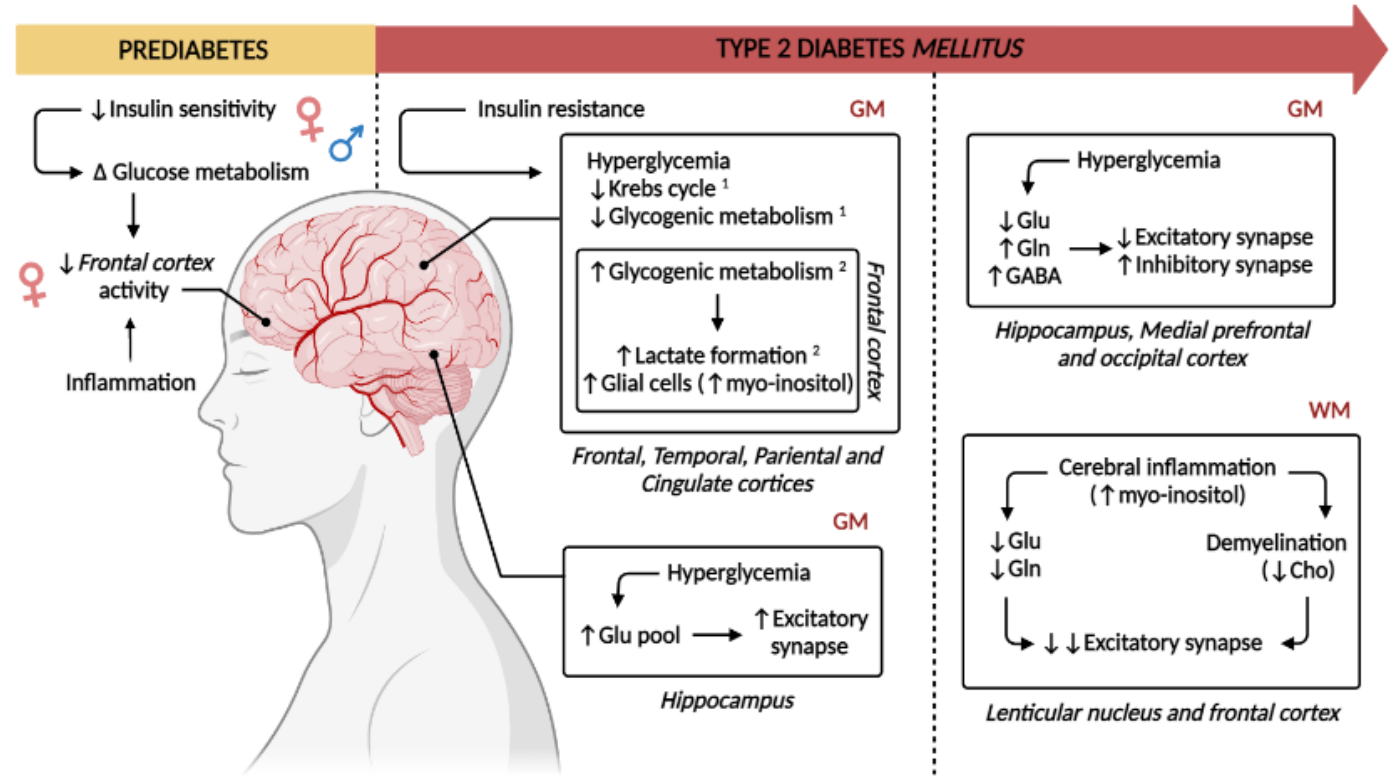

Figure 10. Prediabetes, T2DM and its cerebral neurometabolic alterations.

Little is known regarding the impairment of neurometabolism in prediabetes. Nonetheless, only in female patients, the altered glucose metabolism affected the activity of the frontal cortex. Meanwhile, in the earlier stages of T2DM, only GM alterations are observed. IR promotes hyperglycemia and a metabolic shift, hindering the activity of the Krebs cycle (identified with ↓) and glycogen formation in neurons (numbered with 1) in the frontal, temporal, parietal and cingulate cortices. In contrast, in glial cells and astrocytes (numbered with 2) in the frontal cortex, an ameliorated glycogenic metabolism (represented by ↑) takes place, which promotes lactate formation as a substitute energy font. Ultimately, such potentiates an higher activity of these brain-specific immune cells (as assessed through the higher myo-inositol levels. Simultaneously, hyperglycemia induces the Glu formation, strengthening the excitatory activity in the hippocampus. Nonetheless, this same hallmark impairs its formation and activity in the hippocampus, medial frontal and occipital cortices, while also promoting the synthesis of GABA. The previously mentioned cerebral inflammatory event also participates in the restraint of the glutamatergic synapse in the lenticular nucleus and frontal cortex. Furthermore, inflammation provokes demyelination and consequent diminished Cho levels, suppressing the propagation of the action potential and the excitatory synaptic activity. Image created with Biorender.com.

iii. T2DM, vascular modifications and dementia

Dementia and MCI are promoted by several factors, including metabolic and vascular ones. Despite the strong evidences of a neurometabolic-cognitive decline in a diabetic environment, little is still known, since the majority of the studies take advantage of functional magnetic resonance imaging (fMRI) which only evaluates blood flow alterations and requires specific stimuli, hence limiting these studies. The brain requires exacerbated levels of nutrients, oxygen and ions to exert its functions, when compared to other organs and tissues. However, the hyperglycaemia not only changes brain metabolism, but also potentiates a diminished brain activity through reduction of hemodynamic response[111–113], namely in the hippocampus[114]. Under healthy conditions, an enhancement of CBF takes place upon a stimulus in order to provide the oxygen and metabolites required for synaptic firing and activation of the task-involved brain region, through a process named neurovascular coupling[115,116]. However, in T2DM, this process is impaired due to a reduction of CBF[117–119], since the consequent oxidative stress hinders the bioavailability of vasodilators[120]. Interestingly, the synaptic imbalance between Glu and GABA is also here involved[121,122]. Upon a stimulus, Glu is released and induces nitric oxide (NO) production, through the activation of the NMDAR present in neurons. Moreover, it also promotes the production of prostaglandins through the binding to astrocyte-located metabotropic receptors. However, given the lower Glu levels and GABA overactivation observed in diabetic individuals, such pathways are compromised[123]. Also, AGE production affects the biomechanical properties of the vessels, contributing to an enhanced stiffness and reduced compliance[117–119], not to mention that the superoxide anion reacts with NO to form peroxynitrite, interfering with its bioavailability[124]. Although both GM and WM are sensitive to hypoperfusion, the latter is highly composed of capillaries, when compared to GM. Therefore, WM is more sensitive to vascular factors[125]. In fact, studies involving DTI showed the presence of WM hyperintensities in prediabetes, as a consequence of cerebral microvascular changes, including cerebral microbleeds[112,126]. Such lesions were suggested to potentiate cognitive dysfunction in early stages of the metabolic syndrome[69,112,126,127]. Given that WM interprets sensory information from various regions and transmits neuronal inputs

between several GM areas[128], vascular impairment promotes fewer and weaker WM network connections and compromise synaptic transmission[129]. Among others, and given the vulnerability of the hippocampus to T2DM, the default mode network (DMN) activity is considered the most affected network by this disease[74]. Studies involving fMRI demonstrated that the latter network's connectivity is enhanced between the left hippocampus and left inferior frontal gyrus[74,130] in young diabetic individuals, which is related to a better executive function[74]. The enhanced activity, which might constitute an adaptative compensatory mechanism, is then replaced by a loss of function in older T2DM patients, including those with MCI. This is reflected in an impaired deactivation and hypoactivation of task-relevant regions in the DMN, even in the presence of a normal cognitive performance[73,111,129].

In early stages of T2DM, hyperconnectivity between posterior cingulate cortex and left inferior parietal lobule takes place, while there is a weaker network connectivity in visual and insula areas[129]. Furthermore, prior to the onset of dementia, the connectivity between left frontal–parietal network and sensorimotor network, which includes the precentral and postcentral gyrus, ie, motor and somatosensory regions, respectively, is also increased, possibly as an adaptive mechanism to compensate memory and executive function declines[131].

Taken together, available data suggest the presence of a differential functional organization and activation pattern depending on prediabetes and T2DM severity[74,99,130,132,133], possibly due to an initial increased excitatory activity[104]. Upon disease progression and onset of MCI, the weaker DMN functional connectivity in the left calcarine and bilateral posterior cerebellum culminates in a weaker episodic memory. Such further aggravates the cognitive performance, including visual-spatial ability, memory, and attention executive function[83,132]. Also, apart from the hippocampus, the fMRI-evaluated CBF is compromised in other specific brain regions of subjects with diabetes, including the inferior parietal cortex, inferior temporal cortex and middle frontal regions. These ultimately culminate in an impaired executive function and processing speed[115,116,132].

Osborne et al. showed that chronic noise exposure and the associated psychological disturbances, including poor sleep, were related with a greater CT-assessed visceral adiposity and an enhanced risk for the development of T2DM. Such associations seem to be mediated by the augmented metabolic activity of the noise stress responsive-brain area, i.e., the amygdala, as assessed by ^{18}F-FDG-PET. Such might be, at least partly, explained by the sympathetic nervous system's activation which induces systemic inflammation, endothelial dysfunction, as well as oxidative stress[134].

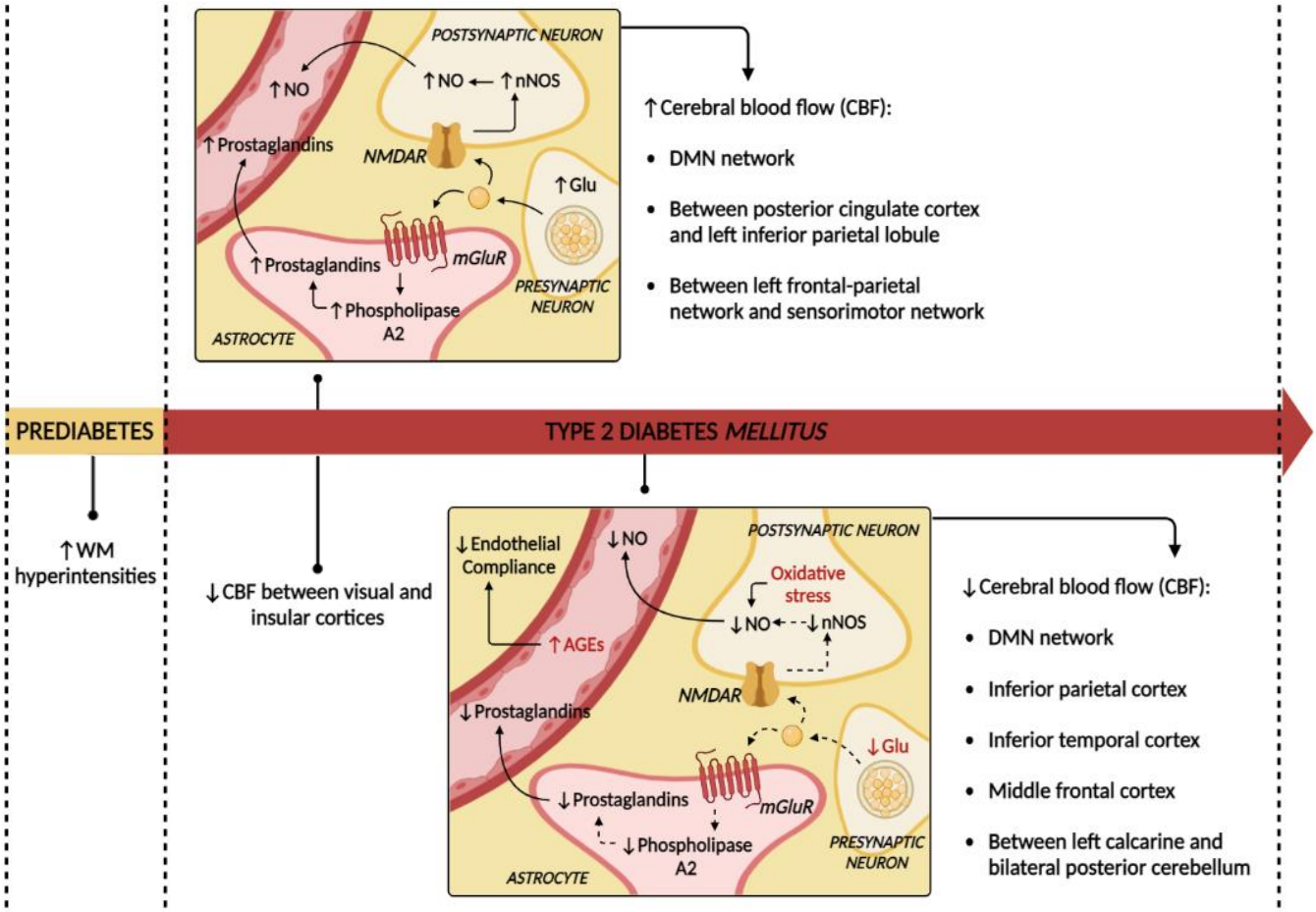

Figure 11. Prediabetes, T2DM and its cerebral vascular alterations.

Concurrent to the firstly enhanced Glu levels and excitatory synaptic activity (represented with ↑), in an earlier stage of T2DM, possibly due to an enhanced production of vasodilators, an higher hemodynamic response is observed in various areas of the brain, including the DMN network. Simultaneously, however, a decreased connectivity (identified with ↓) is present in the network responsible for the connection of the visual and insular cortices. In later stages, cerebral hyperglycemia not only induces an overall stronger inhibitory activity and oxidative

stress, both of which reduce the bioavailability of the vasodilators, but also promotes the formation of AGE which reduces the compliance of the endothelial cells (hyperglycemic consequences represented in red). Altogether, the previously enhanced hemodynamic responses are replaced by its decline. Weakened activities are represented by dashed arrows, while the ameliorated activities are symbolized by continuous arrows. Image created with Biorender.com.

Scientific Framework

Obesity has been shown to promote systemic inflammation, which, in turn, induces the onset of oxidative stress in the hippocampus[135] and the cerebral cortex[136]. This deleterious event is further worsened in T2DM due to hyperglycemia and insulin resistance in the hippocampus[137] and cerebral cortex[138]. Simultaneously, in high-fat diet (HFD)-fed rats, decreased GABA levels were found in the hippocampus[139] and the visual cortex[140]. Such is, then, replaced by, possibly as a protective effect against oxidative stress[141], an amelioration of these levels, accompanied by a greater inhibitory activity in the hippocampus[142] and the visual cortex[143]. d'Almeida *et al.* demonstrated that these neurometabolic alterations preceded structural abnormalities[104]. However, all diagnostic protocols adopted clinically are only standardized for the assessment of morphological alterations, most of which are usually in an irreversible status. Meanwhile, an MRS sequence has been developed named "Hadamard Encoding and Reconstruction of MEGA-Edited Spectroscopy" (HERMES) which enables the simultaneous detection of GABA and glutathione (GSH).

Main objective

This project aimed to investigate the early neurometabolic alterations observed in obesity and T2DM, namely the simultaneous measure of GABAergic synapse and oxidative stress.

Specific objectives

To address the previous objective, this project was divided on 2 specific ones:

1. Evaluate what neurometabolic alterations occurring as a result of obesity and T2DM, and how early these take place;
2. Assess alterations regarding oxidative stress and synapse as early predictors of neuronal metabolic changes in obese or type 2 diabetic animal models.

Materials and Methods

Reagents

Salts and organic solvents used in this study were all purchased from Sigma-Aldrich/Merck Portugal (Oeiras, Portugal) and Fischer Scientific (Pittsburgh, PA, USA), unless stated elsewhere.

Antibodies and ELISA (Enzyme-linked immunosorbent assay) kits

For the Western blot protocol, primary antibodies were used to target calnexin (Sicgen, Cantanhede, Portugal); catalase, glyoxalase-1 (Glo-1), heme oxygenase-1 (HO-1), nitrotyrosine (Nitrotyr), phosphorylated insulin receptor (Y972) (p-IR), Glut. C, $GABA_AR$, vGAT, vGLUT, glucose transporter 3 (GLUT3) (Abcam, Cambridge, UK); argpyrimidine (ArgPyr) (Nordic-MUbio, Susteren, Netherlands); N^{δ}-(5-hydro-5-methyl-4-imidazolon-2-yl)ornithine (MG-H1) (Hycult Biotech, Uden, Netherlands); amyloid precursor protein (APP), total insulin receptor (IR-T), phosphorylated GSK3-β (S9) (p-GSK3β), Akt, PSD-95 (Cell Signaling Technology, Danvers, MA, USA); and synapsin (Synaptic Systems, Göttingen, Germany). The previous were then probed with secondary antibodies, namely anti-mouse (GE Healthcare, Chicago, IL, USA), anti-rabbit and anti-goat (Bio-rad, Hercules, CA, USA).

Plasma insulin concentrations were determined with the Rat Insulin ELISA Kit (Mercodia AB, Uppsala, Sweden).

Table 1. Primary antibodies used in Western blot

Antibody	Molecular weight	Manufacturer	Secondary Antibody	Dilution
Anti-Calnexin	90 kDa	Sicgen	Anti-Goat	1:2000
Anti-Catalase	60 kDa	Abcam	Anti-Rabbit	1:1000
Anti-Glo-1	21 kDa	Abcam	Anti-Rabbit	1:1000
Anti-HO-1	33 kDa	Abcam	Anti-Rabbit	1:1000
Anti-Nitrotyr	-	Abcam	Anti-Mouse	1:750
Anti-p-IR (Y972)	95 kDa	Abcam	Anti-Rabbit	1:1000
Anti-$GABA_AR$	52 kDa	Abcam	Anti-Rabbit	1:1000
Anti-Glut. C	65 kDa	Abcam	Anti-Rabbit	1:1000
Anti-vGAT	57 kDa	Abcam	Anti-Mouse	1:1000
Anti-vGLUT	62 kDa	Abcam	Anti-Rabbit	1:1000
Anti-GLUT3	49-52kDa	Abcam	Anti-Rabbit	1:1000
Anti-APP	100-140 kDa	Cell Signaling	Anti-Rabbit	1:1000
Anti-IR-T	95 kDa	Cell Signaling	Anti-Rabbit	1:1000
Anti-p-GSK3β (S9)	47 kDa	Cell Signaling	Anti-Rabbit	1:1000
Anti-Akt	60 kDa	Cell Signaling	Anti-Rabbit	1:1000
Anti-PSD-95	95 kDa	Cell Signaling	Anti-Mouse	1:1000
Anti-ArgPyr	-	Nordic-Mubio	Anti-Mouse	1:750
Anti-MG-H1	-	Hycult Biotech	Anti-Mouse	1:750
Anti-Synapsin	77 kDa	Synaptic Systems	Anti-Mouse	1:1000

Animal Treatment and Maintenance

Twelve-week old Wistar rats were randomly divided into 3 groups (n = 8 / group) which were differently treated during a ten-week period. Then, within a given group, these were kept in pairs (2 rats/cage). These animals had free access to food and water, while being kept under standard conditions, including temperature at 22-24 ºC, 50-60% humidity and standard light cycle (12 hours of light and 12 hours of darkness). The first group (1 - control) was fed with a standard diet (SD) (3% triglyceride and 50% carbohydrates, A04, SAFE, France) during the entire *in vivo* experiments. Moreover, the second group (2 - HFD) was fed with HFD (40% triglycerides and 10% carbohydrates, 231 HF, SAFE, France), which culminated in the onset of the obesity. Finally, the last group (3 – HFD+STZ) was also fed with HFD for ten weeks, although, on the fourth week, the rats were injected with a low dose (35 mg/kg) of streptozotocin (STZ) (S0130-500MG, Sigma-Aldrich/Merck Portugal, Oeiras, Portugal), in order to potentiate the development of T2DM phenotype. Taken together, 3 groups were designed: (1) a control group (SD), (2) an obesity group (HFD) and (3) a T2DM group (HFD+STZ) (**Figure 12**).

On the day prior to the completion of the ten-weeks period, insulin tolerance test (ITT) was performed. 0.25U/kg insulin (Humulin, 1000 UI/mL Lilly, Lisboa, Portugal) was intraperitoneally administrated, which was promptly followed by glycemia measurement at several time points, namely 0, 15, 30, 60 and 120 minutes, through the tail vein, resorting to a glucometer (Contour Next, Bayer, Leverkusen, Germany) and test strips. The insulin response was expressed by the area under the curve (AUC). Meanwhile, in the same day, ^{1}H-MRS protocols were performed on the 3 groups (later discussed).

In the following day, 6-hour fasting glycemia, body weight, serum triglycerides, food and water intake were measured. Rats were then anesthetized with an intraperitoneal 2:1 (v/v) 50 mg/kg ketamine (100 mg/mL) / 2.5% chlorpromazine (5 mg/mL) injection, blood samples were collected by cardiac puncture, and were sacrificed through cervical dislocation, moment in which the brain was collected. It is noteworthy that 50% of the brains were preserved as a whole (later discussed

procedure), while in the remaining 50%, the hippocampus and visual cortex were individually collected and stored at – 80 ºC. Finally, the blood samples were centrifuged (2200xg, 4 ºC), from which serum and plasma were aliquoted and stored at -80 ºC for further biochemical analysis.

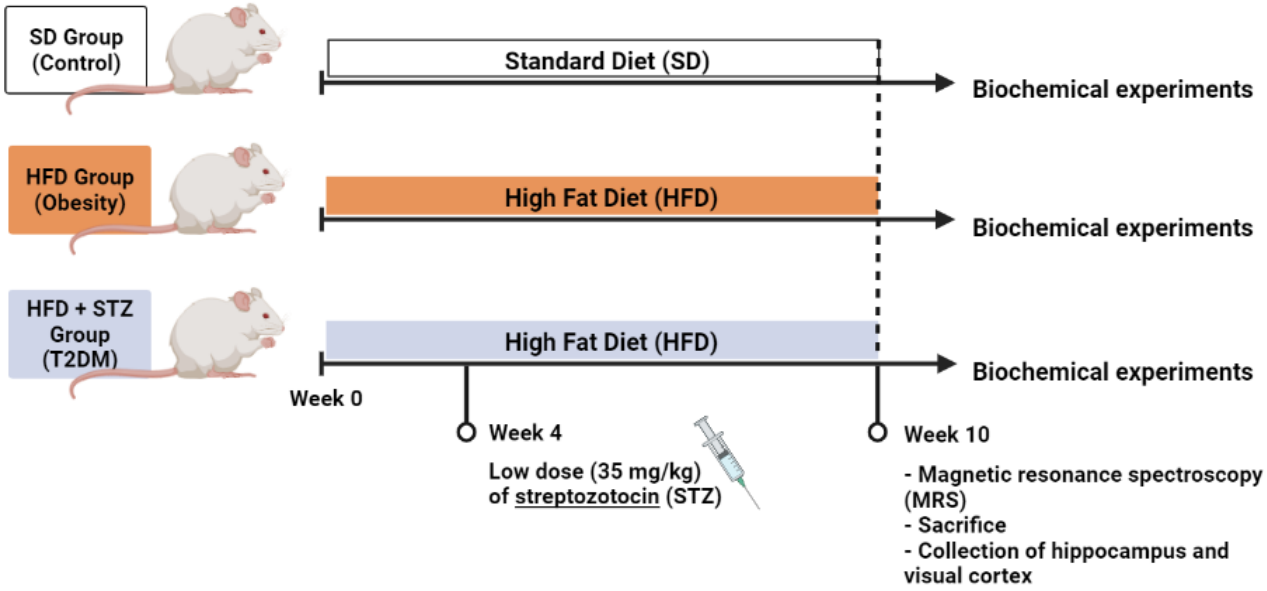

Figure 12. Timeline of the animal *in vivo* experiments.

For 10 weeks, Wistar rats were fed with either SD or HFD. On the 4th week, the latter group was injected with a low dose of STZ in order to partially promoting cellular death of the β-pancreatic cells. Image created with Biorender.com.

^{1}H-Magnetic resonance spectroscopy

Through the non-invasive and high-resolution ^{1}H-MRS, brain metabolites of the hippocampus and visual cortex were calculated using the HERMES sequence, which enables the specific measurement of GABA and GSH[144]. Data was acquired with the BioSpec 9.4 T MRI scanner (Bruker BioSpin, Ettlingen, Germany). Wistar rats were kept anesthetized with isoflurane (2-3%), 100% O_2 and a stable body temperature of 37 ºC. During the procedure, the rats' respiration was monitored (SA Instruments SA, Stony Brook, USA). Spectral data quantification was performed with LC model.

Preparation of samples' extracts

For the preparation of the samples' extracts of the individual hippocampus and visual cortices, a homogenization buffer was previously prepared: firstly 25 mM Tris-hydrochloride (Tris-HCl) and 100 mM sodium chloride (NaCl) were measured, which, once both compounds were dissolved, was followed by the adjusting of pH to 7.4. Then, 5 mM ethylenediaminetetraacetic acid (EDTA), 5 mM ethylene glycol-bis(2-aminoethylether)-N, N, N', N'-tetraacetic acid (EGTA), 20 mM sodium fluoride (NaF), 10 mM β- glycerophosphate, 2.5 mM sodium pyrophosphate and sodium metavanadate ($NaVO_3$) were added to the previous solution, which, once dissolved, was followed by the volume correction with ultrapure water (MiliQ water). $NaVO_3$ requires anticipated activation. Therefore, 200 mM $NaVO_3$ solution was prepared with the pH adjustment to 10, which provides a yellowish colour to the solution. Then, the latter is boiled until it becomes colourless. Upon its cooling, the pH is readjusted, and the solution is boiled once again until it becomes colourless. Such is then followed by its cooling and this protocol has to be repeated until the moment the solution remains at a pH equivalent to 10 for up to 2-3 cycles. Once such succeeds, the solution is kept at -20 ºC.

On the day of the extracts' preparation, 1% Triton X-100, 10 mM phenylmethylsulfonyl fluoride (PMSF) and 5% protease inhibitor were added to the previously prepared homogenization buffer, in order to prepare the lysis buffer. While keeping, through the entire procedure, the samples in ice or cooled structures to avoid thawing and denaturation, the hippocampus and cortex visual were promptly dissolved in lysis buffer in order to produce extracts with a concentration of 100 mg/mL each. The tissues were, then, disrupted using Tissue Lyser II (Qiagen, Germany), which was followed by the samples' centrifugation at 14 000 rotations per minute (rpm), for 20 minutes at 4 ºC. As a result, a lipidic top-layer, a pellet composed of cellular membranes and nucleic acids, and a protein-enriched supernatant were obtained, from which only the latter was collected. The supernatant was centrifugated, once again, at 14 000 rpm at 4 ºC, for 15 minutes, which resulted in the same 3 phases. The supernatant was collected and kept at – 80 º C.

Western blot

To quantify the protein concentration in the extracts, BCA Protein Assay kit (Novagen, Fisher scientific, Massachusetts, USA) was carried out. A calibration curve was designed for 0.0125, 0.025, 0.05, 0.125, 0.25, 0.5, 1, 2 mg/ mL of bovine serum albumin (BSA) solution. In a 96-well plate, 25 µL of each calibration curve points and aliquots of the samples (1:8 diluted in water) was pipetted, to which 200 µL of a solution composed with 98% of BCA solution and 2% of a 4% cupric sulphate solution. Enrolled in an aluminium sheet to protect the photosensitive solution, the multi-well plate was incubated at 37 ºC for 30 minutes. Once the incubation time was completed, the absorbance at 562 nm was measured in a plate reader. Considering the Beer-Lambert equation, the previous dilution (1:8) of the samples and the calibration curve, the total protein concentration of each sample was calculated. Then, the samples were denatured and diluted in 2x Laemmli buffer pH 6.8. The latter was prepared with 62.5 mM Tris-HCl, 10% glycerol, 2% Sodium dodecyl sulphate (SDS), 5% β-mercaptoethanol and 0.01% bromophenol blue. Meanwhile, the pH was adjusted to 6.8, taking into consideration to only add the detergent SDS only after the electrode use, thus avoiding its damage.

The Laemmli buffer-diluted brain samples were sonicated and boiled at 90-95 ºC for 3 minutes. Vertical electrophoresis was performed with 10% polyacrylamide gels composed with either resolving (0.75 M Tris-HCl, 0.2% SDS, pH 8.8) or stacking buffer (0.25 M Tris-HCl, 0.2% SDS, pH 6.8), both of which are supplemented with acrylamide, MiliQ water, ammonium persulfate (APS) and N-tetramethylethylenediamine (TEMED). Samples' volume corresponding to 10 µg of total protein, as well as a molecular weight ladder (GRiSP, Research Solutions, Portugal), were loaded into the SDS-PAGE gels. The latter were translocated to an electrophoresis system (Bio-Rad, USA), which was filled with running buffer composed of 25 mM Tris-base, 480 mM glycine, 1% SDS and a pH 8.8. The protein migration was primarily executed at 80 V, which was augmented until a maximum of 120 V once the proteins passed through the stacking gel. Following, in a sandwich-like protocol, the gels were electrophoretically transferred onto polyvinylidene difluoride (PVDF) membranes (Advansta, San Jose, CA, USA), which were previously activated in methanol, rinsed in

MiliQ water and washed in transfer buffer (50 mM 3-(Cyclohexylamino)-1-propanesulfonic acid (CAPS), 2% sodium hydroxide (NaOH), 10% methanol, pH 11). The transfer procedure was performed for 2 hours at 750 mA, guaranteeing a voltage inferior to 130, while keeping the entire system below 4 ºC. The resulting membranes were, then, blocked with a 5% BSA solution for 2 hours at room temperature or overnight at 4 ºC, following their incubation with a primary antibody (listed above in table 1) for the same time periods as the blockage step. The antibodies are diluted in a tris-buffered saline (TBS) solution (250 mM Tris, 1.5 mM NaCl, pH=7.6) supplemented with 0.01% Tween 20 detergent and 1% BSA. The obtained membranes are rinsed with a wash buffer (TBS plus 0.1% Tween 20 detergent) for 1 hour under constant agitation, followed by their probing in the corresponding secondary antibody for 2 hours at room temperature or overnight at 4 ºC. These are washed once again, which is followed by their revelation through a chemiluminescent method using an enhanced chemiluminescence (ECL) substrate 1:1 (Advansta, San Jose, USA) and the luminescence detection system ImageQuant LAS500 (GE Healthcare, Chicago, IL, USA). The concentration of the specific immunodetected protein was calculated using Quantity One software (Bio-Rad, Hercules, CA, USA) and ImageQuant software (Cytiva Life Sciences, USA). Calnexin was used as a loading control to guarantee each well carried an equal protein quantity.

Brain samples' processing

The samples preserved as a whole brain were used for the assessment of the oxidative stress and associated ROS in both the hippocampus and the visual cortex. In the moment the rats were sacrificed, the brain was collected and submerged in a formol solution for 5 days at room temperature. Upon this period, the organs were put in a 30% sucrose solution for 5 more days at room temperature. Then, the brain was properly dried, wrapped in parafilm and stored at -80 ºC until their usage.

Immunohistochemistry (IHC) of brain sections

Horizontal sections of the visual cortex (n = 4) with a thickness of 30 µm were cut in the cryostat (Leica, Wetzlar, Germany) and directly transferred to glass slides. These were promptly used once these dried, shortly after being cut.

Once the glass slides were dry, the brain slices were fixed with cooled (-20 ºC) acetone for 10 minutes at room temperature. Then, the slides were washed with a phosphate-buffer saline (PBS) solution for 5 minutes, which step was repeated 3 times. After a total of 15 minutes, the brain slices were permeabilized with a 0,25% Triton X-100 solution diluted in PBS for 15 minutes. Once the time period ceased, these were washed one more time in PBS for 5 minutes, which was followed by the blockage of the slices with 1% BSA diluted in PBS, forming a PBA solution, for 30 minutes in a moist chamber in order to avoid their drying. Then, the slices were incubated in 10 µM dihydroethidium (DHE) (D23107, Invitrogen, Waltham, MA, USA) diluted in PBA solution for evaluation of superoxide anion levels. Concurrently, 4',6-diamidino-2-phenylindole (DAPI) was used to counter-stain the nuclei for 30 minutes at 37 ºC, taking into account the photosensitivity of the probes. The glass slides were washed with PBS 3 times, which were 5 minutes each. Then, these were mounted in an aqueous mounting medium (Fischer Scientific, Pittsburgh, PA, USA). Finally, the images of the hippocampus and visual cortex were captured in a fluorescence Zeiss microscope (Zeiss Axio Observer Z1) with the incorporated camera (Zeiss, Jena, Germany), detected with 587 nm of excitation and 610 nm of emission for DHE, while DAPI was detected with 353 nm of excitation and 465 nm of emission. The same settings were kept constant for all analysis. Fluorescence of the acquired images was then measured through the ImageJ software (Fiji).

Statistical analysis

Statistical analysis was performed with GraphPad Prism 8.0 (GraphPad, San Diego, SA, USA) and IBM SPSS Statistics Software (IBM, Armonk, NY, USA Data is expressed as the mean ± standard error of the mean (SEM) and compared by the parametric method one-way analysis of variance (ANOVA), if our samples followed a normal distribution, or the non-parametric Kruskal-Wallis test in case of a non-normal distribution. During the analysis, p value inferior to 0.05 was considered significant.

Results

Characterization of the animal models

As previously stated in the "Material and Methods" section, Wistar rats were divided into 3 groups: (1) the SD group, which was composed the control group and is represented in all graphics of this manuscript in a black colour; (2) the HFD group, also denominated as the obesity model and is represented in orange to be easily identified in the following figures; and (3) a HFD+STZ group which constituted the T2DM model and is represented in a blue colour.

In regard to body weight, the SD group (n = 8) presented a 18.61 ± 1,5% weight gain, while the HFD group (n = 8) had a 26.12 ± 3.3 % of weight gain (**Figure 13A**) during the 10-week time period the *in vivo* experiments took place. Although the weight gain of the latter group was not significant, they experienced a significant increment in weight on week 9 ($p = 0.0460$) and 10 ($p = 0.0426$), in comparison to the SD group. In contrast, HFD+STZ (n = 8) group showed a weaker overall weight variation in comparison to HFD group ($p = 0.0013$). However, on week 3, the T2DM group presented a significantly greater weight than the control group ($p = 0.0386$). After this timepoint, which matched with the STZ injection, this group began to lose weight, which culminated in a body weight of 453.25 ± 17.3 g (**Figure 13B**) on week 10. In concern to triglycerides, all groups presented similar levels: the SD group presented 195.50 ± 24.9 mg/dL; while the HFD and HFD+STZ group showed 252.75 ±44.9 and 241.12 ± 26.1 mg/dL, respectively (**Figure 13C**).

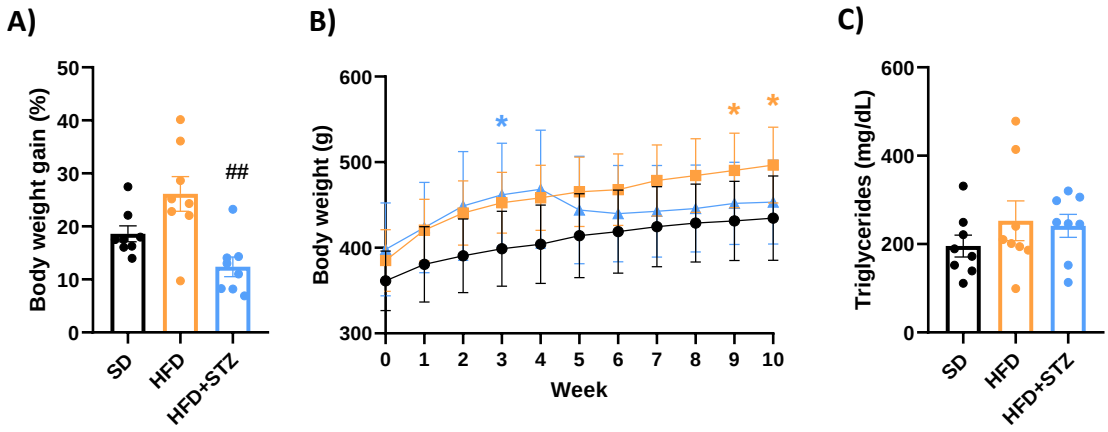

Figure 13. The effect of HFD and STZ on body weight.

In contrast to the HFD group, HFD+STZ group showed an increase of weight gain in the 3rd group (HFD+STZ group) that was lost after STZ injection (A, B). Furthermore, neither of the treatments promoted the loss of triglycerides' homeostasis (C). Statistical analysis obtained through one-way ANOVA test (parametric) and/or Kruskal-Wallis test (non-parametric), mean ±. SEM; n = 8; * vs SD; # vs HFD. * $p < 0.05$; ** $p < 0.01$; *** $p < 0.001$.

Next, we assessed insulin sensitivity. While SD and HFD group presented similar plasma insulin levels of 3.27 ± 0.3 and 2.35 ± 0.4 µg/L, the HFD+STZ group had 0.97 ± 0.2 µg/L, a statistically significant decrease in comparison to SD group ($p = 0.0003$) (**Figure 14A**). Such was to be expected given the genotoxic effects of STZ, potentiated by DNA alkylating activity which ultimately culminates in the apoptosis of pancreatic beta-cells. However, since a low dose of the drug was injected, these cells are only partially killed[145–147]. As a result, in the last ITT performed, it was observed a weaker effect of this hormone in the HFD+STZ group, compared to SD ($p < 0.0001$) and HFD group ($p = 0.0005$) (**Figure 14B**). Specifically, while on week 0 (**Figure 14C**), and week 4 (**Figure 14D**), no differences were observed during either the performed ITT; on week 10, a statistical increment of blood glucose was detected in all time points of the ITT when compared to the other 2 groups: 0 (SD: $p < 0.0001$; HFD: $p < 0.0001$), 15 (SD: $p < 0.0001$; HFD: $p = 0.0001$), 30 (SD: $p < 0.0001$; HFD: $p = 0.0002$), 60 (SD: $p = 0.0006$; HFD: $p = 0.0016$) and 120 minutes (SD: $p = 0.0002$; HFD: $p = 0.0003$) (**Figure 14E**).

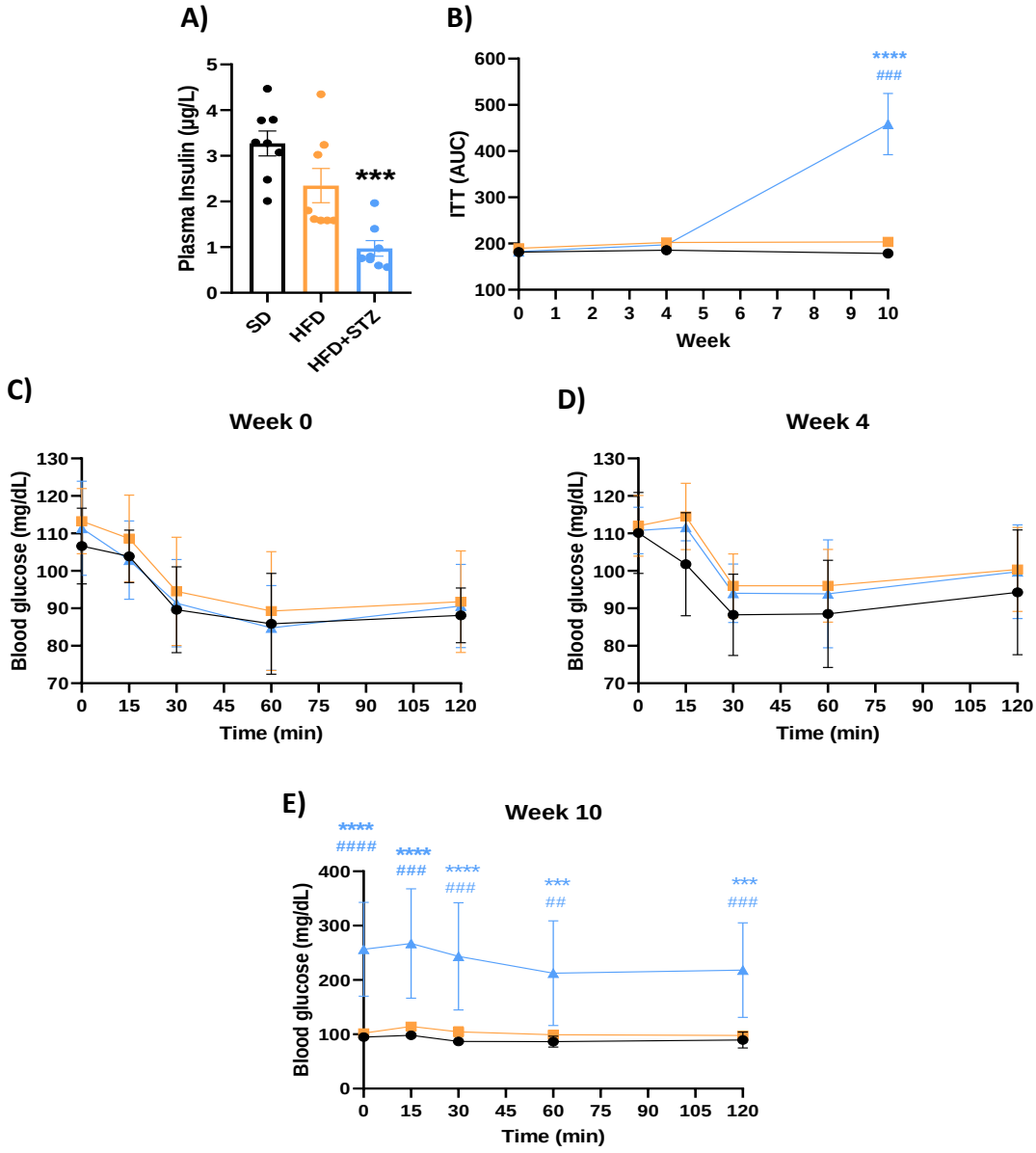

Figure 14. The effect of HFD and STZ on insulin levels and tolerance.

The STZ injection successfully reduced the production of insulin (A). As a result, following week 4, ie the administration of this drug, insulin activity is hindered in the HFD+STZ group on week 10 (B, C, D; E). Statistical analysis obtained through one-way ANOVA test (parametric) and/or Kruskal-Wallis test (non-parametric), mean ±. SEM. n = 8; * vs SD; # vs HFD. * $p < 0.05$; ** $p < 0.01$; *** $p < 0.001$.

Meanwhile, although blood glycemia remained similar throughout the 10-week period in the SD and HFD group (**Figure 15A**), the same did not occur for the HFD+STZ group. Upon the administration of the drug, blood glucose levels peaked from 107.13 ± 2.2 to 314.00 ± 12.5 mg/dL, which constituted a significant enhancement when compared to SD ($p = 0.0008$) and HFD group ($p = 0.0109$). From then forward, week 6 (SD: $p < 0.0001$; HFD: $p < 0.0001$), 7 (SD: $p < 0.0001$; HFD: $p < 0.0001$), 8 (SD: $p = 0.0002$; HFD: $p = 0.0003$), 9 (SD: $p < 0.0001$; HFD: $p < 0.0001$) and 10 (SD: $p < 0.0001$; HFD: $p < 0.0001$) showed statistically significant increases in the HFD+STZ group (**Figure 15B**).

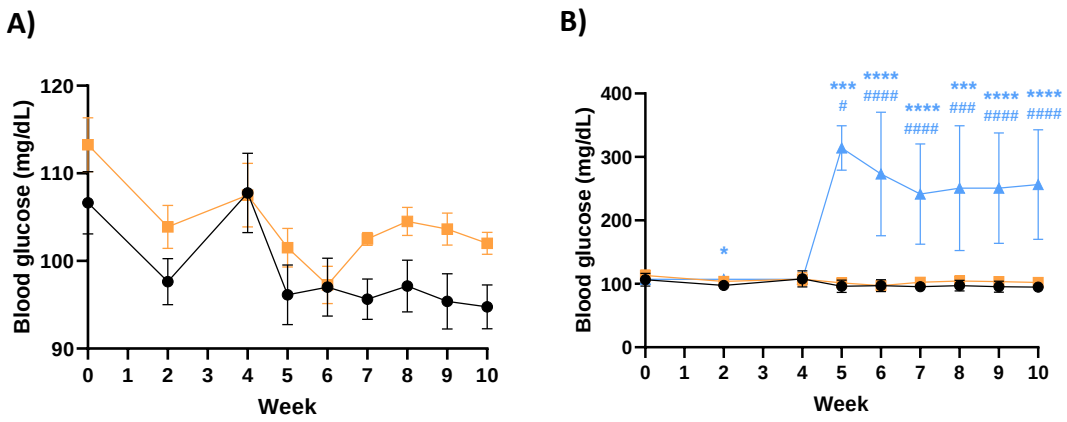

Figure 15. The effect of HFD and STZ on fasting glycaemia.

In contrast to SD and HFD group in which significantly statistical differences were not observed on blood glycaemia (A), in the HFD+STZ group, blood glucose levels reach deleterious concentrations from week 5 to week 10 (B). Statistical analysis obtained through one-way ANOVA test (parametric) and/or Kruskal-Wallis test (non-parametric), mean ±. SEM. n=8; * vs SD; # vs HFD. * $p < 0.05$; ** $p < 0.01$; *** $p < 0.001$.

Obesogenic and type 2 diabetic conditions compromised hippocampal glycaemic homeostasis and metabolism

Concurrent to the blood hyperglycaemia, hippocampal glucose levels were only elevated in the HFD+STZ group, in comparison to the SD group ($p = 0.0072$) (**Figure 16A**). This was supported by Spearman correlation analysis, which exhibited a positive relation between fasting systemic hyperglycaemia and hippocampal glucose levels, both of which were acquired on week 10 ($r = 0.5385$; $p = 0.0383$) (**Figure 16E**). It is, however, noteworthy that ^{1}H-MRS was not sensitive enough to detect several concentrations of glucose in the SD ($n = 3$) and the HFD group ($n = 4$). Nonetheless, the neuronal glucose transport did not seem to be hampered, given the absence of statistically significant levels' modifications of the insulin-independent GLUT3, which is the most expressed isoform of these transporters in neurons[148] (**Figure 16B**).

Due to the unmodified protein levels of IR-T (**Figure 16C**) and p-IR, the active form of this receptor (**Figure 16D**), and considering the characteristic non-dependence of GLUT3 on insulin[148], it would be expected that insulin activity did not affect glucose levels in the hippocampus. Spearman correlation analysis showed otherwise. While insulin activity evaluated by ITT performed on week 10 was positively influencing glucose levels ($r = 0.5360$; $p = 0.0394$) (**Figure 16F**), plasma insulin was negatively correlated with the monosaccharide levels ($r = - 0.7669$; $p = 0.0008$) (**Figure 16G**).

Hippocampus

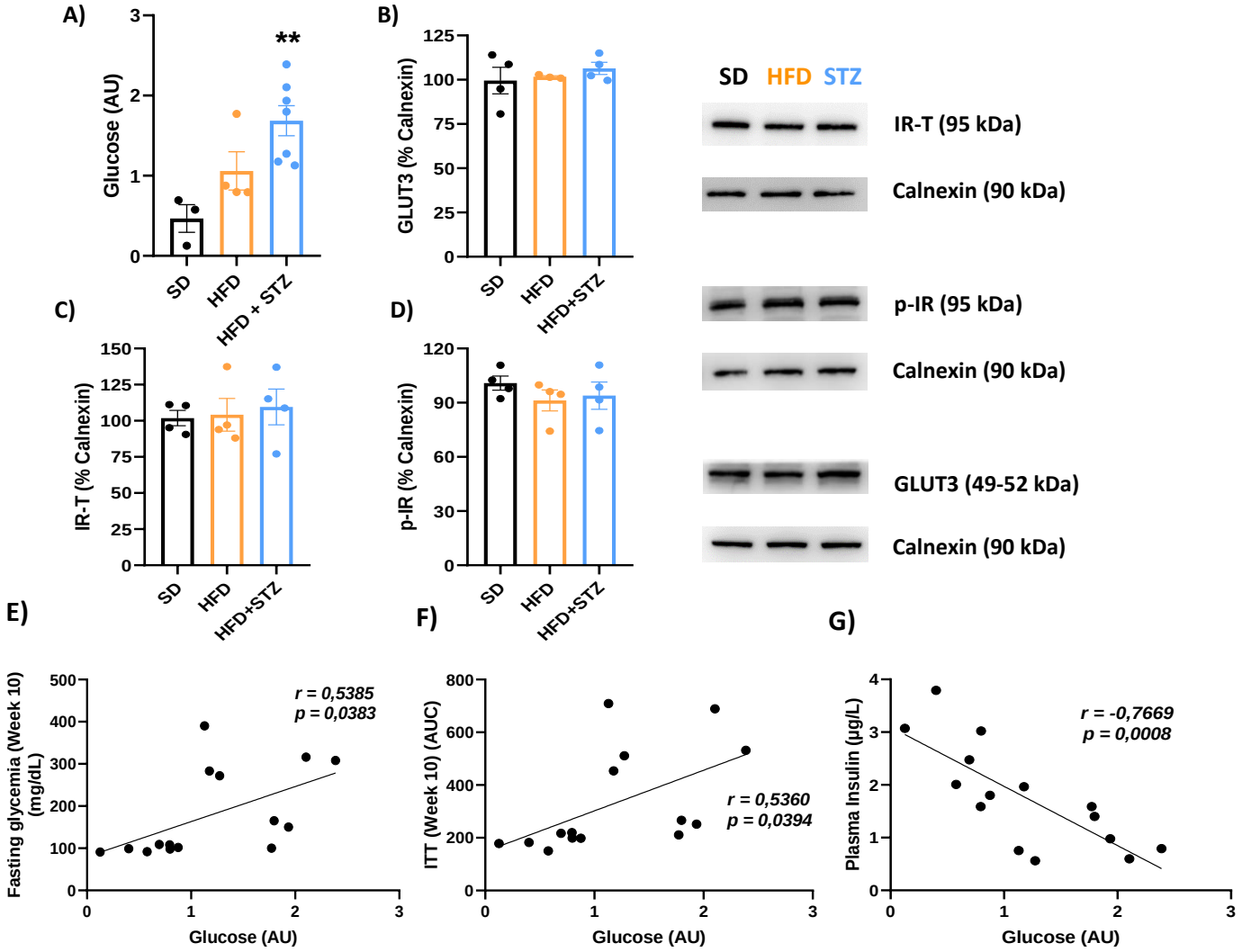

Figure 16. Insulin sensitivity and glucose metabolism in the hippocampus.

Hippocampal glycaemia peaked in the HFD+STZ group (A), despite the non-affected neuronal glucose transport mediated by GLUT3 (B). Meanwhile, insulin seemed not significantly conditioned as assessed through the total (C) and phosphorylated form (active) of the IT (D). Glucose levels, in this brain area did not only correlate with fasting glycemia on week 10 (E), but also with insulin activity (ITT) (F) and levels (G). Statistical analysis obtained through one-way ANOVA test (parametric) and/or Kruskal-Wallis test (non-parametric), mean ±. SEM. n=8 for magnetic resonance spectroscopy, n=4 for Western blot; * vs SD; # vs HFD. * $p < 0.05$; ** $p < 0.01$; *** $p < 0.001$. Correlations were calculated through Pearson correlation analysis.

Simultaneously, in the obese model group, Ala levels were lower than the control group (p = 0.0449). These were, then, tendentially restored in HFD+STZ group (p = 0.0637) (**Figure 17A**). Similar to the latter metabolite, Asp is involved in Glu formation in a Glu dehydrogenase-mediated reaction. Nonetheless, despite Ala levels being affected, Asp concentration in the hippocampus was not altered in none of the groups (**Figure 17B**).

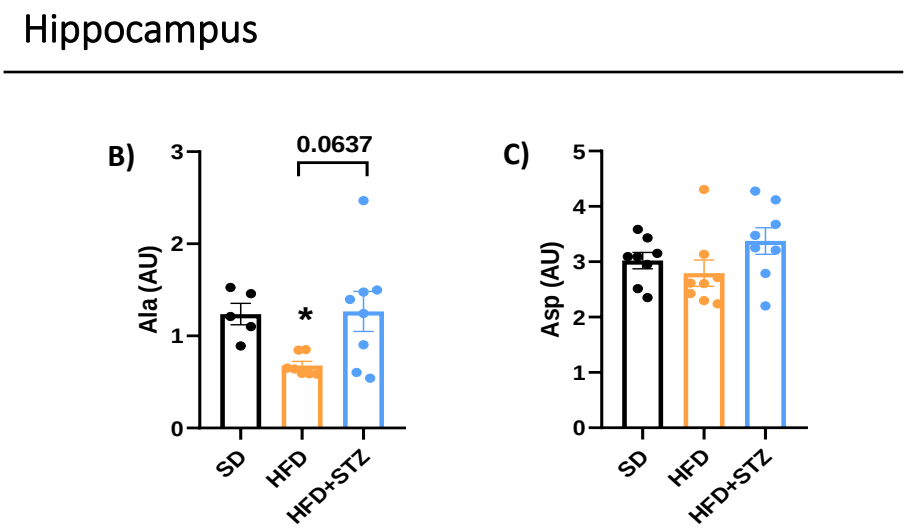

Figure 17. Effect of HFD and STZ on the substrates of Glu synthesis.

While Ala levels were diminished in the HFD group which is followed by a tendency to restoration (A), Asp levels were not affected (B). Statistical analysis obtained through one-way ANOVA test (parametric) and/or Kruskal-Wallis test (non-parametric), mean ±. SEM. n=8 for magnetic resonance spectroscopy, n=4 for Western blot; * vs SD; # vs HFD. * $p < 0.05$; ** $p < 0.01$; *** $p < 0.001$. Correlations were calculated through Pearson correlation analysis.

Obese and T2DM models did not promote the formation of AGE nor the establishment of oxidative stress in the hippocampus

Hyperglycaemia commonly induces (1) the formation of AGE[149] and (2) the onset of oxidative stress potentiated by a higher mitochondrial respiration rate (not evaluated in this manuscript) and AGE-activated mechanisms. Since both are involved in diabetic complications[150], we firstly aimed to investigate whether the hyperglycaemic conditions instigated these hallmarks. We started by evaluating protein adducts formed by

methylglyoxal (MG), a cytotoxic subproduct of glycolysis, which included ArgPyr (**Figure 18A**) and MG-H1 (**Figure 18B**) that were not statistically different among the groups. Accordingly, Glo-1, an ubiquitous cellular enzyme involved in the MG detoxification[151], and its levels did not alter significantly (**Figure 18C**).

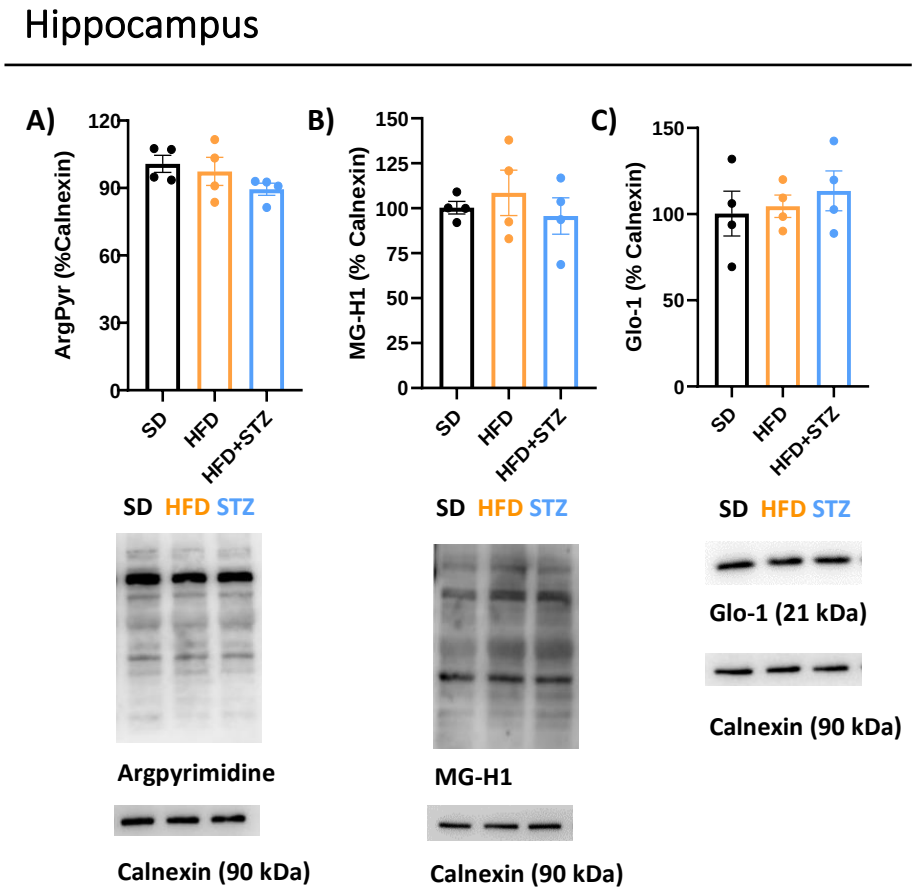

Figure 18. Hippocampal glycation on the obese and T2DM animal models.

Despite the elevated hyperglycemia in 3rd designed groups, ArgPyr (A) and MG-H1 (B), both of which are AGE, were not overly synthesized. Accordingly, Glo-1, an enzyme involved in the MG detoxification and consequently MG-induces AGE, levels did not alter significantly between the 3 groups (C). Statistical analysis obtained through one-way ANOVA test (parametric) and/or Kruskal-Wallis test (non-parametric), mean ±. SEM. n=4 for Western blot; * vs SD; # vs HFD. * $p < 0.05$; ** $p < 0.01$; *** $p < 0.001$.

In turn, among others, AGE promote ROS formation[149]. As a response to the latter generation and consequent deleterious event, antioxidant defences are recruited. These included GSH, an antioxidant defence that prevents ROS-induced cellular

death[152]; catalase, an enzyme that catalyses hydrogen peroxide into non-toxic molecules (water and oxygen)[153]; and HO-1, an enzyme that catalyses heme breakdown[154]. While the latter two molecules were found to not be significantly altered (**Figure 19B and 19C,** respectively), GSH was increased in the HFD group in comparison to the SD group (p = 0.0449). Likewise, through the evaluation of Nitrotyr, which results from the reaction of RNS and tyrosine[155], it was indirectly concluded that RNS were not altered in any group. However, a tendency to its increment was observed in the HFD group (p = 0.0930, vs SD) (**Figure 19D**).

Hippocampus

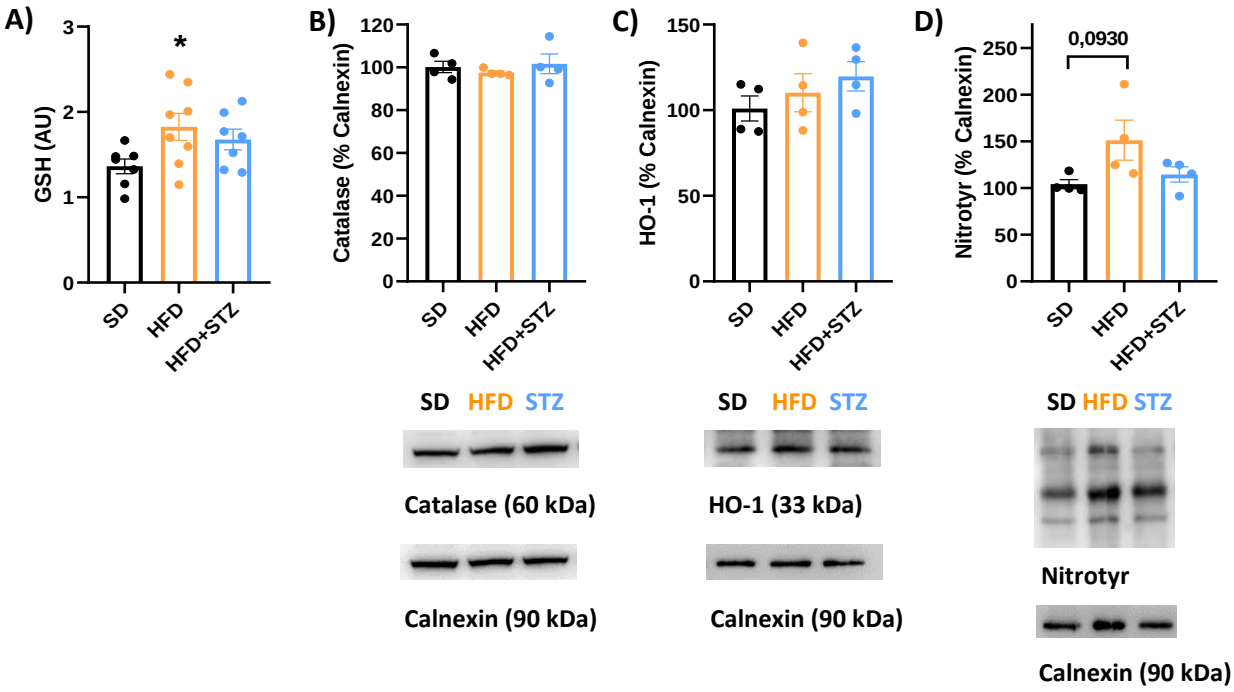

Figure 19. Hippocampal oxidative stress on the obese and T2DM animal models.

While GSH (A) showed to be enhanced in the HFD group, different antioxidant defences, including catalase (B) and HO-1 (C), were not modified. Likewise, Nitrotyr levels (D) show that RNS levels did not reach statistical significance. Statistical analysis obtained through one-way ANOVA test (parametric) and/or Kruskal-Wallis test (non-parametric), mean ±. SEM. n=8 for magnetic resonance spectroscopy, n=4 for Western blot; * vs SD; # vs HFD. * $p < 0.05$; ** $p < 0.01$; *** $p < 0.001$.

In the hippocampus, obesity promoted a possible compensatory mechanism, involving N-acetylasptartylglutamic acid (NAAG) and GSH

Given the metabolic alterations previously observed, we hypothesized whether the glutamatergic and/or GABAergic synapses were compromised. The levels of the excitatory neurotransmitter were unaltered in the 3 groups designed for this project (**Figure 20A**), However, hippocampal glucose levels in the designed models were not correlated with Glu (r = - 0.08938, p = 0.7514) (**Figure 20G**). In contrast, Gln levels, ie the primary substrate in Glu synthesis, tended to increase in HFD group (p = 0.0769, vs SD group), while, in the HFD+STZ group, an increment was indeed observed, when compared to the control model (p = 0.0088) (**Figure 20B**). Although the evaluation of Glut. C and its unchanged expression (**Figure 20F**) would suggest that Gln was not being converted into Glu, a Spearman correlation analysis demonstrated otherwise (r = 0.4945, p = 0.0140) (**Figure 20I**). Interestingly, Gln levels in the hippocampus were negatively correlated with plasma insulin (r = - 0.4056, p = 00493) (**Figure 20H**). Altogether, Glx pool, which composes the total concentration of Gln and Glu, were enhanced in the HFD+STZ group, in comparison to SD (p = 0.0073) and HFD group (p = 0.0368) (**Figure 20C**). Furthermore, the expression of vGLUT, a protein involved in the vesicular Glu transport, remained unaltered (**Figure 20E**), revealing a sustained pre-synaptic activity[156,157]. Accordingly, a consequent unmodified excitatory activity was corroborated by the evaluation of the Glu/GABA ratio[158] (**Figure 20D**).

Hippocampus

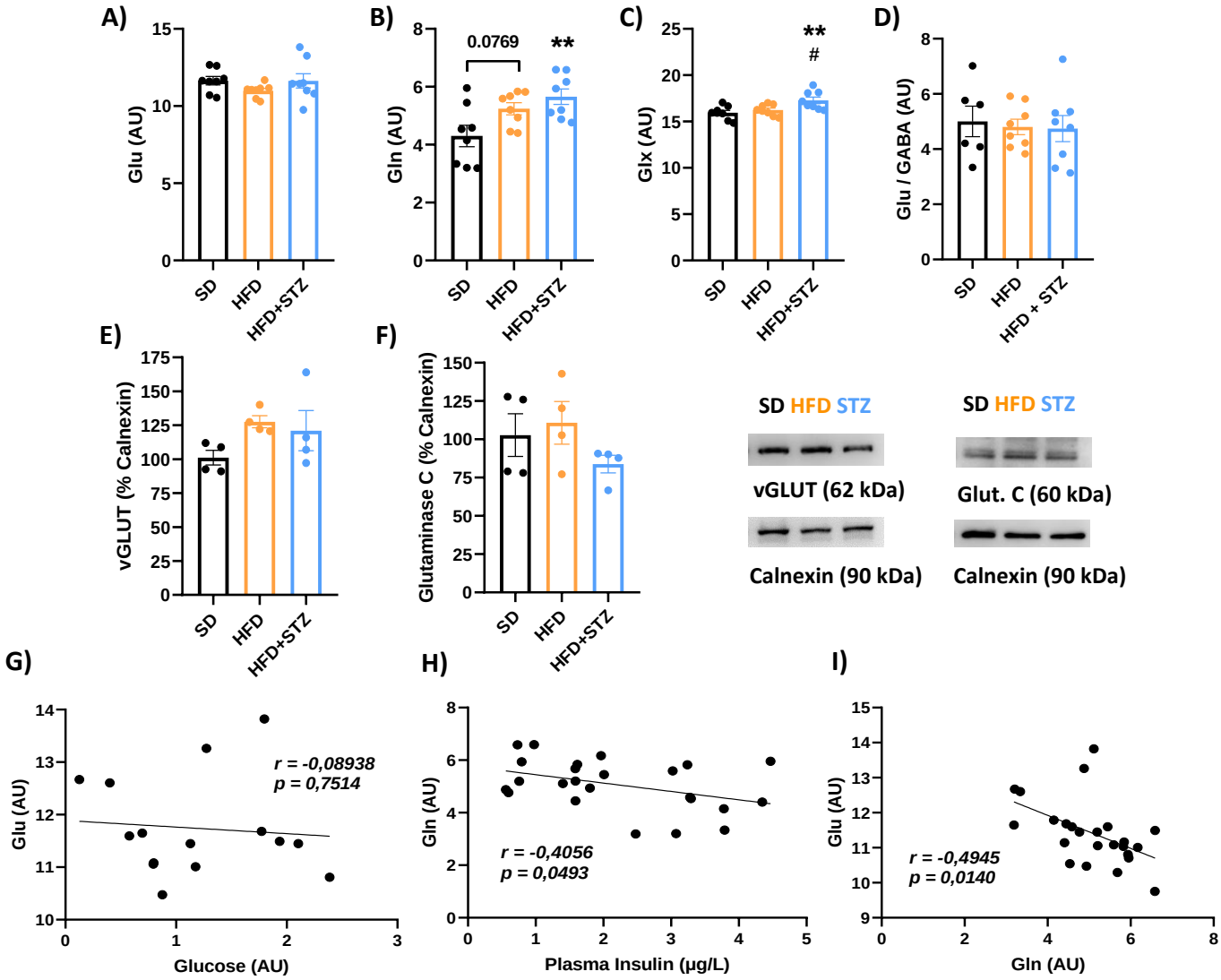

Figure 20. Glutamatergic pool increased in the hippocampus of diabetic rats and related to plasma insulin levels.

Although Glu was not altered (A), its main substrate Gln (B) and Glx pool (C) were augmented in T2DM conditions. Such resulted in a sustained Glu/GABA ratio (D) and vesicular glutamate transport as given by vGLUT (E). This data is usually translated in a stable excitatory activity. However, Glut. C showed similar levels (F). Furthermore, while Glu was not with hippocampal glucose levels (G), Gln was shown to be negatively correlated with Glu (H) and with plasma insulin (I). Statistical analysis obtained through one-way ANOVA test (parametric) and/or Kruskal-Wallis test (non-parametric), mean ±. SEM. n=8 for magnetic resonance spectroscopy, n=4 for Western blot; * vs SD; # vs HFD. * $p < 0.05$; ** $p < 0.01$; *** $p < 0.001$. Correlations were calculated through Pearson correlation analysis.

In agreement with the apparently sustained excitatory synaptic activity, GABA levels, the main inhibitory neurotransmitter, were unaltered among the 3 groups (**Figure 21A**). Furthermore, the levels of $GABA_AR$, which constitutes the most expressed isoform of this receptor (**Figure 21B**), and vGAT, a protein involved in vesicular GABA transport (**Figure 21C**) were also unmodified. These results suggest revealing a sustained pre-synaptic inhibitory activity. In contrast, NAAG levels, an abundant dipeptide that negatively modulates the glutamatergic synapse[159], was augmented in the HFD group ($p = 0.0037$, vs SD group). In turn, the latter levels were downregulated in the T2DM model group ($p = 0.0365$) (**Figure 21D**). Interestingly, a similar levels' variation pattern of NAAG (**Figure 21D**) and GSH (**Figure 21A**) suggested a correlation, which led to their evaluation and confirmation through a Spearman correlation analysis ($r = 0.4652$, $p = 0.0336$) (**Figure 21E**).

Hippocampus

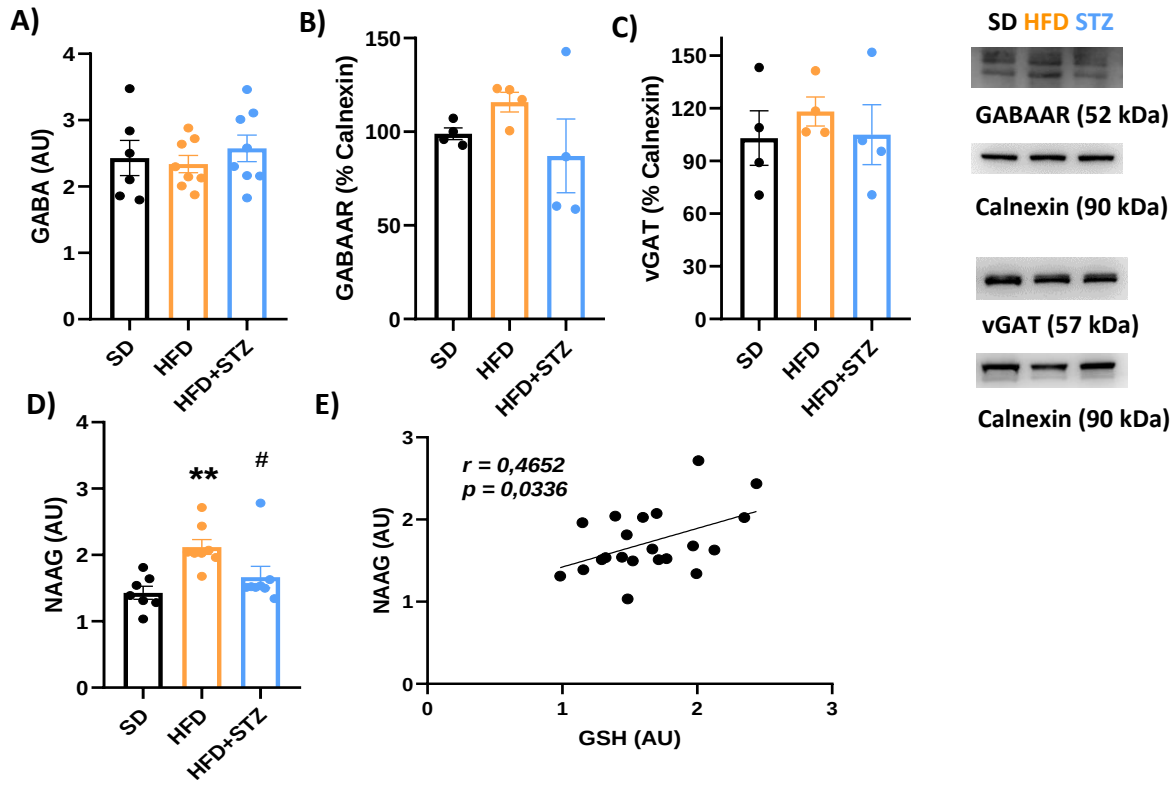

Figure 21. A possible compensatory mechanism involving NAAG and GSH in the hippocampus of obese but not diabetic rats.

GABA levels were not modified significantly (A). Likewise, the inhibitory activity potentiated by $GABA_AR$ (B), and the vesicular transport mediated by vGAT (C) were not compromised. In contrast, a secondary inhibitory neurotransmitter, NAAG, was increased in an obesogenic environment (F). The latter showed a positive correlation with GSH (E). Statistical analysis obtained through one-way ANOVA test (parametric) and/or Kruskal-Wallis test (non-parametric), mean ±. SEM. n=8 for magnetic resonance spectroscopy, n=4 for Western blot; * vs SD; # vs HFD. * $p < 0.05$; ** $p < 0.01$; *** $p < 0.001$. Correlations were calculated through Pearson correlation analysis.

The NAAG-GSH-involving mechanism preceded structural alterations in the hippocampus

Once this neurometabolic pattern was observed in obesogenic conditions and given that the main objective of this project was to detect early biomarkers of neurological conditions, we proceeded to investigate in which stage of the neurological condition these variations take place. Through the evaluation of N-acetylaspartate (NAA) levels, a marker of neuronal viability[160] and a substrate of NAAG formation[159], it was observed an overall sustained structural integrity (**Figure 22A**). Possibly neurotoxic proteins were not significantly formed, preserving hippocampal viability. Such include not only tau protein which, once excessively or abnormally phosphorylated, form neurofibrillary tangles, disrupting neuron's transport system and consequent hampered synaptic activity (**Figure 22B**)[161]; but also APP, which, once cleaved into beta-amyloid and consequently forming amyloid oligomers channels, disrupts calcium homeostasis and promotes synaptic degeneration (**Figure 22C**)[162]. The production of both protein clusters has been shown to be potentiated by p-GSK3β activity which, in turn, is phosphorylated by Akt. Accordingly, both enzymes did not reach significant variation levels between the groups (**Figure 22E and 22D,** respectively). Although tau protein was not correlated with plasma insulin ($r = -0.3277$, $p = 0.1180$) (**Figure 22G**), correlation analysis revealed the protein levels were correlated with ITT i.e., insulin sensitivity (week 10) ($r = 0.5454$, $p = 00058$) (**Figure 22H**). Taking this into consideration, it is understandable the non-variable levels of these proteins given the apparently preserved insulin sensitivity in the hippocampus, as previously mentioned. On a similar note, fasting glycemia on week 10 was also shown to be correlated with tau protein ($r = 0.5223$; $p = 0.0088$) (**Figure 22F**).

Hippocampus

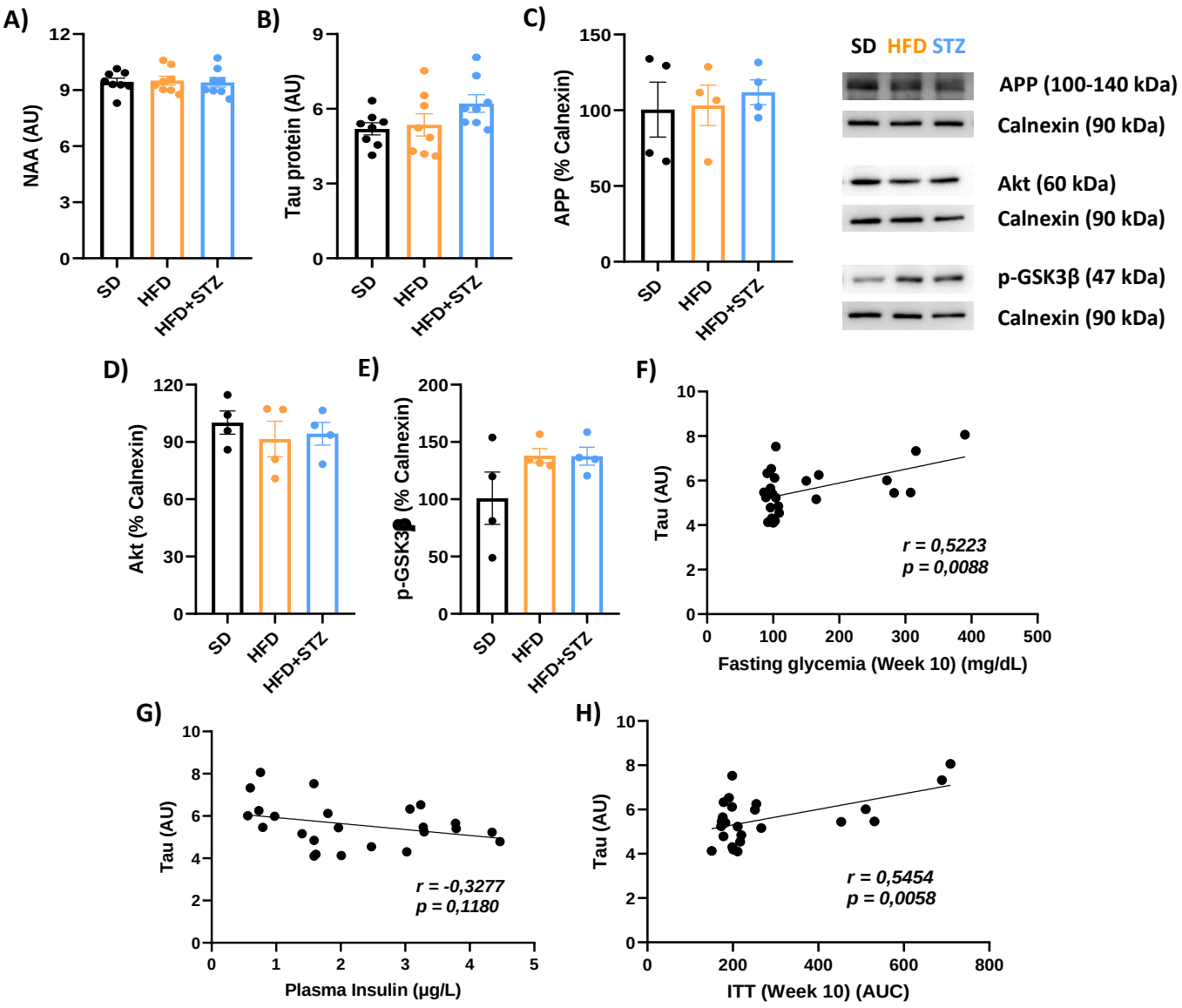

Figure 22. The hippocampal cellular viability was not hindered.

The seemingly identical NAA levels (A) encode an intact cellular viability, possibly due to the non-significant alterations of total tau protein (B) and APP (C). Such might rise from an unaffected insulin sensitivity, which resulted in equivalent levels of Akt (D) and p-GSK3β (E). Interestingly, although tau protein levels were not related with plasma insulin (G), these were with fasting glycemia on week 10 (F) and ITT on week 10 (H). Statistical analysis obtained through one-way ANOVA test (parametric) and/or Kruskal-Wallis test (non-parametric), mean ±. SEM. n=8 for magnetic resonance spectroscopy, n=4 for Western blot; * vs SD; # vs HFD. * $p < 0.05$; ** $p < 0.01$; *** $p < 0.001$. Correlations were calculated through Pearson correlation analysis.

Accordingly, synaptic markers were not significantly altered, including synapsin levels (**Figure 23A**), a membrane protein located on synaptic vesicles with a role in the release of neurotransmitters and cytoskeletal organization given it binds all vesicle types to the actin filaments[163]. We also studied another synaptic marker named PSD-95 which anchors NMDAR in the postsynaptic neuronal membrane, meaning it is specific for excitatory synapses[164]. Similar to synapsin, PSD-95 levels did not reach statistical significance. However, there was a tendency for its increment in the HFD ($p = 0.0887$) and HFD+STZ group ($p = 0.0940$), in comparison to the SD group (**Figure 23B**). Altogether, it was shown a maintained synaptic integrity.

Hippocampus

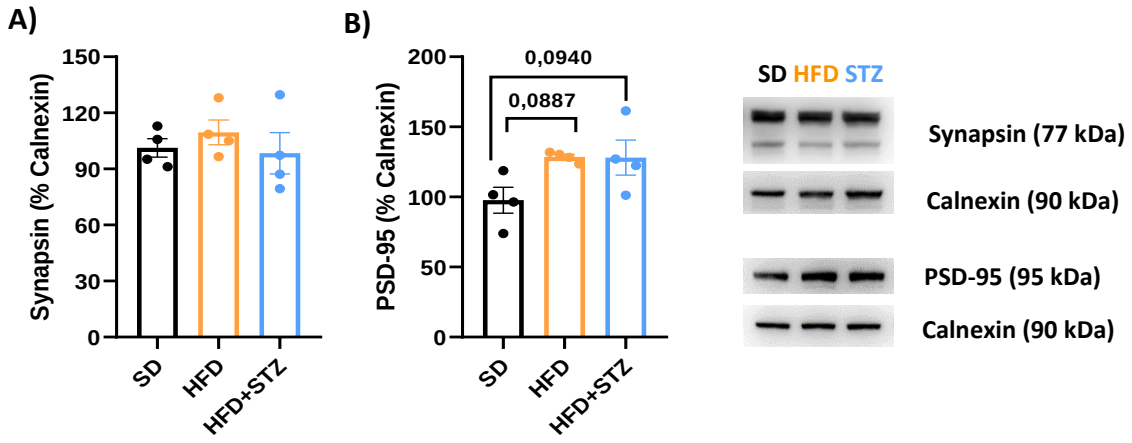

Figure 23. The hippocampal synaptic integrity was not impaired.

Synapsin (A) and PSD-95 (B) levels did not reach statistical significance, showing a sustained synaptic integrity. Statistical analysis obtained through one-way ANOVA test (parametric) and/or Kruskal-Wallis test (non-parametric), mean ±. SEM. n=4 for Western blot; * vs SD; # vs HFD. * $p < 0.05$; ** $p < 0.01$; *** $p < 0.001$. Correlations were calculated through Pearson correlation analysis.

Hyperglycaemia was developed in the visual cortex of T2DM-induced rats

Following the analysis of the hippocampus, we proceeded to evaluate the treatment effects on cerebral metabolism in the visual cortex. Similar to what was observed in the hippocampus, elevated brain glucose levels were only observed in the HFD+STZ group in comparison to the HFD ($p = 0.0005$) and HFD+STZ group ($p = 0.0271$) (**Figure 24A**). The latter was shown to be correlated with fasting glycemia on week 10 ($r = 0.7857$, $p < 0.0001$) (**Figure 24C**). Furthermore, although the correlation between the visual cortex's glucose and plasma insulin did not reach statistical significance ($r = 0.7522$, $p = 0.0511$) (**Figure 24E**), its levels were positively correlated with insulin activity on week 10 ($r = 0.7437$, $p = 0.0003$) (**Figure 24D**). However, through the evaluation of IR-T and its unaltered expression, insulin sensitivity in the visual cortex seemed to be maintained (**Figure 24B, representative WB on the left side of the figure**).

Visual Cortex

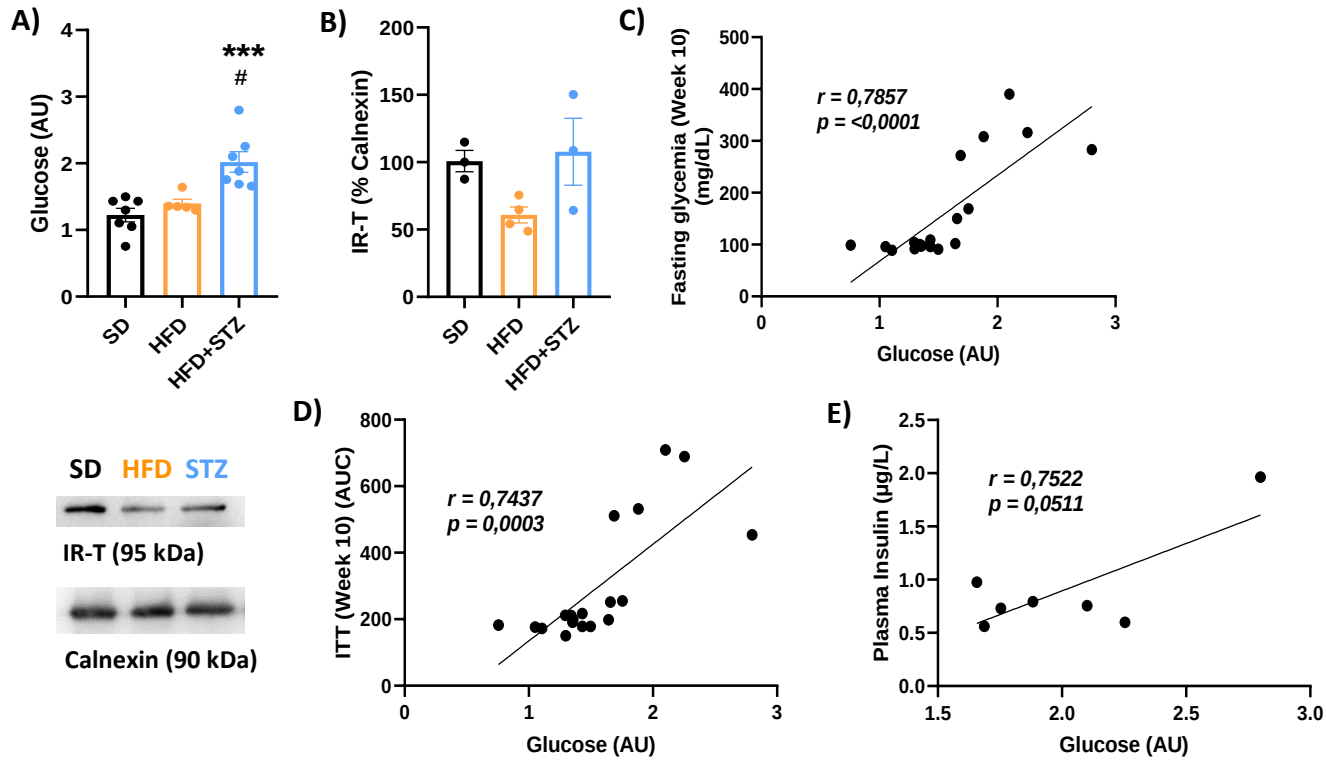

Figure 24. Hyperglycemia was promoted in the visual cortex of STZ-injected rats.

Glucose levels (A) were only augmented in the visual cortex of the T2DM group. In contrast, the expression of IR-T (B) did not reach statistically significant variations. In this brain region, cerebral glucose levels were correlated with the fasting glycemia on week 10 (C), the ITT performed on week 10 (D), and, lastly, a correlative tendency with plasma insulin (E). Statistical analysis obtained through one-way ANOVA test (parametric) and/or Kruskal-Wallis test (non-parametric), mean ±. SEM. n=8 for magnetic resonance spectroscopy, n=4 for Western blot; * vs SD; # vs HFD. * $p < 0.05$; ** $p < 0.01$; *** $p < 0.001$. Correlations were calculated through Pearson correlation analysis.

Meanwhile, the levels of substrates involved in glutamate synthesis, including Ala (**Figure 25A**) and Asp (**Figure 25B**), remained unaltered.

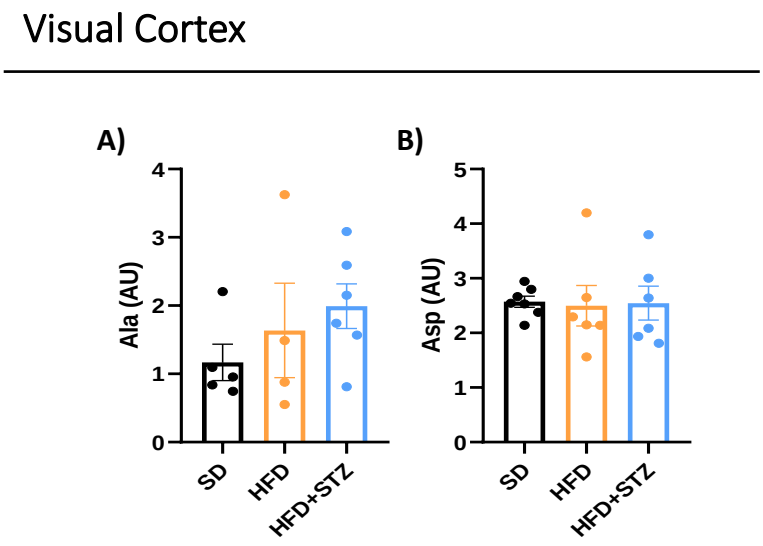

Figure 25. Glu synthesis' substrates were not altered in the visual cortex.

In the visual cortex, amino acids involved in Glu synthesis, namely Ala (A) and Asp (B) were unaltered. Statistical analysis obtained through one-way ANOVA test (parametric) and/or Kruskal-Wallis test (non-parametric), mean ±. SEM. n=8 for magnetic resonance spectroscopy; * vs SD; # vs HFD. * $p < 0.05$; ** $p < 0.01$; *** $p < 0.001$.

Glycation and oxidative stress were not promoted in the visual cortex

Similar to the hippocampus, protein adducts resulting of glucose reactivity, which contribute to a possible oxidative stress, remained unaltered through the different groups, including ArgPyr (**Figure 26A**) and MG-H1 (**Figure 26B**). In concordance, the enzyme involved in their detoxification, Glo-1, was also found to not be altered (**Figure 26C**).

Visual Cortex

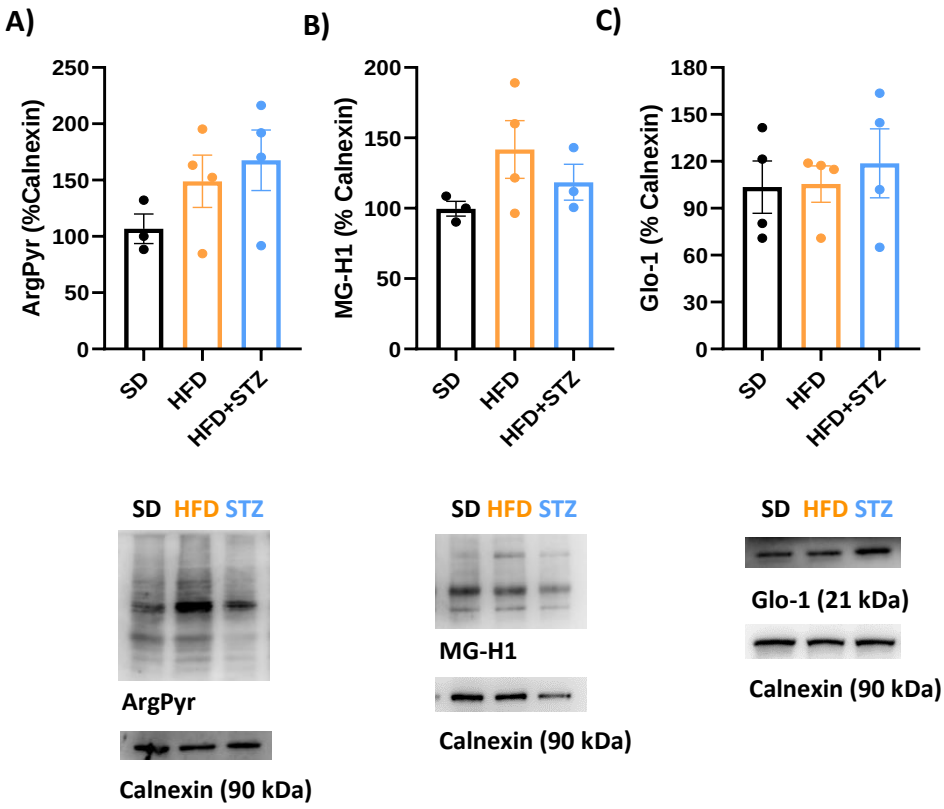

Figure 26. Deleterious events involving glycation were not observed in the visual cortex.

Despite hyperglycemia in the visual cortex being observed in the HFD+STZ group, no variation regarding the glycation products was verified, including in ArgPyr (A) and MG-H1 (B). In concordance with the lack of significant AGE' variance, Glo-1 levels (C) were not altered either. Statistical analysis obtained through one-way ANOVA test (parametric) and/or Kruskal-Wallis test (non-parametric), mean ±. SEM. n=4 for Western blot; * vs SD; # vs HFD. * $p < 0.05$; ** $p < 0.01$; *** $p < 0.001$.

Resorting to the DHE probe, we were able to indirectly assess the levels of superoxide anion and hydrogen peroxide. DHE is an uncharged compound, which, due to its hydrophobicity, crosses extracellular and intracellular cells i.e., plasmatic membrane and nuclear membrane, respectively. Upon its exposure to the previous ROS, DHE is oxidized and converted into a positively-charged and fluorescent molecule

named ethidium. The latter intercalates with the DNA through electrostatic interactions with the phosphate groups and hydrophobic interactions. Consequently, it is accumulated in the cell, enabling its measurement[165,166]. Nonetheless, despite of the unfavourable hallmarks of obesity and T2DM, HFD and HFD+STZ group did not show variable levels of these specific ROS (**Figure 27**).

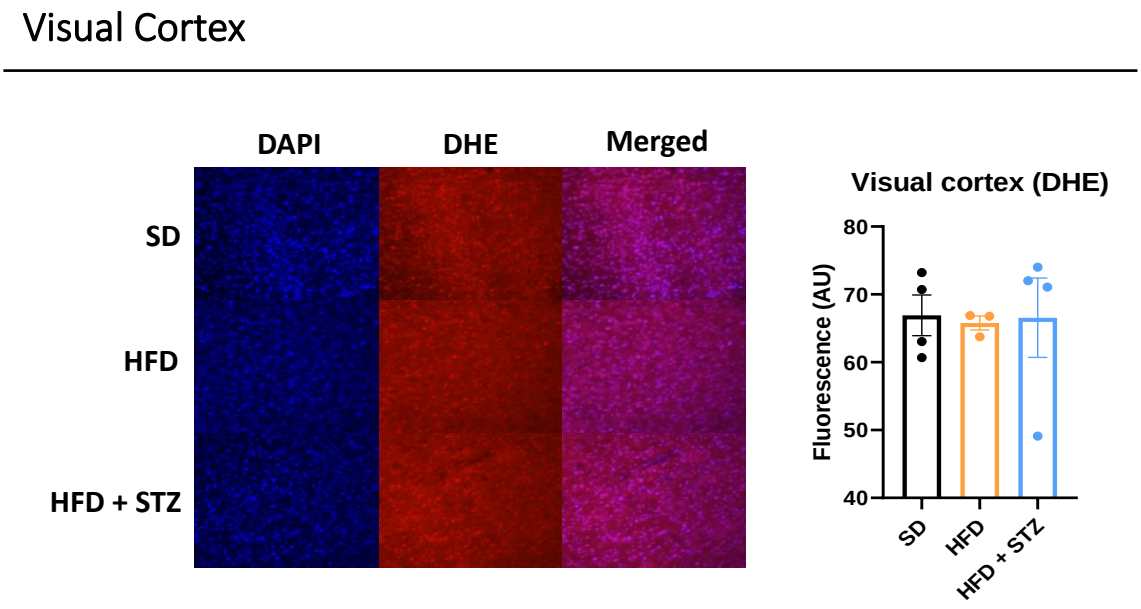

Figure 27. The HFD feeding and/or STZ administration did not generate superoxide anion or hydrogen peroxide.

Through the probing the visual cortex with DHE, we indirectly quantified superoxide anion and hydrogen peroxide. A difference on their levels was not observed in any of the groups. Statistical analysis obtained through one-way ANOVA test (parametric) and/or Kruskal-Wallis test (non-parametric), mean ±. SEM. n=4 for immunohistochemistry; * vs SD; # vs HFD. * $p < 0.05$; ** $p < 0.01$; *** $p < 0.001$.

In concordance, antioxidant defences, including catalase (**Figure 28B**) and HO-1 (**Figure 28C**), did not reach statistically significance. However, GSH tended to be decreased in HFD+STZ group in comparison to the HFD group ($p = 0.0577$) (**Figure 28A**), possibly as an initial indicator of antioxidant defences imbalance and consequent oxidative stress' onset. Likewise, through the assessment of Nitrotyr expression, we indirectly exhibited a non-statistically significant variability of RNS (**Figure 28D**). It is

noteworthy that the results regarding the visual cortex are more variable, since it is a brain area with a particularly small volume in the Wistar rats' brain. Such interfered with the success of the visual cortex extraction, which led to the collection of other surrounding brain areas.

Visual Cortex

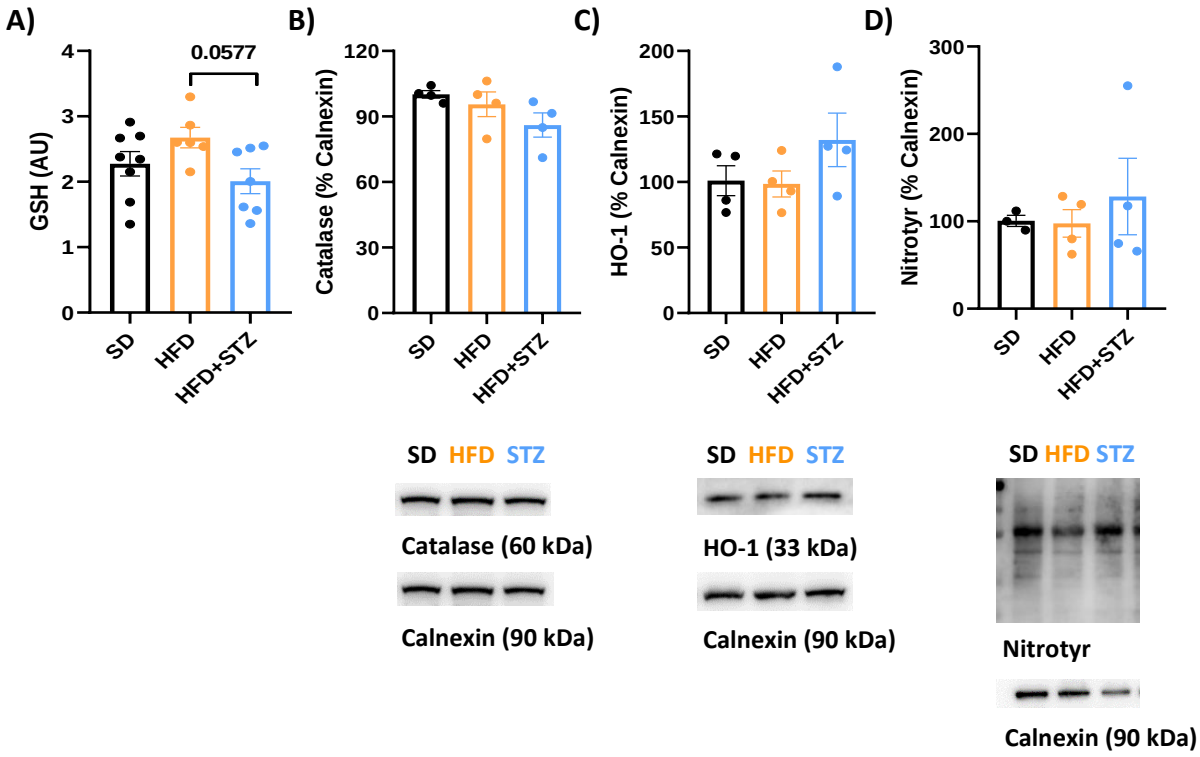

Figure 28. Detrimental events involving oxidative stress were not detected in the visual cortex.

In contrast to the GSH imbalance (A), other antioxidant defences, such as catalase (B) and HO-1 (C) were not altered. Likewise, Nitrotyr (D) levels also remained unchanged between groups. Statistical analysis obtained through one-way ANOVA test (parametric) and/or Kruskal-Wallis test (non-parametric), mean ±. SEM. n=8 for magnetic resonance spectroscopy, n=4 for Western blot; * vs SD; # vs HFD. * $p < 0.05$; ** $p < 0.01$; *** $p < 0.001$.

The NAAG-GSH paradigm was not observed in the visual cortex of obese rats

In agreement with the unchanged levels of Ala and Asp, Glu levels were not significantly changed (**Figure 29A**). The synthetic mechanism involving both these metabolites is coupled with the conversion of oxaloacetate, which results from glucose conversion. Given so and in concordance with the unchanged levels of the substrates, Glu levels were not correlated with brain glucose levels ($r = 0.1644$, $p = 0.5013$) (**Figure 29F**). Meanwhile, the major substrate involved in the formation of this excitatory neurotransmitter was overconcentrated in the HFD+STZ group, when compared to the SD group ($p = 0.0252$) (**Figure 29B**), which resulted in an augmented Glx pool in the same group ($p = 0.0494$) (**Figure 29C**). Through Pearson correlation analysis, this Gln variation was shown to be negatively correlated with plasma insulin ($r = - 0.4715$, $p = 0.0200$) (**Figure 29I**). Interestingly, although the expression of Glut. C was increased or tending to in the HFD ($p = 0.0246$) and the HFD+STZ group ($p = 0.0613$), respectively, in relation to the SD one (**Figure 29E**), the Glu levels were not correlated with the Gln ones ($r = - 0.02117$, $p = 0.9218$) (**Figure 29G**). Altogether, a seemingly sustained excitatory activity was observed, given the evaluated by the Glu/GABA ratio (**Figure 29D**).

Visual Cortex

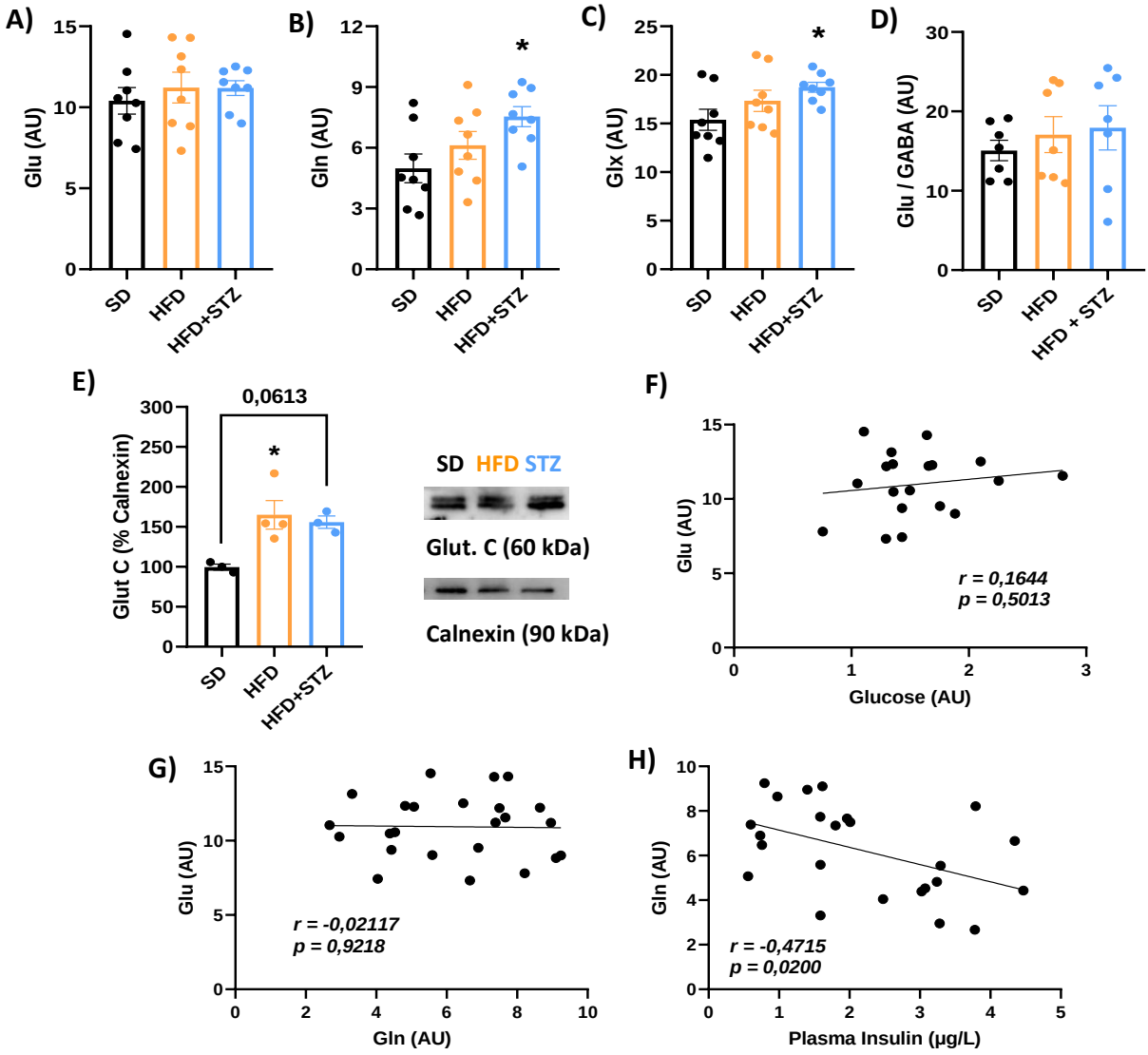

Figure 29. A excitatory synaptic imbalance was not observed in the visual cortex despite some insulin-related neurometabolic changes.

Although Glu (A) levels were shown to not be significantly changed between the groups, Gln (B) and consequently the Glx pool (C) exhibited increments in the HFD+STZ group. In agreement with the maintained excitatory neurotransmitter's concentration, the Glu/GABA ratio (D), a measure representative of synaptic strength, was not modified. However, despite there not being Glu variations, Glut. C (E) levels were elevated or tending to be in obese and T2DM rats, respectively. Pearson correlations showed that Glu levels were not with cerebral glucose in the visual cortex (F), nor was Glu and Gln concentrations (G). In contrast, this analytic method exhibited a correlation between Gln levels located in the visual cortex and plasma insulin (H).

Statistical analysis obtained through one-way ANOVA test (parametric) and/or Kruskal-Wallis test (non-parametric), mean ±. SEM. n=8 for magnetic resonance spectroscopy, n=4 for Western blot; * vs SD; # vs HFD. * $p < 0.05$; ** $p < 0.01$; *** $p < 0.001$. Correlations were calculated through Pearson correlation analysis.

The latter synaptic activity's maintenance was further contributed by the non-significantly variation of GABA levels (**Figure 30A**) and $GABA_AR$ expression (**Figure 30C**). Likewise, other inhibitory neurotransmitters, such as NAAG, were not significantly altered (**Figure 30B**). Consequently, and in contrast to what was observed in the hippocampus, a correlation between NAAG and GSH in the visual cortex was not found ($r = -0.2111$, $p = 0.3857$) (**Figure 30D**).

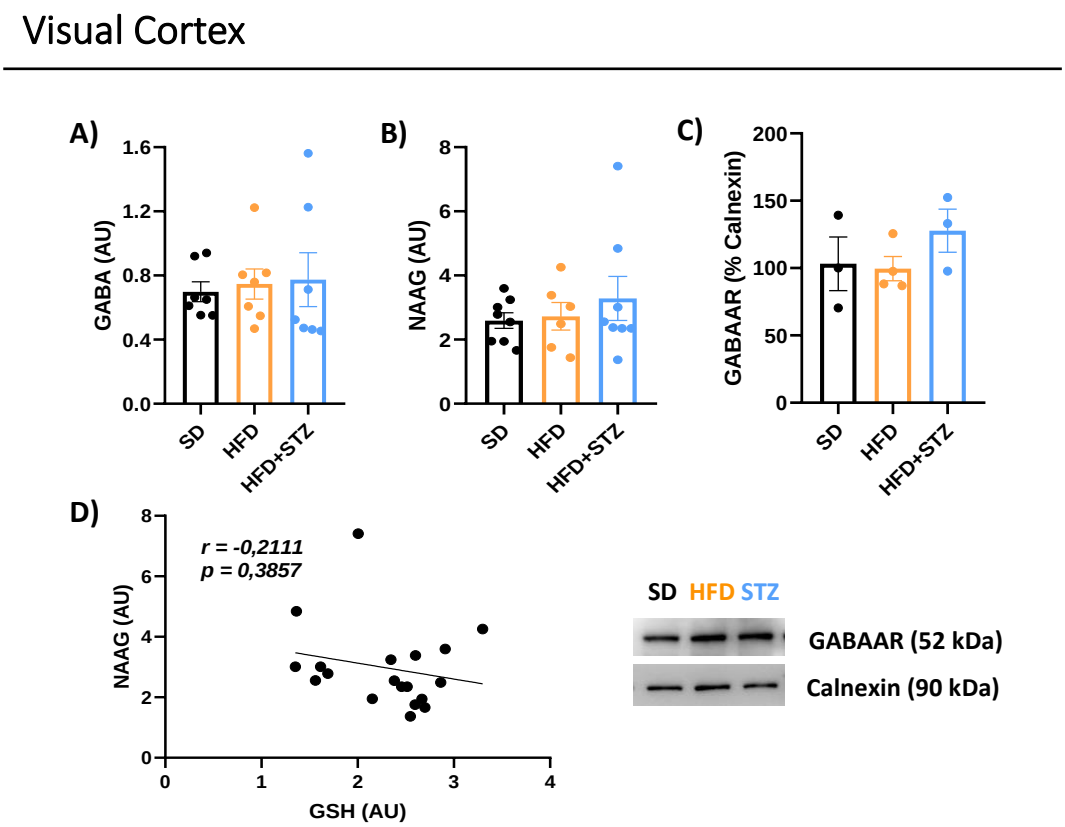

Figure 30. An inhibitory synaptic imbalance was not detected in the visual cortex.

GABA (A) levels were not statistically affected. Likewise, and in contrast to the hippocampus, a secondary inhibitory neurotransmitter, NAAG (B), did not present altered levels either. Accordingly, in regards of the $GABA_AR$ (C), its levels were not altered. Pearson analysis showed no significant correlation between NAAG and GSH. Statistical analysis obtained through one-

way ANOVA test (parametric) and/or Kruskal-Wallis test (non-parametric), mean ±. SEM. n=8 for magnetic resonance spectroscopy, n=4 for Western blot; * vs SD; # vs HFD. * $p < 0.05$; ** $p < 0.01$; *** $p < 0.001$. Correlations were calculated through Pearson correlation analysis.

Cellular viability of the visual cortex was not compromised in the obese nor the T2DM models

Through the assessment of NAA levels, it was concluded that the overall integrity of the visual cortex was preserved throughout the designed groups (**Figure 31A**). Although APP levels were not altered (**Figure 31C**), total tau protein levels were elevated or tending to in the HFD+STZ group, when comparison to the HFD ($p = 0.0326$) and the SD group ($p = 0.0863$), respectively (**Figure 31B**). These potentially neurotoxic levels were correlated with blood glycemia on week 10 ($r = 0.6396$, $p = 0.0014$) (**Figure 31F**). Furthermore, these were yet negatively related to plasma insulin levels ($r = - 0.4751$, $p = 0.0254$) (**Figure 20G**) and positively to insulin sensitivity ($r = 0.6264$, $p = 0.0018$) (**Figure 31H**). However, no changes were observed in proteins downstream in the insulin receptor pathway, including Akt (**Figure 31D**) and p-GSK3β (**Figure 31E**).

Visual Cortex

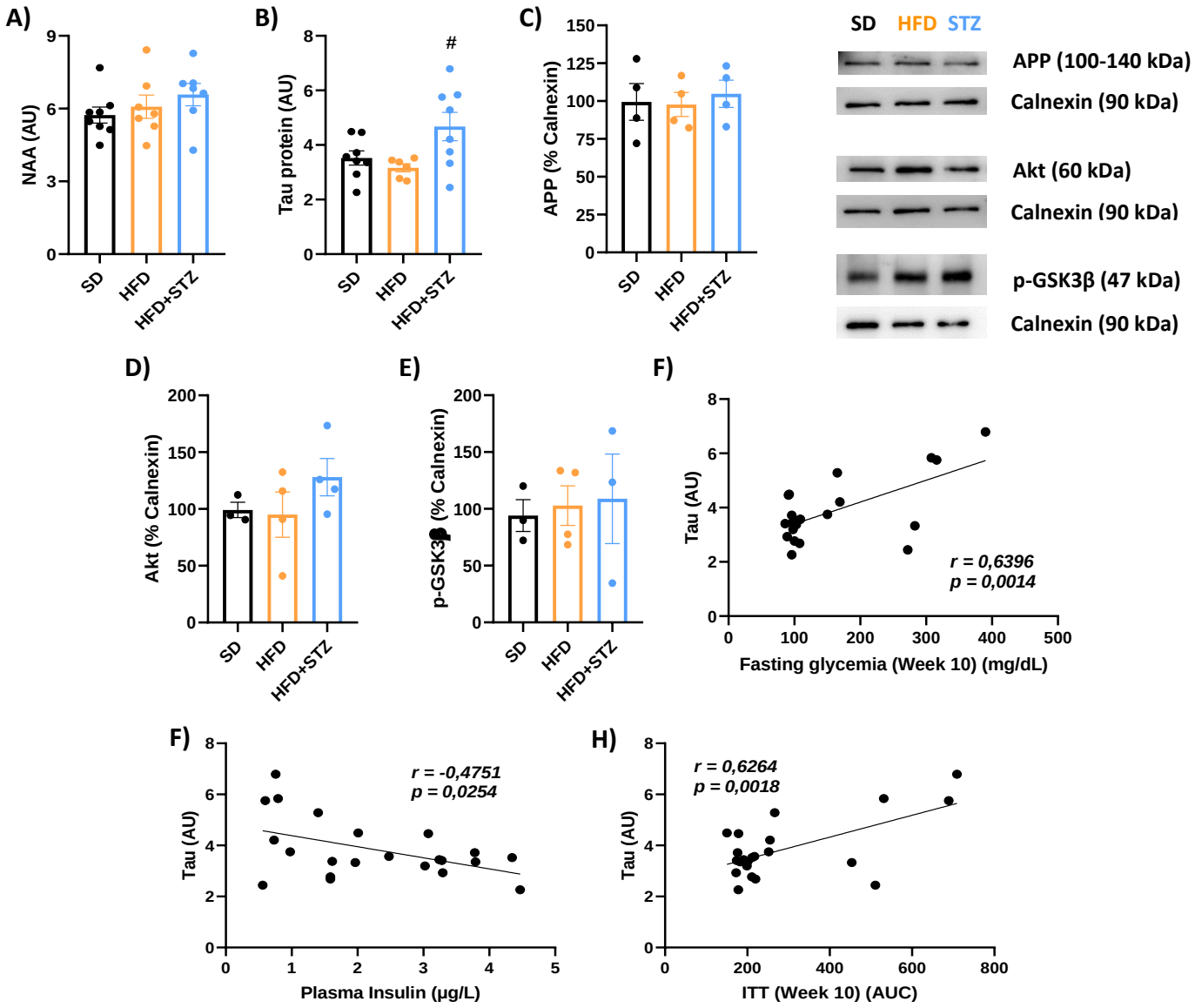

Figure 31. The overall visual cortex integrity was maintained although an insulin-related Tau increase in diabetic rats.

The NAA (A) levels were not significantly altered, suggesting a preservation of cellular integrity. However, total tau protein (B) levels were observed in the HFD+STZ group, in contrast to the APP (C) levels which remained with equivalent concentrations. Although the enzymes modulated by insulin did not exhibit a statistically relevant alteration, including Akt (D) and p-GSK3β (E), tau protein levels were shown to be related with fasting glycemia (F), plasma insulin (G), and ITT performed on week 10 (H). Statistical analysis obtained through one-way ANOVA test (parametric) and/or Kruskal-Wallis test (non-parametric), mean ±. SEM. n=8 for magnetic

resonance spectroscopy, n=4 for Western blot; * vs SD; # vs HFD. * $p < 0.05$; ** $p < 0.01$; *** $p < 0.001$. Correlations were calculated through Pearson correlation analysis.

The HERMES sequence successfully measured GSH levels in the hippocampus and visual cortex, while GABA levels were only valid in the hippocampus

This project used a novel MRS sequence specific for the measurement of both GABA and GSH entitled HERMES sequence. The quality of the obtained MRS data was evaluated by an estimated standard deviation (% SD), which value should be under 30% in order to be considered reliable data[167]. Recurring to this method, we concluded the metabolites' concentrations obtained from both brain regions were valid, in exception for GABA in the visual cortex (**Table 2**).

Table 2. Estimated standard deviation of GABA and GSH measurement in the hippocampus and visual cortex

% SD	SD Group	HFD Group	HFD+STZ Group
GABA (Hippocampus)	22.67 ± 2.51%	23.63 ± 1.78%	21.63 ± 1.29%
GABA (Visual Cortex)	88.50 ± 7.97%	92.71 ± 10.12%	108.71 ± 19.39%
GSH (Hippocampus)	24.14 ± 2.21%	19.50 ± 1.77%	19.71 ± 1.82%
GSH (Visual Cortex)	26.86 ± 2.62%	22.00 ± 0.97%	33.71 ± 4.70%

In concordance, the coherence of the values within the population given by inter-subject coefficient of variance (CV) aligned with the intra-subject signal quality (% SD). Regarding GABA levels, although relatively homogeneous in the hippocampus, the levels' measurement on the visual cortex was hampered. Interestingly, despite the SD group presenting a similar CV value to the ones obtained in the hippocampus (22.91%), the metabolic dysfunctional models prevent a greater CV (HFD: 33.29%; HFD+STZ: 57.33%), even though this neurotransmitter levels do not alter. Simultaneously, the measurement of GSH, which was the innovative tool of this

sequence, showed fairly homogenous CV among groups and brain regions (hippocampus: CV = 23.83%; visual cortex: CV 23.61%) (**Table 3**).

Table 3. Inter-subject coefficient of variance of GABA and GSH measurement in the hippocampus and visual cortex

CV (%)	SD Group	HFD Group	HFD+STZ Group	All groups
GABA (Hippocampus)	26.70	15.67	21.93	20.91
GABA (Visual Cortex)	22.91	33.29	57.33	39.89
GSH (Hippocampus)	16.81	24.66	19.06	23.82
GSH (Visual Cortex)	24.59	14.26	25.05	23.61

However, the accuracy for GABA assessment between the hippocampus and visual cortex was statistically significant (r = 0.5135, p = 0.0245) (**Figure 32A**). While, in contrast, the same was not observed for GSH (r = 03379, p = 0.1570) (**Figure 32B**).

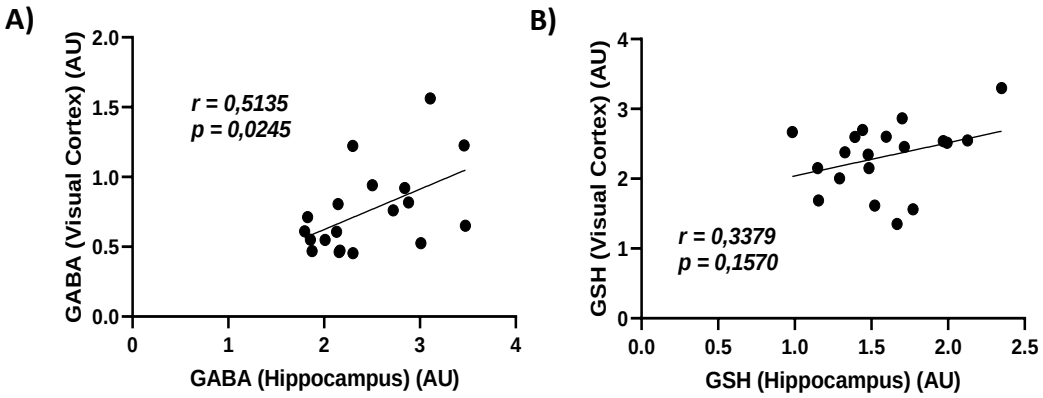

Figure 32. The measurements' accuracy between the hippocampus and the visual cortex.

While GABA levels from the hippocampus showed a positive relation with the levels measured in the visual cortex (A), the opposite occurs for the levels of GSH between the same brain areas (B). Correlations were calculated through Pearson correlation analysis. These were considered statistically relevant when $p < 0.05$.

Discussion

This project aimed to firstly identify early neurometabolic alterations in the hippocampus and the visual cortex of Wistar rats, resorting to a novel ^{1}H-MRS sequence: the HERMES sequence. Following, we proposed to analyse whether the observed alterations could be used as biomarkers for early neurological conditioning in the same model. Although only performed once in the T2DM patients, specifically in the visual cortex[143], other previous studies have quantified GABA levels in different brain regions using Mescher–Garwood Point Resolved Spectroscopy (MEGA-PRESS) during a standardized and relatively prolonged procedure. However, other existing metabolites share the same chemical shift as this inhibitory neurotransmitter, which hinders its quantification[168]. The coexistence of molecules and their assessment is further worsened when measuring metabolites in low concentrations of which GSH is example, which limits the reliably quantified metabolites. These measurements are usually corrected by J-difference editing in which overlying, more concentrated molecules are removed from the spectrum[169]. However, for the later procedure to be successfully performed, only one metabolite can be measured, or at maximum molecules in the vicinity of the chemical shift of the molecule of interest, during the ^{1}H-MRS scan. Meanwhile, the HERMES sequence allows the same editing method used with the MEGA-PRESS sequencing, but for two molecules (or more) simultaneously[144]. As far as our knowledge goes, the HERMES sequence has been used for the simultaneous quantification of GABA and GSH in only two other comparative projects (MEGA-PRESS vs HERMES), both of which in healthy human subjects: (1) in the dorsal anterior cingulate cortex (n = 12)[170] and (2) in the whole brain (n = 8)[171]. Our project was the first one to attempt an optimization of the HERMES sequence in only rats (animal model), aiming to translate its use to individuals with obesity and T2DM. Furthermore, we also pioneered by analysing the hippocampus and visual cortex with this same sequence. In regard to GABA assessment, the hippocampus presented a lower CV and hence more homogenous results than the visual cortex which presented a CV nearly 2 times higher than the memory-involving brain region. Prisciandaro *et al.* measured the same metabolite with a CV equivalent to 16.7%, a coinciding value to the one obtained using

the standardized MEGA-PRESS sequence[170]. Our obtained results in the hippocampus were comparable to the previous project, in contrast to the visual cortex. Meanwhile, another recent study presented a more accurate evaluation. The latter group acquired an improved population variability (CV = 3%) with the HERMES sequence, when compared to the MEGA-PRESS one (CV = 7%)[171]. However, the main obstacle with the HERMES sequence is the not yet optimized GSH quantification. Nonetheless, our results showed similar CV values in the hippocampus (CV = 23.82%) and the visual cortex (CV = 23.61%) between brain areas, and in comparison to the hippocampal GABA determination (CV = 20.91%). While the first paper showed a worsened CV (19%) with the HERMES sequence compared to the MEGA-PRESS (CV = 7.3%)[170], Saleh *et al.* displayed congruent concentration levels in both sequences (CV = 16%)[171]. The obtained difference between our and these projects may arise, among other reasons, from (1) the small volume presented by the distinct rat brain areas than the human ones; (2) greater difficulty to maintain a continuous immobility in rats, which is required for a more precise estimation of the metabolites' concentration; and (3) the use of MRI scanners with different magnetic flux density.

It has been reported that insulin is not necessary for cerebral glucose transport. However, it may facilitate the process[172]. Although higher glucose levels were found in the diabetic group, the process was not compromised by a deficiency of GLUT3, the most expressed isoform of this transporter in the neurons[148]. Instead, the glucose transport may be hampered through other mechanisms, namely the insulin-independent[173] GLUT1 which is expressed in endothelial cells of the BBB, enabling glucose entry into astrocytes[174,175]. Although, considering a correlation between glucose levels in the hippocampus and insulin activity was identified, it is plausible the expression difference may be attributed to GLUT4, an insulin-dependent isoform shown to be present in the hippocampus, among other brain regions[176]. Although no isoform was analysed in the visual cortex, it is likely that a similar scenario is observed in this brain area due to the presence of a relation between insulin activity (assessed by ITT) and glucose levels.

Given the proximity of chemical shifts to GABA and GSH, other metabolites were quantified simultaneously, of which was example the peptide NAAG, a neuromodulator of the glutamatergic synapse composed of NAA and glutamate[159]. The levels of NAAG

were upregulated in the hippocampus of HFD-fed rats, similarly to what was observed by Raider *et al.*[177]. NAAG has been described in the literature as a postsynaptic neuron-produced peptide which release is potentiated by the active ionotropic glutamate receptors (NMDAR). Once in the synaptic cleft, NAAG binds to the presynaptic metabotropic glutamate receptor 3 (mGluR3), an isoform moderately expressed in hippocampus which, in a negative feedback, constrains Glu release and hence the excitatory activity[159]. Such enables a protective effect over excitotoxicity, which, among others, promotes oxidative stress and apoptosis[178]. Although it has been associated with various brain disorders including epilepsy, its effect on obesity has yet to be determined. In a similar increment pattern, GSH, an anti-oxidant constituted of glycine, cysteine and Glu, was shown to be positively correlated with the previous excitatory neuromodulator. Despite not shown yet in obese animal or human models, this paradox has been shown in perinatal hypoxic-ischemic injury[179,180] and traumatic brain injury models[181]. These present oxidative stress and cell apoptotic conditions, respectively. In a co-culture of neurons and Schwann cells treated with elevated glucose concentrations and an agonist of mGluR3 (2R,4R-4-aminopyrrolidine-2,4-dicarboxylate), GSH synthesis was promptly increased as a protective response to a neuronal glucose-induced oxidative stress[182–184]. Likewise, in a neonatal cerebral hypoxia-ischemia injury, a pathology characterized by a great glutamate release and accumulation in the synaptic cleft, GSH production was ameliorated upon NAAG treatment. Conversely, despite there being reduced ROS levels, the activity of other antioxidant enzymes, such as catalase, did not differ between controls and the treated groups, concurrent to our observations. The latter suggests NAAG might primarily inhibit ROS production rather than its removal[179]. Therefore, it is plausible that, in the obesogenic environment, the increased substrates (Gln and Ala) of Glu synthesis may be, in fact, producing the excitatory neurotransmitter. However, the latter might be promptly being used to produce both NAAG and GSH, hence the unmodified levels of Glu at the moment of the MRS scan. In the hippocampus, the concentration of Glu and Glut. C were not modified significantly, despite there being enhanced levels of Gln, the major substrate of Glu synthesis. This enzyme converts Gln, which was increased in the T2DM group, into Glu that is primarily used for excitatory synaptic activity[14]. Similarly, Ala presented augmented levels and a

tendency in an obesogenic and type 2 diabetic environment, respectively; and it is also involved in the Glu synthesis. While Ala is converted into pyruvate through a alanine aminotransferase, a coupled reaction transforms the oxaloacetate (a product of glucose metabolism) into Glu[185]. Such would suggest that Gln was not being greatly transformed into Glu and that Ala-involving mechanisms would be preferentially recurred to the Glu synthesis. However, it is noteworthy that we did not measure the activity of Glut. C, only its expression. In fact, the presence of a Pearson correlation between Gln and Glu and a lack of one between Glu and cerebral glucose levels suggest that Glu may be preferentially formed by Gln conversion. In a similar note, Asp, a secondary excitatory neurotransmitter, can also participate in the synthesis of the previous excitatory neurotransmitter. In fact, Asp can (1) act as a neurotransmitter itself; or (2) participate in the conversion of oxaloacetate into Glu through a biochemically-coupled process. However, its levels were not modified either. Furthermore, it is plausible that NAAG was inhibiting Glu release and redirecting it into the formation of GSH. However, the expected Glu pool resulting from this inhibition would hamper the synaptic activity, which is refuted by the sustained excitatory activity strength and synaptic integrity. Thus, since it does not seem to be a response to an overactivation of the glutamatergic synapse, it is probable this NAAG-GSH paradox is a compensatory mechanism preventive of oxidative stress potentiated by a high-fat diet. This compensatory mechanism seemed to be later lost once T2DM is established. Furthermore, NAAG also seemed to promote the expression of the transforming growth factor β (TGF-β), which confers anti-apoptotic and neuroregenerative properties. It resulted in a higher number of living cells in the hippocampal CA1 region of perinatal hypoxic rats[179] and animal models with traumatic brain injury[181]. Accordingly, although we are not capable of guaranteeing a causality between the growth factor and neuronal viability, the obese animal model did not show a compromised cellular and overall cerebral viability. The NAAG-GSH paradox seems not only to be a preventive mechanism observed exclusively in obesity, but also seems to be region-specific, since the augmented levels and correlation between both molecules is absent in the visual cortex. Altogether, this response seems to precede glycation, oxidative stress, neuronal compromise, glutamatergic and GABAergic synaptic imbalance, hence precedes the onset on several

hallmarks of the neurological complications observed in obesity and T2DM. Despite the need of clinical trials, which comprehends the next task, this HERMES sequence-measured paradox may constitute a novel biomarker capable of an early detection of cerebral alterations, prior to nocuous events.

Conclusion and future perspectives

In the animal models designed for this project, except for GABA levels on the visual cortex, HERMES sequence provided seemingly reliable and accurate levels of GABA and GSH in the hippocampus and visual cortex, given the comparability of variances with other published studies. With this same sequence and resort to Pearson analysis, a compensatory mechanism involving GSH and NAAG in obesogenic conditions. The latter seems to be potentiating the formation of GSH, while plausibly redirecting Glu prevenient of Gln conversion to the synthesis of this antioxidant. This paradox precedes prejudicial hallmarks of diabetic neuronal complications, namely synaptic imbalance, oxidative stress and loss of cellular viability. Therefore, the simultaneous presence of ameliorated GSH and NAAG may constitute an innovative and valuable imaging marker for the early detection of neurological comorbidities. Nonetheless, to confirm the possibility of its use in the clinic, human studies have to be performed, which compromises the following task of this project.

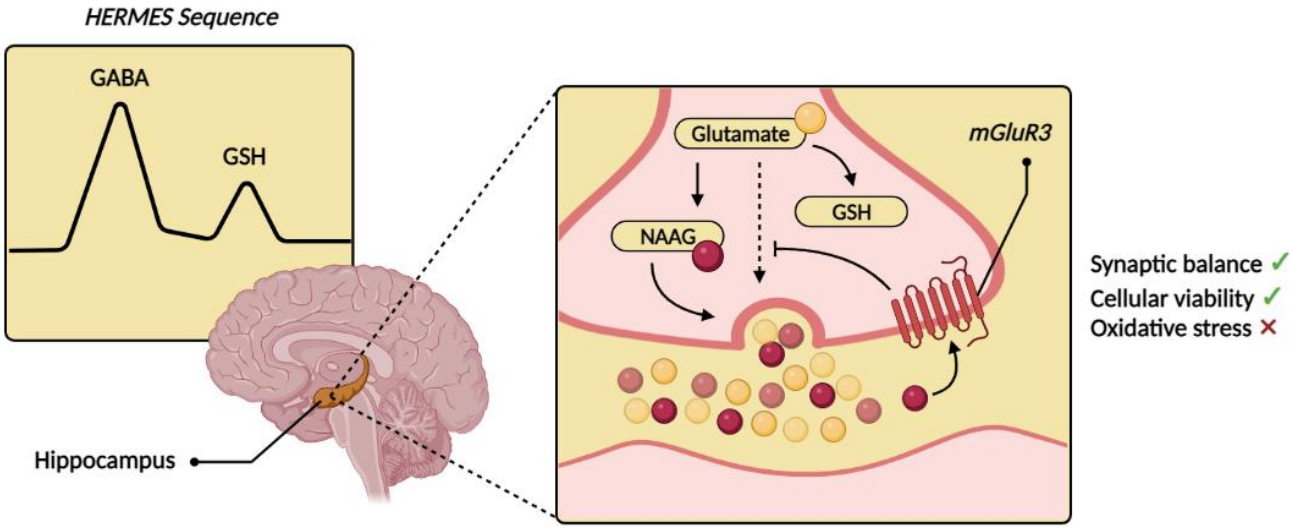

Figure 33. A HERMES sequence revealed a compensatory mechanism mediated by NAAG and GSH in response to obesogenic conditions.

Prior to synaptic imbalance, compromised cellular viability and oxidative stress, an enhancement of NAAG levels promotes the formation of GSH in obesity. Weakened activities are represented by dashed arrows, while the ameliorated activities are symbolized by continuous arrows. Image created with Biorender.com.

Bibliography

1. Park JH, Moon JH, Kim HJ, Kong MH, Oh YH. Sedentary Lifestyle: Overview of Updated Evidence of Potential Health Risks. *Korean J Fam Med*. 2020;41(6):365-373. doi:10.4082/kjfm.20.0165

2. Hardy OT, Czech MP, Corvera S. What causes the insulin resistance underlying obesity? *Curr Opin Endocrinol Diabetes Obes*. 2012;19(2):81-87. doi:10.1097/MED.0b013e3283514e13

3. Obradovic M, Sudar-Milovanovic E, Soskic S, et al. Leptin and Obesity: Role and Clinical Implication. *Front Endocrinol*. 2021;12:585887. doi:10.3389/fendo.2021.585887

4. Lima JEBF, Moreira NCS, Sakamoto-Hojo ET. Mechanisms underlying the pathophysiology of type 2 diabetes: From risk factors to oxidative stress, metabolic dysfunction, and hyperglycemia. *Mutat Res Toxicol Environ Mutagen*. 2022;874-875:503437. doi:10.1016/j.mrgentox.2021.503437

5. Izquierdo AG, Crujeiras AB, Casanueva FF, Carreira MC. Leptin, Obesity, and Leptin Resistance: Where Are We 25 Years Later? *Nutrients*. 2019;11(11):2704. doi:10.3390/nu11112704

6. Galicia-Garcia U, Benito-Vicente A, Jebari S, et al. Pathophysiology of Type 2 Diabetes Mellitus. *Int J Mol Sci*. 2020;21(17):6275. doi:10.3390/ijms21176275

7. Zaragozá R. Transport of Amino Acids Across the Blood-Brain Barrier. *Front Physiol*. 2020;11:973. doi:10.3389/fphys.2020.00973

8. Hawkins RA. The blood-brain barrier and glutamate. *Am J Clin Nutr*. 2009;90(3):867S-874S. doi:10.3945/ajcn.2009.27462BB

9. Hogstad S, Svenneby G, Torgner IAa, Kvamme E, Hertz L, Schousboe A. Glutaminase in neurons and astrocytes cultured from mouse brain: Kinetic properties and effects of phosphate, glutamate, and ammonia. *Neurochem Res*. 1988;13(4):383-388. doi:10.1007/BF00972489

10. Schousboe A, Scafidi S, Bak LK, Waagepetersen HS, McKenna MC. Glutamate Metabolism in the Brain Focusing on Astrocytes. In: Parpura V, Schousboe A, Verkhratsky A, eds. Vol 11. Advances in Neurobiology. Springer International Publishing; 2014:13-30. doi:10.1007/978-3-319-08894-5_2

11. Burger PM, Mehl E, Cameron PL, et al. Synaptic vesicles immunoisolated from rat cerebral cortex contain high levels of glutamate. *Neuron*. 1989;3(6):715-720. doi:10.1016/0896-6273(89)90240-7

12. Chen X, Levy JM, Hou A, et al. PSD-95 family MAGUKs are essential for anchoring AMPA and NMDA receptor complexes at the postsynaptic density. *Proc Natl Acad Sci*. 2015;112(50):E6983-E6992. doi:10.1073/pnas.1517045112

13. Norenberg MD, Martinez-Hernandez A. Fine structural localization of glutamine synthetase in astrocytes of rat brain. *Brain Res*. 1979;161(2):303-310. doi:10.1016/0006-8993(79)90071-4

14. Andersen JV, Markussen KH, Jakobsen E, et al. Glutamate metabolism and recycling at the excitatory synapse in health and neurodegeneration. *Neuropharmacology*. 2021;196:108719. doi:10.1016/j.neuropharm.2021.108719

15. Roth FC, Draguhn A. GABA Metabolism and Transport: Effects on Synaptic Efficacy. *Neural Plast*. 2012;2012:805830. doi:10.1155/2012/805830

16. Jin H, Wu H, Osterhaus G, et al. Demonstration of functional coupling between γ-aminobutyric acid (GABA) synthesis and vesicular GABA transport into synaptic vesicles. *Proc Natl Acad Sci*. 100(7):4293-4298. doi:10.1073/pnas.0730698100

17. Jacob TC, Bogdanov YD, Magnus C, et al. Gephyrin Regulates the Cell Surface Dynamics of Synaptic GABAA Receptors. *J Neurosci*. 2005;25(45):10469-10478. doi:10.1523/JNEUROSCI.2267-05.2005

18. Conti F, Melone M, de Biasi S, Minelli A, Brecha NC, Ducati A. Neuronal and glial localization of GAT-1, a high-affinity γ-aminobutyric acid plasma membrane transporter, in human cerebral cortex: With a note on its distribution in monkey cortex. *J Comp Neurol*. 1998;396:51-63. doi:10.1002/(SICI)1096-9861(19980622)396:1<51::AID-CNE5>3.0.CO;2-H

19. Minelli A, DeBiasi S, Brecha NC, Vitellaro Zuccarello L, Conti F. GAT-3, a High-Affinity GABA Plasma Membrane Transporter, Is Localized to Astrocytic Processes, and It Is Not Confined to the Vicinity of GABAergic Synapses in the Cerebral Cortex. *J Neurosci*. 1996;16(19):6255-6264. doi:10.1523/JNEUROSCI.16-19-06255.1996

20. Picó C, Palou M, Pomar CA, Rodríguez AM, Palou A. Leptin as a key regulator of the adipose organ. *Rev Endocr Metab Disord*. 2022;23(1):13-30. doi:10.1007/s11154-021-09687-5

21. Li RJW, Zhang SY, Lam TKT. Interaction of glucose sensing and leptin action in the brain. *Mol Metab*. 2020;39:101011. doi:10.1016/j.molmet.2020.101011

22. Kim YB, Uotani S, Pierroz DD, Flier JS, Kahn BB. In Vivo Administration of Leptin Activates Signal Transduction Directly in Insulin-Sensitive Tissues: Overlapping but Distinct Pathways from Insulin. *Endocrinology*. 2000;141(7):2328-2339. doi:10.1210/endo.141.7.7536.

23. Karlsson HK, Tuulari JJ, Hirvonen J, et al. Obesity Is Associated with White Matter Atrophy: A Combined Diffusion Tensor Imaging and Voxel-Based Morphometric Study. *Obesity*. 2013;21(12):2530-2537. doi:10.1002/oby.20386

24. Bernardes G, IJzerman RG, ten Kulve JS, et al. Cortical and subcortical gray matter structural alterations in normoglycemic obese and type 2 diabetes patients: relationship with adiposity, glucose, and insulin. *Metab Brain Dis*. 2018;33(4):1211-1222. doi:10.1007/s11011-018-0223-5

25. Roy B, Ehlert L, Mullur R, et al. Regional Brain Gray Matter Changes in Patients with Type 2 Diabetes Mellitus. *Sci Rep*. 2020;10(1):9925. doi:10.1038/s41598-020-67022-5

26. Zhang B, Tian X, Tian D, et al. Altered Regional Gray Matter Volume in Obese Men: A Structural MRI Study. *Front Psychol*. 2017;8:125. doi:10.3389/fpsyg.2017.00125

27. Chen EY, Eickhoff SB, Giovannetti T, Smith DV. Obesity is associated with reduced orbitofrontal cortex volume: A coordinate-based meta-analysis. *NeuroImage Clin*. 2020;28:102420. doi:10.1016/j.nicl.2020.102420

28. Bakker W, Eringa EC, Sipkema P, van Hinsbergh VWM. Endothelial dysfunction and diabetes: roles of hyperglycemia, impaired insulin signaling and obesity. *Cell Tissue Res*. 2009;335(1):165-189. doi:10.1007/s00441-008-0685-6

29. Meza CA, La Favor JD, Kim DH, Hickner RC. Endothelial Dysfunction: Is There a Hyperglycemia-Induced Imbalance of NOX and NOS? *Int J Mol Sci*. 2019;20(15):3775. doi:10.3390/ijms20153775

30. Bouhrara M, Alisch JSR, Khattar N, et al. Association of cerebral blood flow with myelin content in cognitively unimpaired adults. *BMJ Neurol Open*. 2020;2:e000053. doi:10.1136/bmjno-2020-000053

31. Kullmann S, Callaghan MF, Heni M, et al. Specific white matter tissue microstructure changes associated with obesity. *NeuroImage*. 2016;125:36-44. doi:10.1016/j.neuroimage.2015.10.006

32. Stanek KM, Grieve SM, Brickman AM, et al. Obesity Is Associated With Reduced White Matter Integrity in Otherwise Healthy Adults. *Obesity*. 2011;19(3):500-504. doi:10.1038/oby.2010.312

33. Repple J, Opel N, Meinert S, et al. Elevated body-mass index is associated with reduced white matter integrity in two large independent cohorts. *Psychoneuroendocrinology*. 2018;91:179-185. doi:10.1016/j.psyneuen.2018.03.007

34. Metzler-Baddeley C, Mole JP, Leonaviciute E, et al. Sex-specific effects of central adiposity and inflammatory markers on limbic microstructure. *NeuroImage*. 2019;189:793-803. doi:10.1016/j.neuroimage.2019.02.007

35. Kullmann S, Abbas Z, Machann J, et al. Investigating obesity-associated brain inflammation using quantitative water content mapping. *J Neuroendocrinol*. 2020;32(12):e12907. doi:10.1111/jne.12907

36. Cazettes F, Cohen JI, Yau PL, Talbot H, Convit A. Obesity-mediated inflammation may damage the brain circuit that regulates food intake. *Brain Res*. 2011;1373:101-109. doi:10.1016/j.brainres.2010.12.008

37. Puig J, Blasco G, Daunis-i-Estadella J, et al. Hypothalamic Damage Is Associated With Inflammatory Markers and Worse Cognitive Performance in Obese Subjects. *J Clin Endocrinol Metab*. 2015;100(2):E276-E281. doi:10.1210/jc.2014-2682

38. Lee D, Thaler JP, Berkseth KE, Melhorn SJ, Schwartz MW, Schur EA. Longer T_2 relaxation time is a marker of hypothalamic gliosis in mice with diet-induced obesity. *Am J Physiol-Endocrinol Metab*. 2013;304(11):E1245-E1250. doi:10.1152/ajpendo.00020.2013

39. Di Marzo V, Goparaju SK, Wang L, et al. Leptin-regulated endocannabinoids are involved in maintaining food intake. *Nature*. 2001;410(6830):822-825. doi:10.1038/35071088

40. Kantonen T, Pekkarinen L, Karjalainen T, et al. Obesity risk is associated with altered cerebral glucose metabolism and decreased μ-opioid and CB1 receptor availability. *Int J Obes*. 2022;46(2):400-407. doi:10.1038/s41366-021-00996-y

41. Joutsa J, Karlsson HK, Majuri J, et al. Binge eating disorder and morbid obesity are associated with lowered mu-opioid receptor availability in the brain. *Psychiatry Res Neuroimaging*. 2018;276:41-45. doi:10.1016/j.pscychresns.2018.03.006

42. Burghardt PR, Rothberg AE, Dykhuis KE, Burant CF, Zubieta JK. Endogenous Opioid Mechanisms Are Implicated in Obesity and Weight Loss in Humans. *J Clin Endocrinol Metab*. 2015;100(8):3193-3201. doi:10.1210/jc.2015-1783

43. Dunn JP, Kessler RM, Feurer ID, et al. Relationship of Dopamine Type 2 Receptor Binding Potential With Fasting Neuroendocrine Hormones and Insulin Sensitivity in Human Obesity. *Diabetes Care*. 2012;35(5):1105-1111. doi:10.2337/dc11-2250

44. Werther GA, Hogg A, Oldfield BJ, et al. Localization and Characterization of Insulin Receptors in Rat Brain and Pituitary Gland Using *in Vitro* Autoradiography and Computerized Densitometry. *Endocrinology*. 1987;121(4):1562-1570. doi:10.1210/endo-121-4-1562

45. Volkow ND, Wise RA. How can drug addiction help us understand obesity? *Nat Neurosci*. 2005;8(5):555-560. doi:10.1038/nn1452

46. Erritzoe D, Frokjaer VG, Haahr MT, et al. Cerebral serotonin transporter binding is inversely related to body mass index. *NeuroImage*. 2010;52(1):284-289. doi:10.1016/j.neuroimage.2010.03.086

47. Haahr ME, Rasmussen PM, Madsen K, et al. Obesity is associated with high serotonin 4 receptor availability in the brain reward circuitry. *NeuroImage*. 2012;61(4):884-888. doi:10.1016/j.neuroimage.2012.03.050

48. Thanos PK, Michaelides M, Gispert JD, et al. Differences in response to food stimuli in a rat model of obesity: in-vivo assessment of brain glucose metabolism. *Int J Obes*. 2008;32(7):1171-1179. doi:10.1038/ijo.2008.50

49. Kullmann S, Heni M, Veit R, et al. Selective Insulin Resistance in Homeostatic and Cognitive Control Brain Areas in Overweight and Obese Adults. *Diabetes Care*. 2015;38(6):1044-1050. doi:10.2337/dc14-2319

50. Han P, Roitzsch C, Horstmann A, Pössel M, Hummel T. Increased Brain Reward Responsivity to Food-Related Odors in Obesity. *Obesity*. 2021;29(7):1138-1145. doi:10.1002/oby.23170

51. Belfort-DeAguiar R, Seo D, Lacadie C, et al. Humans with obesity have disordered brain responses to food images during physiological hyperglycemia. *Am J Physiol-Endocrinol Metab*. 2018;314(5):E522-E529. doi:10.1152/ajpendo.00335.2017

52. DelParigi A, Chen K, Salbe AD, Reiman EM, Tataranni PA. Sensory experience of food and obesity: a positron emission tomography study of the brain regions affected by tasting a liquid meal after a prolonged fast. *NeuroImage*. 2005;24(2):436-443. doi:10.1016/j.neuroimage.2004.08.035

53. Kullmann S, Heni M, Linder K, et al. Resting-state functional connectivity of the human hypothalamus: Hypothalamus Functional Connectivity Networks. *Hum Brain Mapp*. 2014;35(12):6088-6096. doi:10.1002/hbm.22607

54. Avery JA, Powell JN, Breslin FJ, et al. Obesity is associated with altered mid-insula functional connectivity to limbic regions underlying appetitive responses to foods. *J Psychopharmacol (Oxf)*. 2017;31(11):1475-1484. doi:10.1177/0269881117728429

55. Li G, Hu Y, Zhang W, et al. Resting activity of the hippocampus and amygdala in obese individuals predicts their response to food cues. *Addict Biol*. 2021;26(3):e12974. doi:10.1111/adb.12974

56. Girault FM, Sonnay S, Gruetter R, Duarte JMN. Alterations of Brain Energy Metabolism in Type 2 Diabetic Goto-Kakizaki Rats Measured In Vivo by 13C Magnetic Resonance Spectroscopy. *Neurotox Res*. 2019;36(2):268-278. doi:10.1007/s12640-017-9821-y

57. Gazdzinski SP, Gaździńska AP, Orzeł J, et al. Intragastric balloon therapy leads to normalization of brain magnetic resonance spectroscopic markers of diabetes in morbidly obese patients. *NMR Biomed*. 2018;31(9):e3957. doi:10.1002/nbm.3957

58. Picciotto MR, Higley MJ, Mineur YS. Acetylcholine as a Neuromodulator: Cholinergic Signaling Shapes Nervous System Function and Behavior. *Neuron*. 2012;76(1):116-129. doi:10.1016/j.neuron.2012.08.036

59. Contreras-Rodríguez O, Martín-Pérez C, Vilar-López R, Verdejo-Garcia A. Ventral and Dorsal Striatum Networks in Obesity: Link to Food Craving and Weight Gain. *Biol Psychiatry*. 2017;81(9):789-796. doi:10.1016/j.biopsych.2015.11.020

60. Volkow ND, Wang GJ, Tomasi D, Baler RD. The Addictive Dimensionality of Obesity. *Biol Psychiatry*. 2013;73(9):811-818. doi:10.1016/j.biopsych.2012.12.020

61. Ding Y, Ji G, Li G, et al. Altered Interactions Among Resting-State Networks in Individuals with Obesity. *Obesity*. 2020;28(3):601-608. doi:10.1002/oby.22731

62. Farr OM, Mantzoros CS. Obese individuals with more components of the metabolic syndrome and/or prediabetes demonstrate decreased activation of reward-related brain centers in response to food cues in both the fed and fasting states: a preliminary fMRI study. *Int J Obes*. 2017;41(3):471-474. doi:10.1038/ijo.2016.231

63. Letra L, Matafome P, Rodrigues T, et al. Association between Adipokines and Biomarkers of Alzheimer's Disease: A Cross-Sectional Study. *J Alzheimers Dis*. 2019;67(2):725-735. doi:10.3233/JAD-180669

64. Tschritter O, Preissl H, Hennige AM, et al. High cerebral insulin sensitivity is associated with loss of body fat during lifestyle intervention. *Diabetologia*. 2012;55(1):175-182. doi:10.1007/s00125-011-2309-z

65. Pan W, Kastin AJ. Adipokines and the blood-brain barrier. *Peptides*. 2007;28(6):1317-1330. doi:10.1016/j.peptides.2007.04.023

66. Rhea E, Banks WA. Regulation of insulin transport across the blood-brain barrier by CNS insulin receptor signaling: Impact of CNS insulin signaling in Alzheimer's disease. *Alzheimers Dement*. 2020;16(S3). doi:10.1002/alz.039508

67. Fang F, Zhan YF, Zhuo YY, Yin DZ, Li KA, Wang YF. Brain atrophy in middle-aged subjects with Type 2 diabetes mellitus, with and without microvascular complications. *J Diabetes*. 2018;10(8):625-632. doi:10.1111/1753-0407.12646

68. Qiao J, Lawson CM, Rentrup KFG, Kulkarni P, Ferris CF. Evaluating blood–brain barrier permeability in a rat model of type 2 diabetes. *J Transl Med*. 2020;18(1):256. doi:10.1186/s12967-020-02428-3

69. Markus MRP, Ittermann T, Wittfeld K, et al. Prediabetes is associated with lower brain gray matter volume in the general population. The Study of Health in Pomerania (SHIP). *Nutr Metab Cardiovasc Dis*. 2017;27(12):1114-1122. doi:10.1016/j.numecd.2017.10.007

70. Whitlow CT, Sink KM, Divers J, et al. Effects of Type 2 Diabetes on Brain Structure and Cognitive Function: African American–Diabetes Heart Study MIND. *Am J Neuroradiol*. 2015;36(9):1648-1653. doi:10.3174/ajnr.A4321

71. Boucher J, Kleinridders A, Kahn CR. Insulin Receptor Signaling in Normal and Insulin-Resistant States. *Cold Spring Harb Perspect Biol*. 2014;6(1):a009191. doi:10.1101/cshperspect.a009191

72. Freude S, Plum L, Schnitker J, et al. Peripheral Hyperinsulinemia Promotes Tau Phosphorylation In Vivo. *Diabetes*. 2005;54(12):3343-3348. doi:10.2337/diabetes.54.12.3343

73. den Heijer T, Vermeer SE, van Dijk EJ, et al. Type 2 diabetes and atrophy of medial temporal lobe structures on brain MRI. *Diabetologia*. 2003;46(12):1604-1610. doi:10.1007/s00125-003-1235-0

74. Fang F, Lai MY, Huang JJ, et al. Compensatory Hippocampal Connectivity in Young Adults With Early-Stage Type 2 Diabetes. *J Clin Endocrinol Metab*. 2019;104(7):3025-3038. doi:10.1210/jc.2018-02319

75. Bingham EM, Hopkins D, Smith D, et al. The Role of Insulin in Human Brain Glucose Metabolism. *Diabetes*. 2002;51(12):3384-3390. doi:10.2337/diabetes.51.12.3384

76. Novak V, Zhao P, Manor B, et al. Adhesion Molecules, Altered Vasoreactivity, and Brain Atrophy in Type 2 Diabetes. *Diabetes Care*. 2011;34(11):2438-2441. doi:10.2337/dc11-0969

77. Franke K, Gaser C, Manor B, Novak V. Advanced BrainAGE in older adults with type 2 diabetes mellitus. *Front Aging Neurosci*. 2013;5:90. doi:10.3389/fnagi.2013.00090

78. Lee S, Kim TD, Kim RY, et al. Hippocampal subregional alterations and verbal fluency in the early stage of type 2 diabetes mellitus. *Eur J Neurosci*. 2021;54(10):7550-7559. doi:10.1111/ejn.15505

79. Kerti L, Witte AV, Winkler A, Grittner U, Rujescu D, Floel A. Higher glucose levels associated with lower memory and reduced hippocampal microstructure. *Neurology*. 2013;81(20):1746-1752. doi:10.1212/01.wnl.0000435561.00234.ee

80. Brundel M, van den Heuvel M, de Bresser J, Kappelle LJ, Biessels GJ. Cerebral cortical thickness in patients with type 2 diabetes. *J Neurol Sci*. 2010;299(1-2):126-130. doi:10.1016/j.jns.2010.08.048

81. Dong S, Dongwei L, Zhang J, Liang J, Sun Z, Fang J. Individuals in the prediabetes stage exhibit reduced hippocampal tail volume and executive dysfunction. *Brain Behav*. 2019;9(8):e01351. doi:10.1002/brb3.1351

82. Anan F, Masaki T, Shimomura T, et al. Abdominal visceral fat accumulation is associated with hippocampus volume in non-dementia patients with type 2 diabetes mellitus. *NeuroImage*. 2010;49(1):57-62. doi:10.1016/j.neuroimage.2009.08.021

83. Zhang YW, Zhang JQ, Liu C, et al. Memory Dysfunction in Type 2 Diabetes Mellitus Correlates with Reduced Hippocampal CA1 and Subiculum Volumes. *Chin Med J (Engl)*. 2015;128(4):465-471. doi:10.4103/0366-6999.151082

84. Yang X, Chen Y, Zhang W, et al. Association Between Inflammatory Biomarkers and Cognitive Dysfunction Analyzed by MRI in Diabetes Patients. *Diabetes Metab Syndr Obes Targets Ther*. 2020;Volume 13:4059-4065. doi:10.2147/DMSO.S271160

85. Milne NT, Bucks RS, Davis WA, et al. Hippocampal atrophy, asymmetry, and cognition in type 2 diabetes mellitus. *Brain Behav*. 2018;8(1):e00741. doi:10.1002/brb3.741

86. Ferreira FS, Pereira JMS, Reis A, et al. Early visual cortical structural changes in diabetic patients without diabetic retinopathy. *Graefes Arch Clin Exp Ophthalmol*. 2017;255(11):2113-2118. doi:10.1007/s00417-017-3752-4

87. Xie Y, Zhang Y, Qin W, Lu S, Ni C, Zhang Q. White Matter Microstructural Abnormalities in Type 2 Diabetes Mellitus: A Diffusional Kurtosis Imaging Analysis. *Am J Neuroradiol*. 2017;38(3):617-625. doi:10.3174/ajnr.A5042

88. Li C, Jin R, Liu K, et al. White Matter Atrophy in Type 2 Diabetes Mellitus Patients With Mild Cognitive Impairment. *Front Neurosci*. 2021;14:602501. doi:10.3389/fnins.2020.602501

89. Rothemund Y, Preuschhof C, Bohner G, et al. Differential activation of the dorsal striatum by high-calorie visual food stimuli in obese individuals. *NeuroImage*. 2007;37(2):410-421. doi:10.1016/j.neuroimage.2007.05.008

90. Zhang B, Tian D, Yu C, et al. Altered baseline brain activities before food intake in obese men: A resting state fMRI study. *Neurosci Lett*. 2015;584:156-161. doi:10.1016/j.neulet.2014.10.020

91. Xiong Y, Sui Y, Zhang S, et al. Brain microstructural alterations in type 2 diabetes: diffusion kurtosis imaging provides added value to diffusion tensor imaging. *Eur Radiol*. 2019;29(4):1997-2008. doi:10.1007/s00330-018-5746-y

92. Xiong Y, Sui Y, Xu Z, et al. A Diffusion Tensor Imaging Study on White Matter Abnormalities in Patients with Type 2 Diabetes Using Tract-Based Spatial Statistics. *Am J Neuroradiol*. 2016;37(8):1462-1469. doi:10.3174/ajnr.A4740

93. Anan F, Masaki T, Eto T, et al. Visceral fat accumulation is a significant risk factor for white matter lesions in Japanese type 2 diabetic patients. *Eur J Clin Invest*. 2009;39(5):368-374. doi:10.1111/j.1365-2362.2009.02103.x

94. Widya RL, Kroft LJM, Altmann-Schneider I, et al. Visceral adipose tissue is associated with microstructural brain tissue damage: Adiposity and Microstructural Brain Damage. *Obesity*. 2015;23(5):1092-1096. doi:10.1002/oby.21048

95. Hsu FC, Yuan M, Bowden DW, et al. Adiposity is inversely associated with hippocampal volume in African Americans and European Americans with diabetes. *J Diabetes Complications*. 2016;30(8):1506-1512. doi:10.1016/j.jdiacomp.2016.08.012

96. Sahin I, Alkan A, Keskin L, et al. Evaluation of in vivo cerebral metabolism on proton magnetic resonance spectroscopy in patients with impaired glucose tolerance and type 2 diabetes mellitus. *J Diabetes Complications*. 2008;22(4):254-260. doi:10.1016/j.jdiacomp.2007.03.007

97. Sundermann EE, Thomas KR, Bangen KJ, et al. Prediabetes Is Associated With Brain Hypometabolism and Cognitive Decline in a Sex-Dependent Manner: A Longitudinal Study of Nondemented Older Adults. *Front Neurol*. 2021;12:551975. doi:10.3389/fneur.2021.551975

98. Lin Y, Zhou J, Sha L, et al. Metabolite Differences in the Lenticular Nucleus in Type 2 Diabetes Mellitus Shown by Proton MR Spectroscopy. *Am J Neuroradiol*. 2013;34(9):1692-1696. doi:10.3174/ajnr.A3492

99. Baker LD, Cross DJ, Minoshima S, Belongia D, Watson GS, Craft S. Insulin Resistance and Alzheimer-like Reductions in Regional Cerebral Glucose Metabolism for Cognitively Normal Adults With Prediabetes or Early Type 2 Diabetes. *Arch Neurol*. 2011;68(1):51-57. doi:10.1001/archneurol.2010.225

100. Ribeiro M, Castelhano J, Petrella LI, et al. High-fat diet induces a neurometabolic state characterized by changes in glutamate and N-acetylaspartate pools associated with early glucose intolerance: An in vivo multimodal MRI study: Neurometabolic Changes Induced by HFD. *J Magn Reson Imaging*. 2018;48(3):757-766. doi:10.1002/jmri.25942

101. Soares AF, Nissen JD, Garcia-Serrano AM, Nussbaum SS, Waagepetersen HS, Duarte JMN. Glycogen metabolism is impaired in the brain of male type 2 diabetic Goto-Kakizaki rats. *J Neurosci Res*. 2019;97(8):1004-1017. doi:10.1002/jnr.24437

102. Magistretti PJ, Allaman I. Lactate in the brain: from metabolic end-product to signalling molecule. *Nat Rev Neurosci*. 2018;19(4):235-249. doi:10.1038/nrn.2018.19

103. Zhang M, Sun X, Zhang Z, et al. Brain metabolite changes in patients with type 2 diabetes and cerebral infarction using proton magnetic resonance spectroscopy. *Int J Neurosci*. 2014;124(1):37-41. doi:10.3109/00207454.2013.816958

104. d'Almeida OC, Violante IR, Quendera B, Moreno C, Gomes L, Castelo-Branco M. The neurometabolic profiles of GABA and Glutamate as revealed by proton magnetic

resonance spectroscopy in type 1 and type 2 diabetes. *PLoS ONE*. 2020;15(10):e0240907. doi:10.1371/journal.pone.0240907

105. Ajilore O, Haroon E, Kumaran S, et al. Measurement of Brain Metabolites in Patients with type 2 Diabetes and Major Depression Using Proton Magnetic Resonance Spectroscopy. *Neuropsychopharmacology*. 2007;32(6):1224-1231. doi:10.1038/sj.npp.1301248

106. Sinha S, Ekka M, Sharma U, P R, Pandey RM, Jagannathan NR. Assessment of changes in brain metabolites in Indian patients with type-2 diabetes mellitus using proton magnetic resonance spectroscopy. *BMC Res Notes*. 2014;7:41. doi:10.1186/1756-0500-7-41

107. Garcia-Serrano AM, Duarte JMN. Brain Metabolism Alterations in Type 2 Diabetes: What Did We Learn From Diet-Induced Diabetes Models? *Front Neurosci*. 2020;14:229. doi:10.3389/fnins.2020.00229

108. Thielen J, Gancheva S, Hong D, et al. Higher GABA concentration in the medial prefrontal cortex of Type 2 diabetes patients is associated with episodic memory dysfunction. *Hum Brain Mapp*. 2019;40(14):4287-4295. doi:10.1002/hbm.24702

109. Luchsinger JA, Palta P, Rippon B, et al. Pre-Diabetes, but not Type 2 Diabetes, Is Related to Brain Amyloid in Late Middle-Age. *J Alzheimers Dis*. 2020;75(4):1241-1252. doi:10.3233/JAD-200232

110. Toppala S, Ekblad LL, Lötjönen J, et al. Midlife Insulin Resistance as a Predictor for Late-Life Cognitive Function and Cerebrovascular Lesions. Bangen K, ed. *J Alzheimers Dis*. 2019;72(1):215-228. doi:10.3233/JAD-190691

111. Espeland MA, Bryan RN, Goveas JS, et al. Influence of Type 2 Diabetes on Brain Volumes and Changes in Brain Volumes. *Diabetes Care*. 2013;36(1):90-97. doi:10.2337/dc12-0555

112. Imamine R, Kawamura T, Umemura T, et al. Does cerebral small vessel disease predict future decline of cognitive function in elderly people with type 2 diabetes? *Diabetes Res Clin Pract*. 2011;94(1):91-99. doi:10.1016/j.diabres.2011.06.014

113. Marder TJ, Flores VL, Bolo NR, et al. Task-Induced Brain Activity Patterns in Type 2 Diabetes: A Potential Biomarker for Cognitive Decline. *Diabetes*. 2014;63(9):3112-3119. doi:10.2337/db13-1783

114. Korf ESC, White LR, Scheltens P, Launer LJ. Brain Aging in Very Old Men With Type 2 Diabetes. *Diabetes Care*. 2006;29(10):2268-2274. doi:10.2337/dc06-0243

115. Bangen KJ, Werhane ML, Weigand AJ, et al. Reduced Regional Cerebral Blood Flow Relates to Poorer Cognition in Older Adults With Type 2 Diabetes. *Front Aging Neurosci*. 2018;10:270. doi:10.3389/fnagi.2018.00270

116. Zhang Y, Zhang X, Ma G, et al. Neurovascular coupling alterations in type 2 diabetes: a 5-year longitudinal MRI study. *BMJ Open Diabetes Res Care*. 2021;9(1):e001433. doi:10.1136/bmjdrc-2020-001433

117. Yu Y, Yan LF, Sun Q, et al. Neurovascular decoupling in type 2 diabetes mellitus without mild cognitive impairment: Potential biomarker for early cognitive impairment. *NeuroImage*. 2019;200:644-658. doi:10.1016/j.neuroimage.2019.06.058

118. Hu B, Yan LF, Sun Q, et al. Disturbed neurovascular coupling in type 2 diabetes mellitus patients: Evidence from a comprehensive fMRI analysis. *NeuroImage Clin*. 2019;22:101802. doi:10.1016/j.nicl.2019.101802

119. Chung CC, Pimentel Maldonado DA, Jor'dan AJ, et al. Lower cerebral vasoreactivity as a predictor of gait speed decline in type 2 diabetes mellitus. *J Neurol*. 2018;265(10):2267-2276. doi:10.1007/s00415-018-8981-x

120. Hui YY, McAmis WC, Baynes JW, Schaeffer RC, Wolf MB. Effect of advanced glycation end products on oxidative stress in endothelial cells in culture: a warning on the use of cells studied in serum-free media. *Diabetologia*. 2001;44(10):1310-1317. doi:10.1007/s001250100646

121. Andersen JV, Nissen JD, Christensen SK, Markussen KH, Waagepetersen HS. Impaired Hippocampal Glutamate and Glutamine Metabolism in the db/db Mouse Model of Type 2 Diabetes Mellitus. *Neural Plast*. 2017;2017:2107084. doi:10.1155/2017/2107084

122. Duarte AI, Santos MS, Seiça R, Oliveira CR de. Insulin affects synaptosomal GABA and glutamate transport under oxidative stress conditions. *Brain Res*. 2003;977(1):23-30. doi:10.1016/S0006-8993(03)02679-9

123. Harris JJ, Reynell C, Attwell D. The physiology of developmental changes in BOLD functional imaging signals. *Dev Cogn Neurosci*. 2011;1(3):199-216. doi:10.1016/j.dcn.2011.04.001

124. Gryglewski RJ, Palmer RMJ, Moncada S. Superoxide anion is involved in the breakdown of endothelium-derived vascular relaxing factor. *Nature*. 1986;320(6061):454-456. doi:10.1038/320454a0

125. Hase Y, Ding R, Harrison G, et al. White matter capillaries in vascular and neurodegenerative dementias. *Acta Neuropathol Commun*. 2019;7(1):16. doi:10.1186/s40478-019-0666-x

126. Bouvy WH, Zwanenburg JJ, Reinink R, et al. Perivascular spaces on 7 Tesla brain MRI are related to markers of small vessel disease but not to age or cardiovascular risk factors. *J Cereb Blood Flow Metab*. 2016;36(10):1708-1717. doi:10.1177/0271678X16648970

127. Li J, Guo Y, Li Q, et al. Presence of White Matter Lesions Associated with Diabetes-Associated Cognitive Decline in Male Rat Models of Pre-Type 2 Diabetes. *Med Sci Monit*. 2019;25:9679-9689. doi:10.12659/MSM.918557

128. Fields RD. Change in the Brain's White Matter. *Science*. 2010;330(6005):768-769. doi:10.1126/science.1199139

129. Li C, Zhang J, Qiu M, et al. Alterations of Brain Structural Network Connectivity in Type 2 Diabetes Mellitus Patients With Mild Cognitive Impairment. *Front Aging Neurosci*. 2021;12:615048. doi:10.3389/fnagi.2020.615048

130. Xiong Y, Chen X, Zhao X, Fan Y, Zhang Q, Zhu W. Altered regional homogeneity and functional brain networks in Type 2 diabetes with and without mild cognitive impairment. *Sci Rep*. 2020;10(1):21254. doi:10.1038/s41598-020-76495-3

131. Chen Y, Liu Z, Zhang J, et al. Selectively Disrupted Functional Connectivity Networks in Type 2 Diabetes Mellitus. *Front Aging Neurosci*. 2015;7:233. doi:10.3389/fnagi.2015.00233

132. Zhang W, Gao C, Qing Z, et al. Hippocampal subfields atrophy contribute more to cognitive impairment in middle-aged patients with type 2 diabetes rather than microvascular lesions. *Acta Diabetol*. 2021;58(8):1023-1033. doi:10.1007/s00592-020-01670-x

133. Liu D, Duan S, Zhang J, et al. Aberrant Brain Regional Homogeneity and Functional Connectivity in Middle-Aged T2DM Patients: A Resting-State Functional MRI Study. *Front Hum Neurosci*. 2016;10:490. doi:10.3389/fnhum.2016.00490

134. Osborne MT, Naddaf N, Abohashem S, et al. A neurobiological link between transportation noise exposure and metabolic disease in humans. *Psychoneuroendocrinology*. 2021;131:105331. doi:10.1016/j.psyneuen.2021.105331

135. Tucsek Z, Toth P, Sosnowska D, et al. Obesity in Aging Exacerbates Blood-Brain Barrier Disruption, Neuroinflammation, and Oxidative Stress in the Mouse Hippocampus: Effects on Expression of Genes Involved in Beta-Amyloid Generation and Alzheimer's Disease. *J Gerontol A Biol Sci Med Sci*. 2014;69(10):1212-1226. doi:10.1093/gerona/glt177

136. Cavaliere G, Trinchese G, Penna E, et al. High-Fat Diet Induces Neuroinflammation and Mitochondrial Impairment in Mice Cerebral Cortex and Synaptic Fraction. *Front Cell Neurosci*. 2019;13:509. doi:10.3389/fncel.2019.00509

137. Butterfield DA, Di Domenico F, Barone E. Elevated risk of type 2 diabetes for development of Alzheimer disease: A key role for oxidative stress in brain. *Biochim Biophys Acta BBA - Mol Basis Dis*. 2014;1842(9):1693-1706. doi:10.1016/j.bbadis.2014.06.010

138. Maciejczyk M, Żebrowska E, Zalewska A, Chabowski A. Redox Balance, Antioxidant Defense, and Oxidative Damage in the Hypothalamus and Cerebral Cortex of Rats with High Fat Diet-Induced Insulin Resistance. *Oxid Med Cell Longev*. 2018;2018:6940515. doi:10.1155/2018/6940515

139. Sandoval-Salazar C, Ramírez-Emiliano J, Trejo-Bahena A, Oviedo-Solís CI, Solís-Ortiz MS. A high-fat diet decreases GABA concentration in the frontal cortex and hippocampus of rats. *Biol Res*. 2016;49:15. doi:10.1186/s40659-016-0075-6

140. Lunghi C, Daniele G, Binda P, et al. Altered Visual Plasticity in Morbidly Obese Subjects. *iScience*. 2019;22:206-213. doi:10.1016/j.isci.2019.11.027

141. Eltahawy NA, Saada HN, Hammad AS. Gamma Amino Butyric Acid Attenuates Brain Oxidative Damage Associated with Insulin Alteration in Streptozotocin-Treated Rats. *Indian J Clin Biochem*. 2017;32(2):207-213. doi:10.1007/s12291-016-0597-2

142. Tu L, Sun Q, Wei L, Shi J, Li J. Upregulation of GABA receptor promotes long-term potentiation and depotentiation in the hippocampal CA1 region of mice with type 2 diabetes mellitus. *Exp Ther Med*. 2019;18(4):2429-2436. doi:10.3892/etm.2019.7868

143. Sanches M, Abuhaiba SI, d'Almeida OC, et al. Diabetic brain or retina? Visual psychophysical performance in diabetic patients in relation to GABA levels in occipital cortex. *Metab Brain Dis*. 2017;32(3):913-921. doi:10.1007/s11011-017-9986-3

144. Chan KL, Puts NAJ, Schär M, Barker PB, Edden RAE. HERMES: Hadamard encoding and reconstruction of MEGA-edited spectroscopy: HERMES. *Magn Reson Med*. 2016;76(1):11-19. doi:10.1002/mrm.26233

145. Damasceno DC, Netto AO, Iessi IL, et al. Streptozotocin-Induced Diabetes Models: Pathophysiological Mechanisms and Fetal Outcomes. *BioMed Res Int*. 2014;2014(2):819065. doi:10.1155/2014/819065

146. Gheibi S, Kashfi K, Ghasemi A. A practical guide for induction of type-2 diabetes in rat: Incorporating a high-fat diet and streptozotocin. *Biomed Pharmacother*. 2017;95:605-613. doi:10.1016/j.biopha.2017.08.098

147. Wszola M, Klak M, Kosowska A, et al. Streptozotocin-Induced Diabetes in a Mouse Model (BALB/c) Is Not an Effective Model for Research on Transplantation Procedures in the Treatment of Type 1 Diabetes. *Biomedicines*. 2021;9(12):1790. doi:10.3390/biomedicines9121790

148. Simpson IA, Dwyer D, Malide D, Moley KH, Travis A, Vannucci SJ. The facilitative glucose transporter GLUT3: 20 years of distinction. *Am J Physiol-Endocrinol Metab*. 2008;295(2):E242-E253. doi:10.1152/ajpendo.90388.2008

149. Singh VP, Bali A, Singh N, Jaggi AS. Advanced Glycation End Products and Diabetic Complications. *Korean J Physiol Pharmacol*. 2014;18(1):1-14. doi:10.4196/kjpp.2014.18.1.1

150. Burgos-Morón, Abad-Jiménez, Marañón, et al. Relationship Between Oxidative Stress, ER Stress, and Inflammation in Type 2 Diabetes: The Battle Continues. *J Clin Med*. 2019;8(9):1385. doi:10.3390/jcm8091385

151. Thornalley PJ. Glyoxalase I – structure, function and a critical role in the enzymatic defence against glycation. *Biochem Soc Trans*. 2003;31(6):1343-1348. doi:10.1042/bst0311343

152. Braidy N, Zarka M, Jugder BE, et al. The Precursor to Glutathione (GSH), γ-Glutamylcysteine (GGC), Can Ameliorate Oxidative Damage and Neuroinflammation Induced by Aβ40 Oligomers in Human Astrocytes. *Front Aging Neurosci*. 2019;11:177. doi:10.3389/fnagi.2019.00177

153. Nandi A, Yan LJ, Jana CK, Das N. Role of Catalase in Oxidative Stress- and Age-Associated Degenerative Diseases. *Oxid Med Cell Longev*. 2019;2019:9613090. doi:10.1155/2019/9613090

154. Burkhard FZ, Parween S, Udhane SS, Flück CE, Pandey AV. P450 Oxidoreductase deficiency: Analysis of mutations and polymorphisms. *J Steroid Biochem Mol Biol*. 2017;165:38-50. doi:10.1016/j.jsbmb.2016.04.003

155. Ahsan H. 3-Nitrotyrosine: A biomarker of nitrogen free radical species modified proteins in systemic autoimmunogenic conditions. *Hum Immunol*. 2013;74(10):1392-1399. doi:10.1016/j.humimm.2013.06.009

156. Gronborg M, Pavlos NJ, Brunk I, et al. Quantitative Comparison of Glutamatergic and GABAergic Synaptic Vesicles Unveils Selectivity for Few Proteins Including MAL2, a Novel Synaptic Vesicle Protein. *J Neurosci*. 2010;30(1):2-12. doi:10.1523/JNEUROSCI.4074-09.2010

157. Gürth CM, Dankovich TM, Rizzoli SO, D'Este E. Synaptic activity and strength are reflected by changes in the post-synaptic secretory pathway. *Sci Rep*. 2020;10(1):20576. doi:10.1038/s41598-020-77260-2

158. Ford TC, Nibbs R, Crewther DP. Glutamate/GABA+ ratio is associated with the psychosocial domain of autistic and schizotypal traits. Fatemi SH, ed. *PLoS ONE*. 2017;12(7):e0181961. doi:10.1371/journal.pone.0181961

159. Morland C, Nordengen K. N-Acetyl-Aspartyl-Glutamate in Brain Health and Disease. *Int J Mol Sci*. 2022;23(3):1268. doi:10.3390/ijms23031268

160. Moffett JR, Arun P, Ariyannur PS, Namboodiri AMA. N-Acetylaspartate reductions in brain injury: impact on post-injury neuroenergetics, lipid synthesis, and protein acetylation. *Front Neuroenergetics*. 2013;5:11. doi:10.3389/fnene.2013.00011

161. Brion JP, Anderton BH, Authelet M, et al. Neurofibrillary tangles and tau phosphorylation. O'Neill C, Anderton B, eds. *Biochem Soc Symp*. 2001;67:81-88. doi:10.1042/bss0670081

162. Reiss AB, Arain HA, Stecker MM, Siegart NM, Kasselman LJ. Amyloid toxicity in Alzheimer's disease. *Rev Neurosci*. 2018;29(6):613-627. doi:10.1515/revneuro-2017-0063

163. Lugarà E, De Fusco A, Lignani G, Benfenati F, Humeau Y. Synapsin I Controls Synaptic Maturation of Long-Range Projections in the Lateral Amygdala in a Targeted Selective Fashion. *Front Cell Neurosci*. 2019;13:220. doi:10.3389/fncel.2019.00220

164. Sheng M, Pak DT. Glutamate Receptor Anchoring Proteins and the Molecular Organization of Excitatory Synapses. *Ann N Y Acad Sci*. 1999;868:483-493. doi:10.1111/j.1749-6632.1999.tb11317.x

165. Chen J, Rogers SC, Kavdia M. Analysis of Kinetics of Dihydroethidium Fluorescence with Superoxide Using Xanthine Oxidase and Hypoxanthine Assay. *Ann Biomed Eng*. 2013;41(2):327-337. doi:10.1007/s10439-012-0653-x

166. Garbett NC, Hammond NB, Graves DE. Influence of the Amino Substituents in the Interaction of Ethidium Bromide with DNA. *Biophys J*. 2004;87(6):3974-3981. doi:10.1529/biophysj.104.047415

167. Tapper S. *Neurotransmitter Imaging of the Human Brain : Detecting γ-Aminobutyric Acid (GABA) Using Magnetic Resonance Spectroscopy*. Vol 1667. Linköping University Electronic Press; 2019. doi:10.3384/diss.diva-154904

168. Aufhaus E, Weber-Fahr W, Sack M, et al. Absence of changes in GABA concentrations with age and gender in the human anterior cingulate cortex: A MEGA-PRESS study with symmetric editing pulse frequencies for macromolecule suppression: GABA MEGA-PRESS with Macromolecule Suppression. *Magn Reson Med*. 2013;69(2):317-320. doi:10.1002/mrm.24257

169. Near J, Evans CJ, Puts NAJ, Barker PB, Edden RAE. *J* -difference editing of gamma-aminobutyric acid (GABA): Simulated and experimental multiplet patterns: Simulations of GABA-Edited MRS. *Magn Reson Med*. 2013;70(5):1183-1191. doi:10.1002/mrm.24572

170. Prisciandaro JJ, Mikkelsen M, Saleh MG, Edden RAE. An evaluation of the reproducibility of 1H-MRS GABA and GSH levels acquired in healthy volunteers with J-difference editing sequences at varying echo times. *Magn Reson Imaging*. 2020;65:109-113. doi:10.1016/j.mri.2019.10.004

171. Saleh MG, Rimbault D, Mikkelsen M, et al. Multi-vendor standardized sequence for edited magnetic resonance spectroscopy. *NeuroImage*. 2019;189:425-431. doi:10.1016/j.neuroimage.2019.01.056

172. Ghasemi R, Haeri A, Dargahi L, Mohamed Z, Ahmadiani A. Insulin in the Brain: Sources, Localization and Functions. *Mol Neurobiol*. 2013;47(1):145-171. doi:10.1007/s12035-012-8339-9.

173. Ebeling P, Koistinen HA, Koivisto VA. Insulin-independent glucose transport regulates insulin sensitivity. *FEBS Lett*. 1998;436(3):301-303. doi:10.1016/S0014-5793(98)01149-1

174. Veys K, Fan Z, Ghobrial M, et al. Role of the GLUT1 Glucose Transporter in Postnatal CNS Angiogenesis and Blood-Brain Barrier Integrity. *Circ Res*. 2020;127(4):466-482. doi:10.1161/CIRCRESAHA.119.316463

175. Morgello S, Uson RR, Schwartz EJ, Haber RS. The human blood-brain barrier glucose transporter (GLUT1) is a glucose transporter of gray matter astrocytes. *Glia*. 1995;14(1):43-54. doi:10.1002/glia.440140107

176. Vannucci SJ, Koehler-Stec EM, Li K, Reynolds TH, Clark R, Simpson IA. GLUT4 glucose transporter expression in rodent brain: effect of diabetes. 1998;797(1):1-11. doi:10.1016/S0006-8993(98)00103-6

177. Raider K, Ma D, Harris JL, et al. A high fat diet alters metabolic and bioenergetic function in the brain: A magnetic resonance spectroscopy study. *Neurochem Int*. 2016;97:172-180. doi:10.1016/j.neuint.2016.04.008

178. Bondy SC, LeBel CP. The relationship between excitotoxicity and oxidative stress in the central nervous system. *Free Radic Biol Med*. 1993;14(6):633-642. doi:10.1016/0891-5849(93)90144-J

179. Bratek E, Ziembowicz A, Salinska E. N-Acetylaspartylglutamate (NAAG) Pretreatment Reduces Hypoxic-Ischemic Brain Damage and Oxidative Stress in Neonatal Rats. *Antioxidants*. 2020;9(9):877. doi:10.3390/antiox9090877

180. Bratek E, Ziembowicz A, Bronisz A, Salinska E. The activation of group II metabotropic glutamate receptors protects neonatal rat brains from oxidative stress injury after hypoxia-ischemia. Barnes S, ed. *PLOS ONE*. 2018;13(7):e0200933. doi:10.1371/journal.pone.0200933

181. Cao Y, Gao Y, Xu S, et al. Glutamate carboxypeptidase II gene knockout attenuates oxidative stress and cortical apoptosis after traumatic brain injury. *BMC Neurosci*. 2016;17(1):15. doi:10.1186/s12868-016-0251-1

182. Berent-Spillson A, Russell JW. Metabotropic glutamate receptor 3 protects neurons from glucose-induced oxidative injury by increasing intracellular glutathione concentration. *J Neurochem*. 2007;101(2):342-354. doi:10.1111/j.1471-4159.2006.04373.x

183. Bruno V, Battaglia G, Casabona G, Copani A, Caciagli F, Nicoletti F. Neuroprotection by Glial Metabotropic Glutamate Receptors Is Mediated by Transforming Growth Factor-Beta. 18(23):9594-9600. doi:0270-6474/98/189594-07$05.00/0

184. Dobolyi A, Vincze C, Pál G, Lovas G. The Neuroprotective Functions of Transforming Growth Factor Beta Proteins. *Int J Mol Sci*. 2012;13(7):8219-8258. doi:10.3390/ijms13078219

185. Calvetti D, Somersalo E. Quantitative in silico Analysis of Neurotransmitter Pathways Under Steady State Conditions. *Front Endocrinol*. 2013;4:137. doi:10.3389/fendo.2013.00137

Annexes:

Figure 16. Insulin sensitivity and glucose metabolism in the

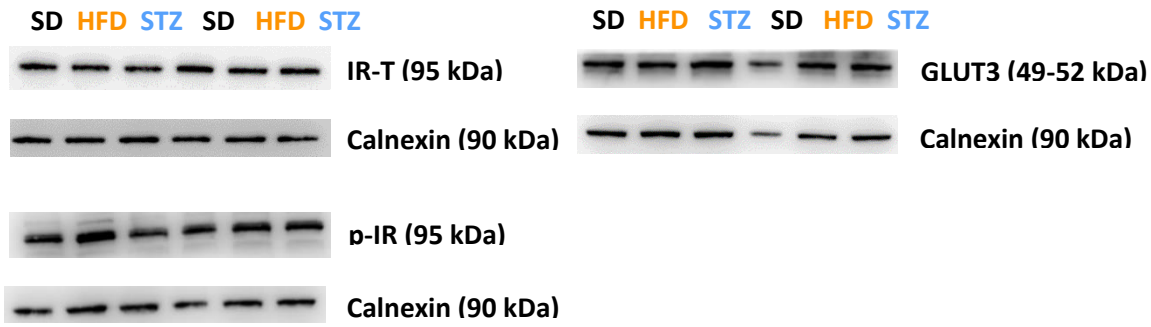

Figure 18. Hippocampal glycation on the obese and T2DM animal

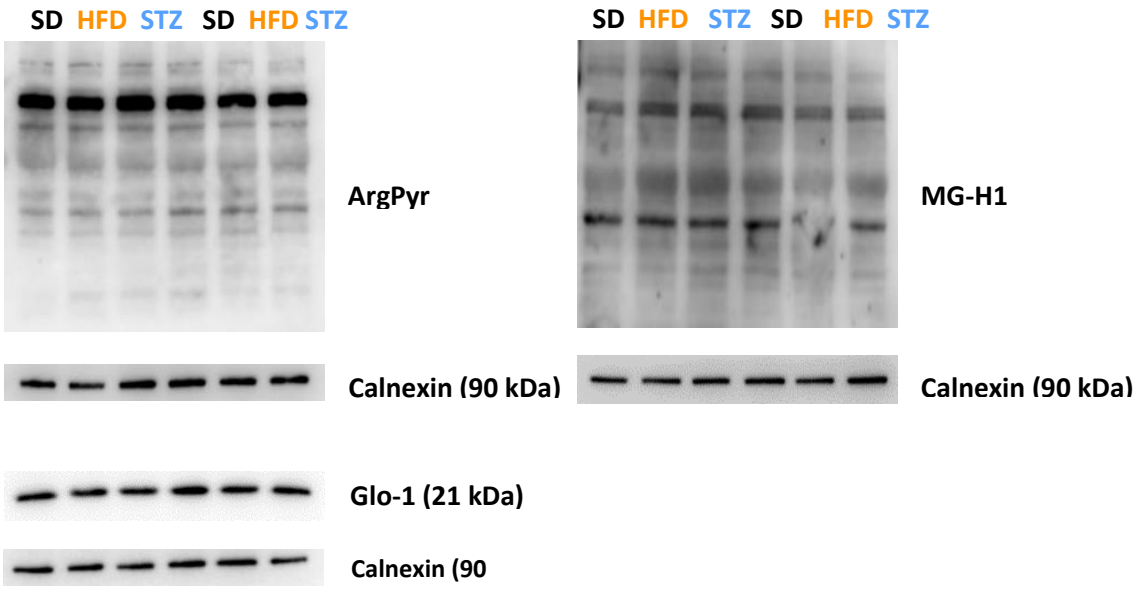

Figure 19. Hippocampal oxidative stress on the obese and T2DM

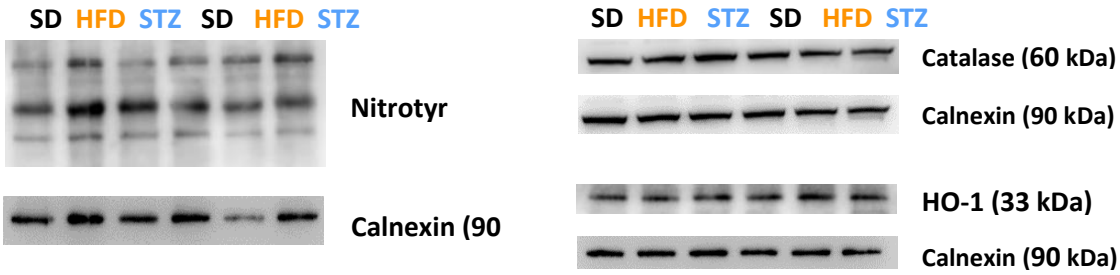

Figure 20. Glutamatergic pool increased in the hippocampus of diabetic rats and related to plasma insulin levels.

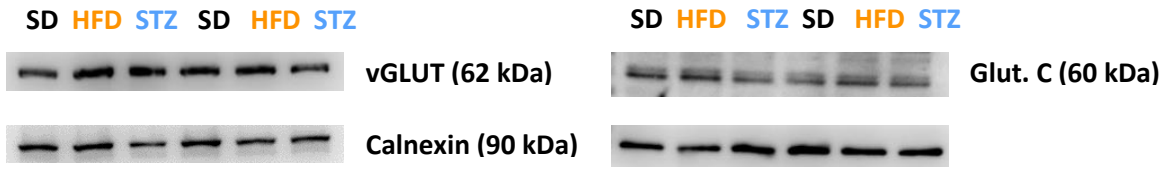

Figure 21. A possible compensatory mechanism involving NAAG and GSH in the hippocampus of obese but not diabetic rats.

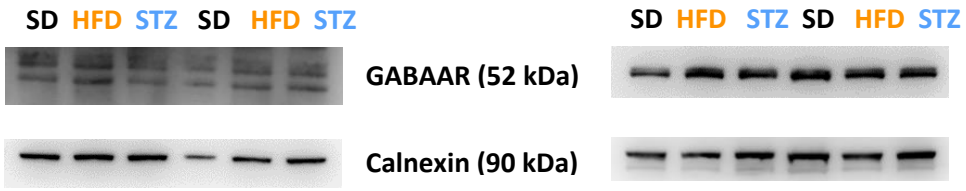

Figure 22. The hippocampal cellular viability was not hindered.

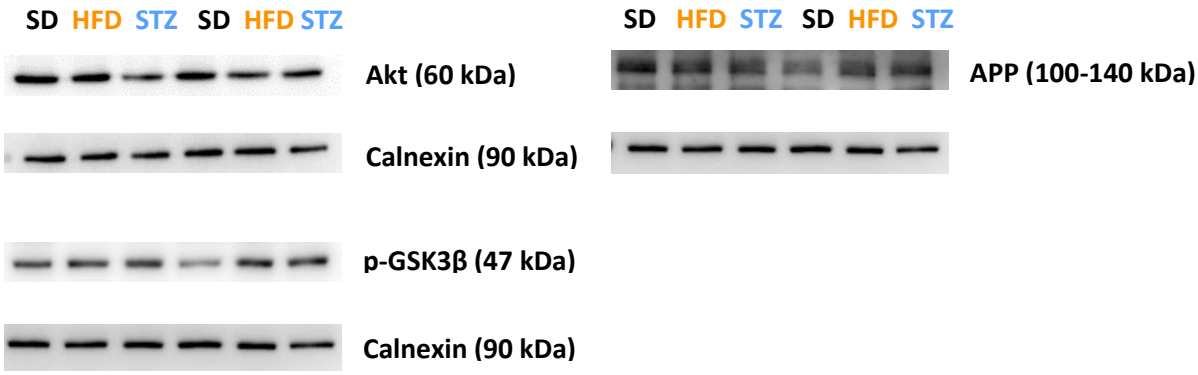

Figure 23. The hippocampal synaptic integrity was not impaired.

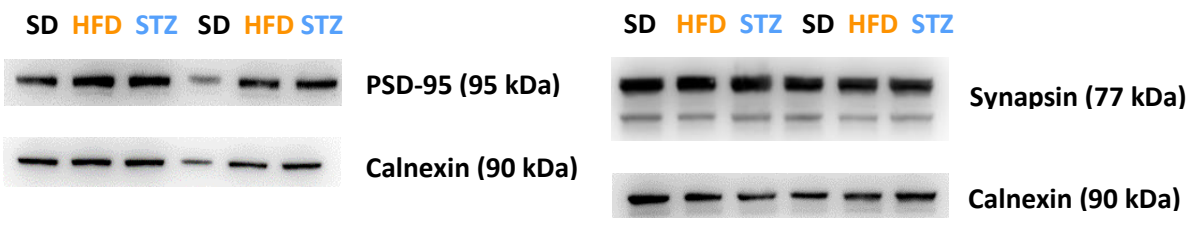

Figure 24. Hyperglycemia was promoted in the visual cortex of STZ-injected rats.

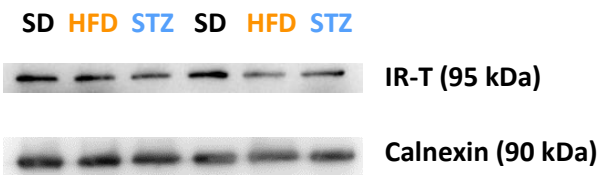

Figure 26. Deleterious events involving glycation were not observed in the visual cortex.

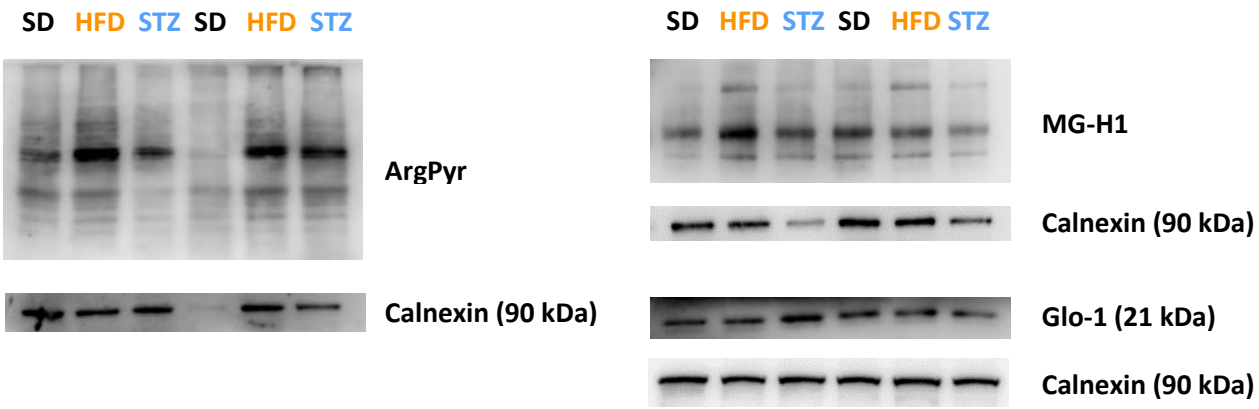

Figure 28. Detrimental events involving oxidative stress were not detected in the visual cortex.

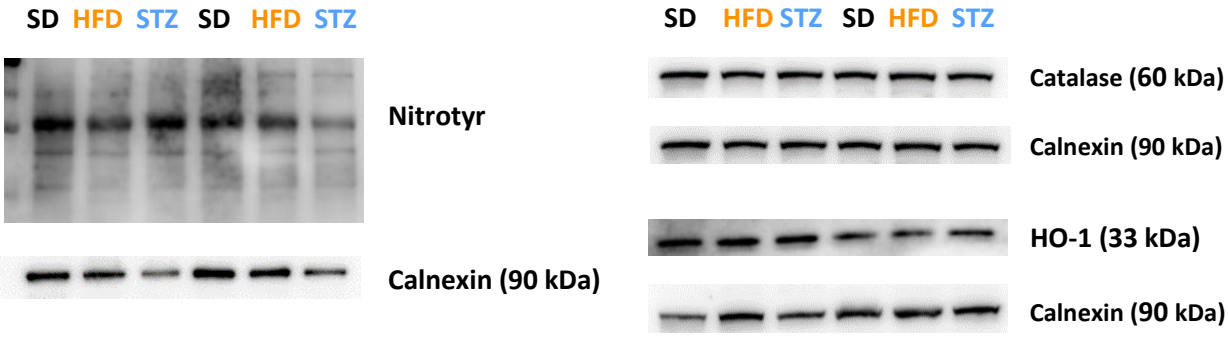

Figure 29. A excitatory synaptic imbalance was not observed in the visual cortex despite some insulin-related neurometabolic changes.

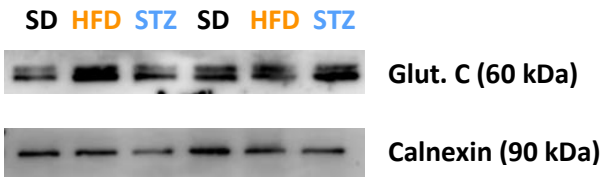

Figure 30. An inhibitory synaptic imbalance was not detected in the visual cortex.

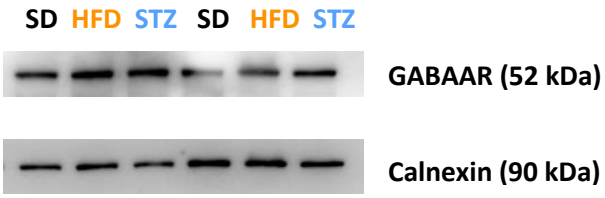

Figure 31. The overall visual cortex integrity was maintained although an insulin-related Tau increase in diabetic rats.